UNIVERSITAT DE BARCELONA

Fluctuations, gene circuit architecture and stem cell quiescence

David Frigola Tubert

Universitat de Barcelona

Ph.D. Thesis

Fluctuations, gene circuit architecture and stem cell quiescence

Author:
David Frigola Tubert

Advisor:
Dra. Marta Ibañes Miguez
Tutor:
Prof. José María Sancho Herrero

Memòria presentada per a optar al grau de Doctor al Programa de Doctorat en Física

Department of Structure and Constituents of Matter
Facultat de Física

November 2015

“ The first principle is that you must not fool yourself — and you are the easiest person to fool.”

Richard Feynman

“Ah, what a fine day for science!”

Dexter

Agradecimientos

De algún modo, esta tesis no se la debo solo a los que han estado a mi lado durante los ultimos años, sino también a quien estuvo antes. Y más extrañamente, no puedo dejar de agradecer cosas que aún estan por venir. En todo caso, tengo un buen puñado de gente a quien agradecer el trabajo aquí presentado, y el que no está aquí también. La lista no es, no puede ser, exhaustiva, ni en las personas que aparecen ni en las razones.

A l'entorn científic.
A la Marta per la paciencia, per la guia, per no descartar mai d'entrada una idea que provingués de mi i per, potser sense adonar-se'n, deixar-me aprendre per mi mateix.
A Jose Maria.
A companys i membres de grup seniors i juniors, per alguns moments compartits i per alguns comentaris científics que han acabat a aquesta tesi.
Als companys de despatx, amb qui també hem compartit dubtes científics, burocràtics i alguna conversa política.
También a los miembros del Caño Lab. En especial a Ana (que siempre me ha hecho sentir valorado), a Pep (pel seu entusiasme) y a Mary Paz (por explicarme hasta la biología más básica).
A Pau y a Irina.

A todas las personas con las que coincidí en la FJI y en D-Recerca. Por haber compartido un espacio de activismo, porque han influido mucho en mi visión de la ciencia y por algunos momentos inolvidables.

Als amics aquí a la facultat.
A Sara. Por más de 10 años de amistad, por todo lo que he aprendido... y

porque no sabría decir cuantas decimas de la media de la carrera te debo, pero es más de una.
Al Mario per ajudar a matar Frigotubi de calcuta.
Al David per ser el millor company de doctorat.
A Juan Camilo, Dani, Pau. Por los descansos dentro y fuera de la facultad.
A la Maria (M), per tants anys... i recentment per mostrarme que tenim futur.
També als companys de la carrera. Julià, Joan Manel, Lluis... et al.

A mis amigos de siempre.
A Carlo por ser un amigo y un espejo en el que reflejé tanto tiempo quién quería y creía ser. Quien soy ahora tiene mucho de aquel reflejo, seguramente más de lo que parece.
A Joan por estar siempre.
A los demás PNWB, porque si no nos hubieran juntado a aquel grupo de raritos no se que habría sido de nosotros.

A mi familia.
A mamá y a papá. Las cosas importantes son obvias, pero aquí quizás os puedo agradecer aquella colección del barco de vapor de color naranja y aquellos libros rojos de 'como funciona el mundo'.
A Albert.
A Elena.
A Boris y a Iker les agradecería la ilusión de verles crecer, pero más bien les pido perdón por no haber estado.

A Maria. Por apoyarme y demostrarme que quieres seguir haciendolo. Por estar, por crecer, por seguir creciendo. Por el futuro que me ayudas a proyectar y a construir.

A ti

Contents

Part I

Introduction

Chapter 1

Dynamics and stochasticity of genetic circuits

1.1 A brief historical perspective

To a physicist, living matter is a wonderfully complex subject of study, but it can also be overwhelming. The physicist's reductionist approach to any problem, trying to find universal laws and use the minimal components that qualitatively define a system, has been used many times to try to answer questions of biological significance, and it has not always succeeded. Let us take a look at the history of physicists and mathematicians that have tried to delve into biological matters, to put in context the work presented in this thesis (Frigola et al., Submitted).

Mathematically-minded scientists (such as physicists) have historically tried to contribute to biology in two main ways. One is the resolve to find some sort of general, simple principles that govern biology, like the ones that can be found in the atomic world or in the heavens. Not completely independent is a second contribution, trying to apply concepts learned from physics and mathematics to biological problems. Of these, the first is still in its infancy (despite having started many decades ago), but the second already has a fertile history of failures and successes upon which to build present science.

The most obvious example of both is the Waddington landscape, the metaphor proposed over 70 years ago that during development cells roll down through valleys that bifurcate, choosing at each new ridge their future cell type (Waddington, 1942). This view of cell differentiation has actually become a commonly used and debated paradigm to interpret cellular states, where the valleys of the landscape are attractors that are reshaped during developmental processes (Ferrell, 2012).

Another such example is the somehow physical concept of positional information, proposed by Lewis Wolpert (Wolpert, 1969). He posited that cells would need to somehow know their position within a developing organism to define their cell fate. Nobel Laureate Francis Crick realized in 1970 that the space and time scales involved in diffusion of biological molecules within the extracellular space meant that these molecules could be creating gradients across developing tissues, to fulfil this role and convey this positional information (Crick, 1970a). Since then, many different molecules have been found to do this type of function (Rogers and Schier, 2011).

These are examples of successful conceptual frameworks that where relatively so from the beginning. A perhaps more paradigmatic example in its mixture of success and failure is the contribution by Alan Turing, most famous from his work in computer science. In a seminal work in 1952, he proposed that patterns arising during development could be the natural output of chemical reactions between an activator and a repressor molecule that diffuse across space with different diffusion coefficients (Turing, 1952). The validity of this idea was later proven experimentally in chemical (not biological) systems (Castets et al., 1990; Vigil et al., 1992). Furthermore, the mechanism was generalized and distilled to its key components (a short range activation and a long range inhibition) by Gierer and Meinhardt (1972). This mechanism became a very popular idea and yet, it is a good example of the failure of the interplay between mathematics and biology.

Despite the Turing mechanism being able to reproduce many biological patterns (the most striking example being the fur and skin patterns of several animals (Murray, 2001)), the molecules that would be enacting the mechanism could not be found for many years. Thus, the kind of beautiful mathematical idea that seduced theorists was shunned by biologists. This is only one instance of models that predicted mechanisms that were not detected in nature, or were

unable to predict changes in patterning that were observed experimentally. Due to these cases, a kind of mutual suspicion between experimental biologists and theorists arose (Lawrence, 2004).

In the last decades, though, an enormous advance in experimental techniques has allowed to bridge this divide. The knowledge of which biological molecules participate in development, as well as the ability to manipulate and observe them in greater spacetime resolution, has allowed mathematical models to become more grounded in biological reality, as well as to reinterpret older models in light of new, more abundant data. As an example, in the last years some new examples (not the first) of the Turing mechanism have been successfully found in fish skin patterning (Kondo et al., 2009). At the same time, theoretical tools did not stop advancing, and relevant progress has been achieved in nonequilibrium statistical mechanics, dissipative systems, nonlinear dynamics and complex systems. This, together with the enormous increase in available computational power, has enabled modelling that is much more relevant to experimental biology (and vice versa). During the last two decades, interdisciplinary research involving members from both communities has become more and more common, and the aforementioned mutual suspicion has progressively diluted (Perrimon and Barkai, 2011). Thus we are now in an exceptionally fertile moment to approach biological problems mathematically, as well as to embrace the challenge of trying to extract some fundamental principles of how living matter works.

1.2 Noise in biochemical systems

One of the most active and fertile of these problems are the ones within the area found between development, gene regulation, and different forms of cell-to-cell communication, only perhaps rivalled by neuroscience. It is in this area that our studies are framed, and to understand them we need to do a condensed review of their biological framework and its relationship to physical concepts.

The cell is a biochemical reactor, with hundreds of different chemical molecules moving around both in the nucleus and in the cytoplasm (in the case of eukaryotes) and interacting in a myriad ways (Alberts et al., 2007). These molecules,

of three main types (DNA, messenger RNA and proteins) have a fundamental relationship that is the basis of all the function in the cell: the *central dogma of molecular biology*. This classic view states that the information encoded in genes (DNA) is transcribed (by RNA polymerase) into messenger RNA (mRNA) molecules which is then decoded and translated (by a ribosome) into the aminoacid chain that later folds into a protein. This view has become more nuanced since its original presentation by Francis Crick in 1970 (Crick, 1970b), with this sequence and information flow still at its core (Figure 1.1).

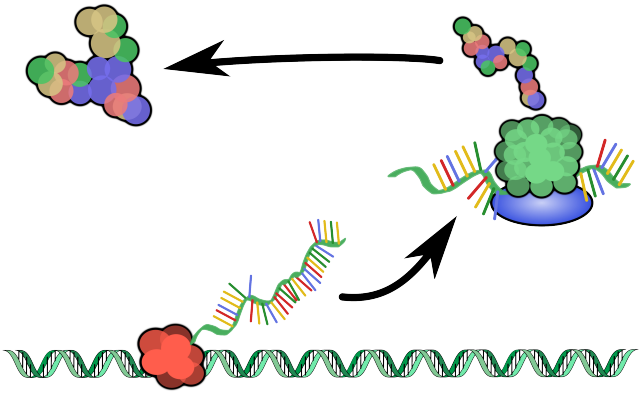

Figure 1.1 Main information flow of the Central Dogma of Molecular Biology. According to it, DNA is transcribed into mRNA which is translated into protein. Not shown are the other information flows: DNA on itself, RNA on itself, and RNA onto protein. According to the classic view, protein can modulate the expression but not change the information contained in DNA or RNA.

Some important additions to this view are RNA chains with functions other than being transcribed intro proteins, proteins that interact with each other, proteins that interact with DNA altering transcription of another specific protein, or proteins that semi-permanently modify DNA (for instance through methylation, the addition of methyl groups at specific DNA regions), in what is known as epigenetics. Of special interest to us will be the proteins that modulate the expression of other proteins. These are called Transcription Factors (TFs), and bind to the promoter, a region of DNA that does not encode proteins and, instead, is responsible for modulating the expression of a specific protein that is encoded adjacent to it.

These processes, and in particular the protein-protein and protein-DNA interactions form an enormous network of interactions that yield the final protein amounts that do all functions in the cell. This network is amenable to study through different mathematical tools. Regardless of how they are studied, it is often necessary to consider the stochasticity that is inherent to these processes. All these processes are chemical reactions, that depend on molecules meeting in space to happen. In a naive view of chemistry, chemical species are very abundant, and well mixed, so the rate at which they react is constant or, at least, evolves deterministically.

In cells, however, many molecules are in low amounts (for instance, many genes have only one copy), which means that whether reactions happen or not at a certain time becomes a matter of chance (Kepler and Elston, 2001; Bialek, 2011). Furthermore, due to these low numbers, any small fluctuation can have a meaningful impact in the behaviour of biological systems. This needs to be accounted for in any model of the cell, or in any description that tries to understand a cellular process, since however they work, cellular mechanisms need to work around this. A lot of study has gone into how the cell may minimize the effects of this noise, learning from the experience of fields such as electronics, liquid crystals, or other nonequilibrium systems (Sagués et al., 2007), but in the last years the idea that cells may not only work despite noise but also profit from it has gained traction and has been demonstrated for several examples (Losick and Desplan, 2008; Eldar and Elowitz, 2010). Some typical examples are a population having a heterogeneous response to the same input (despite having no genetic differences) (Kussell et al., 2005; Veening et al., 2008), tuning the proportion of this heterogeneity (Acar et al., 2008) or the activation and deactivation of cellular processes by noise(Balaban et al., 2004).

This noise can be classified in several ways. One classification that will be useful in this thesis is in the categories of intrinsic and extrinsic. Intrinsic noise comes from the dynamics that are being studied themselves, like the stochastic chance that two molecules meet in space and react, or the chance that the DNA promoter of a protein of study is available for transcription. On the other hand, extrinsic noise is noise that comes from fluctuations that directly affect the system but are not being directly modelled, such as the environment of the cell or the amount of some molecule that is not explicitly part of the model, like RNA polymerase (often not represented as such, but absorbed into the transcription

rate of a protein of interest). It could be said that, in a way, intrinsic noise is noise in (or coming from) the variables of the system, and extrinsic noise is noise in the parameters (Gardiner, 2008; García-Ojalvo and Sancho, 2012). In biological systems, this separation is usually taken further, and intrinsic noise is taken to be the noise inherent to the process of gene expression or the dynamics of a particular protein, whereas extrinsic noise is considered to be noise in other cellular components, affecting all the cell at the same time (Elowitz et al., 2002).

To better understand the two types of noise, we can look at an example in which they have been experimentally quantified. In a beautiful experiment, Elowitz and colleagues prepared transgenic bacteria that expressed two fluorescent proteins of different colors (yellow and red) (Elowitz et al., 2002). The promoters that regulated both proteins were identical, meaning that any modulations of expression affected them in the same way. The difference in expression between both proteins in a given cell was due to intrinsic noise, whereas changes that affected both genes equally, or differences from cell to cell, corresponded to extrinsic noise (be it due to differences in local environment, small internal differences from cell to cell, or variation in molecules such as polymerases) (Elowitz et al., 2002). What this experiment shows is that the distinction between intrinsic and extrinsic is related to the level of description but, at the same time, it has physical significance.

1.3 Modular biology: Network motifs

The vastly complex network formed by all transcriptional regulations exists and acts all at the same time, and the precise responses and functions of the cell are affected by each and every one of the parts of this network. Thus, contrary to the classical biologist's view in which each molecule is responsible for one function, one may think that a network of interacting components needs to be modelled all at the same time (Hartwell et al., 1999; Barabasi and Oltvai, 2004). This is a valid approach and, using knowledge from network theory and complex systems, it often provides insights into the workings of the cell (Barabasi and Oltvai, 2004). However, there is also another approach, that we take here. Less than 15 years ago, analysis of known transcriptional networks showed that there are some highly recurrent (meaning that they happen much more often than would be expected in a randomly wired network) small regulatory patterns,

called network motifs (Milo et al., 2002; Alon, 2006, 2007). Theoretical study of these motifs has shown that each is capable of generating specific dynamics, that can be linked to specific functions (Alon, 2006, 2007). Studying network motifs allows a more detailed level of description which includes, for instance, the different types of noise and how they affect specific functions, as well as an insight into some of the principles used by the undirected design of evolution (Alon, 2003).

One very common motif is Negative Auto Regulation (NAR), in which a protein represses its own expression once it reaches a certain threshold (Alon, 2006, 2007). NAR provides two functions: faster response times and, importantly, a supression of fluctuations (Alon, 2006, 2007). Another common motif is the Feed-Forward Loop (FFL), which consists of a protein A that regulates a protein B which in turn regulates a protein C, but with the particularity that protein A also regulates C directly (thus feeds-forward)(Milo et al., 2002). Depending on the sign of these three interactions (that is, whether they repress or activate), the FFL can do different functions, like acting as a filter against fluctuations or as a pulse generator (Alon, 2006, 2007). The classical FFL classification defined two categories depending on whether the direct wiring from A to C was of the same sign than the one that goes through B (coherent FFL) or of opposite sign (incoherent FFL), with similar deterministic dynamics and function within each category (Alon, 2006, 2007). Interestingly, it has been shown that there is an alternate classification according to their stochastic behaviour, and that this classification is a good predictor of the functions of the cell in which the FFL is found (Kittisopikul and Süel, 2010).

1.4 Bistability

Another feature that network motifs can provide is mutistability. A system is multistable when it has more than one stable state for a given set of parameters (i.e. external and internal conditions). This can be useful to provide two different but well defined responses to the same input, or to avoid changing states until the conditions have clearly changed, in a process that is known as hysteresis (Cherry and Adler, 2000; Ferrell, 2002; Guantes and Poyatos, 2008; Siegal-Gaskins et al., 2009). Hereby we will concentrate on the particular case of two simultaneously stable states, called bistability.

As explained earlier, cells are subject to noisy dynamics and a noisy environment. Due to differences in history, but also due to small differences from one cell to another (extrinsic noise), cell populations may show heterogeneity, with some cells in each state. These states can be experimentally observed: when a histogram of the concentrations in the population is done, a bimodal distribution arises, with one peak at each stable state (Ferrell Jr., 1998; Becskei et al., 2001; Acar et al., 2010) (Figure 1.3 B). This bimodality observed in a single population does not necessarily correspond to bistability and can instead be due to ultrasensitive (Shu et al., 2011) or excitatory behaviours (Kalmar et al., 2009). A theoretical analysis of the system that underlies bimodality can provide evidence as to what dynamic behaviour is generating the bimodality by pinpointing additional specific features that should be expected, such as hysteresis when bistability arising from saddle node bifurcations underlies the bimodality (Becskei et al., 2001).

One very common way of achieving bistability in biology is having a Positive Feedback Loop involving a strong enough nonlinearity (Cherry and Adler, 2000; Ferrell, 2002). A Positive Feedback Loop appears when a protein enhances its own expression, be it by directly binding to its own promoter or by interacting with other proteins that, in turn, interact with its promoter. The direct, most simple case, is called autoactivation. There are other known common PFL motifs. A very simple one is that of Mutual Activation, in which a protein X activates the transcription of a second protein Y, which in turn activates X back. Another simple possibility is mutual repression, in which Y represses X expression, and the positive feedback is achieved when X represses Y in turn, eliminating the repression and thus enhancing its own production (Tyson et al., 2003). Mutual activation, as well as mutual repression and autoactivation, need a strong enough nonlinearity in the transcriptional regulations to drive bistability (Cherry and Adler, 2000). This is commonly achieved through cooperativity: if one protein is not enough to do the regulation, and instead several copies need to be bound at the same time, the regulation scales nonlinearly, with the number of molecules necessary as an exponent.

Other bistable motifs involve interactions other than transcriptional. In particular, a computational exploration through evolutionary algorithms *de novo*, with the ingredients of transcriptional networks, found new circuit architectures that

display bistability. In these circuits, the proteins X and Y interact postranscriptionally, forming a dimer which is then degraded (François and Hakim, 2004). This sort of sequestering of each protein by the other, that has been termed molecular titration, has been shown to enable nonlinear behaviour (Buchler and Louis, 2008). Thanks to this nonlinearity, the linear transcriptional feedback is able to achieve bistability. Two of these motifs are the Mixed Feedback Loop (MFL) and what was termed Autoactivation with Complex (AAC). In the MFL, Y transcriptionally represses X and they form a dimer together, closing the feedback loop through one transcriptional and one post-transcriptional repression (hence the 'mixed' part of the name). In AAC, X autoactivates and also forms a dimer with Y. In both cases, titration through dimer formation is needed to obtain bistability because the transcriptional regulations are linear. Both cases seem to be biologically relevant and the MFL, in particular, has been found to happen in natural circuits with a much higher frequency than would be expected by pure chance (François and Hakim, 2005).

To better understand the phenomenon of bistability (beyond what circuits can generate it), and some of the concepts already discussed here, let us see a specific example of bistable PFL. Imagine a protein X with a basal production rate R (which incorporates both transcription and translation). This protein can activate its own production with cooperativity n, up to an amount $R + r$ when there are very high amounts of protein. For such a system, the dynamic equation for the concentration x could be, as used several times in the literature, (Keller, 1995; Smolen et al., 1998; Becskei et al., 2001; Cheng et al., 2008))

$$\frac{dx}{dt} = R + \frac{rx^n}{K_d + x^n} - k_{deg}x, \tag{1.1}$$

where cooperativity emerges in a Hill function of order n, $K_d^{\frac{1}{n}}$ sets the protein concentration at which autoactivated production is half its maximum value r (and is mechanistically related to the binding-dissociation of protein and DNA) and k_{deg} is the degradation rate of the protein.

To better understand the key parameters and behaviours of the system, it is useful to take dimensionless variables that absorb some of the parameters of the system. To do that, we take k_{deg} as the reference timescale for the system, and $K_d^{\frac{1}{n}}$ as the relevant scale of concentration. This yields the dimensionless dynamic equation

$$\frac{d\widetilde{x}}{d\widetilde{t}} = \widetilde{R} + \widetilde{r}\frac{\widetilde{x}^n}{1+\widetilde{x}^n} - \widetilde{x}, \tag{1.2}$$

where both parameters and variables have been rescaled:

$$\widetilde{x} = \frac{x}{\sqrt[n]{K_d}} \quad , \quad \widetilde{t} = k_{deg}t, \tag{1.3}$$

$$\widetilde{r} = \frac{r}{k_{deg}\sqrt[n]{K_d}} \quad , \quad \widetilde{R} = \frac{R}{k_{deg}\sqrt[n]{K_d}}. \tag{1.4}$$

This dynamic equation tells us the deterministic evolution of the system. By setting the derivative $\frac{dx}{dt} = 0$ and solving the subsequent equation, we can obtain the steady state value x^{st}. By varying a control parameter such as $\widetilde{r}$ and obtaining the steady states, we can obtain a bifurcation diagram (Strogatz, 2014) like the one in Figure 1.2 A. Notice how for $1.8 < r < 4$ there are two stable steady states separated by an unstable steady state (meaning that, although it fulfils $\frac{dx}{dt} = 0$, the smallest perturbation will grow and drive the system away from it).

The shape of this bifurcation diagram is also what enables the hysteresis mentioned earlier: if the system starts at a low r and this maximal transcription rate is progressively increased (due to a change in external conditions, for instance), it will remain at the low x state until it reaches the $r = 4$ threshold, when it will rapidly switch to a high x, whereas if it begins in the high x state, it will need to reach the much lower threshold of $r = 1.8$ to switch (Figure 1.2 A). This has been observed for different systems, but as an example, let us consider the lactose utilization network of model bacterium *E. coli* (Ozbudak et al., 2004). In this example, x would be the concentration of a lactose metabolizing protein, and r would be regulated by lactose in the medium (Figure 1.2 B). If the lactose metabolism is off, there needs to be a large lactose signalling to switch it on, whereas if it is already on lactose needs to drop to very low values for it to switch off (Figure 1.2 B). This may have the biological usefulness of avoiding responding to spurious changes in the environment: activating metabolic pathways is a costly and complex process, and it is therefore beneficial to avoid commiting to a change in these processes unless it is really necessary (Lambert and Kussell, 2014).

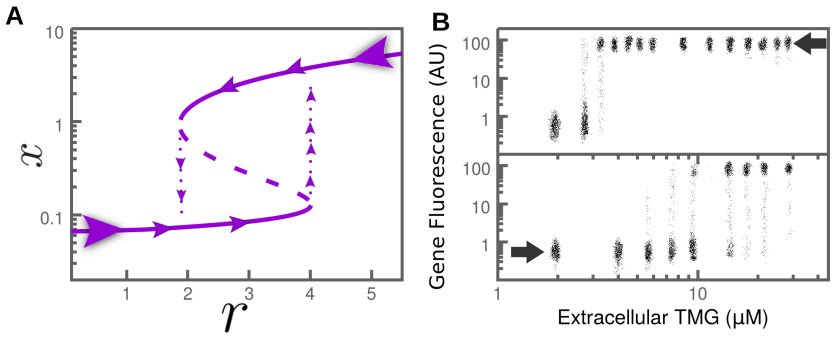

Figure 1.2 Bifurcation diagram and hysteresis. **A** Bifurcation diagram for the steady states x_{st} of equation 1.2, with $\widetilde{R} = 0.063$, $n = 2$. Continuous lines are stable steady states, whereas dashed line represents the unstable steady state. Arrows schematically show the change in concentration of a system starting at high r and lowering it progressively, or starting at the lower end and increasing r. Dotted lines show where each of the systems switch states. **B** Hysteresis in lactose utilization of *E. coli*. Figure is a qualitative reproduction of the results from Ozbudak et al. (2004), with a scatter plot in which cells are put at different concentrations of TMG (a sugar similar to lactose) and fluorescence proportional to the activity of their lactose uptake is measured. Arrows indicate the initial state for each of the subpanels, and it can be seen how depending on their history, they switch states at a different external concentration of TMG. In color in digital version.

Equation (1.1) can be undersood as gradient dynamics arising from a potential defined as $\frac{dx}{dt} = -\frac{dU}{dt}$. We can derive this potential function that underlies the dynamic equation, which will have two minima at the stable states, separated by a barrier, with its peak in the unstable steady state (Figure 1.3 A). Under specific noise conditions, this potential is reciprocal to the bimodal distribution of the concentrations in a population, with the peaks of the distribution at the minima of the potential wells and the width of the peaks related both to the shape of the well and the intensity of fluctuations(Gardiner, 2008; San Miguel and Toral, 2000):

$$P_{st}(x) \sim e^{\frac{-U(x)}{B}}, \tag{1.5}$$

where P_{st} is the steady state distribution of the system and B is a parameter related to noise intensity.

More interestingly, it has long been known from physics that fluctuations can

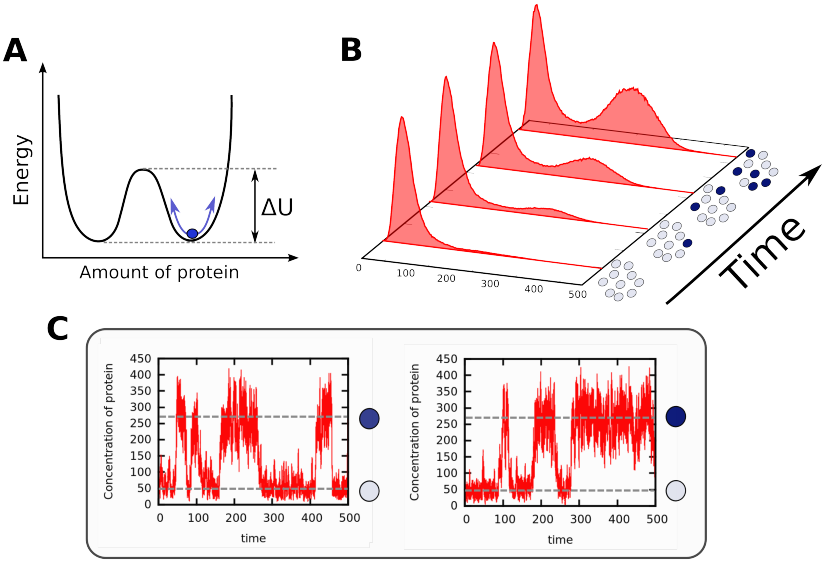

Figure 1.3 Stochastic state switching. **A** From the deterministic dynamics a potential can be derived that has two minima and a barrier separating them. **B** Experimental observation of switching in a population. If the high concentration state is eliminated, it will repopulate over time, yielding information about the state switching. **C** Modelling and observation of switching in a single cell. Stochastic simulations allow us to observe the dynamics of a cell that spontaneously switches states. Figure adapted from (Frigola et al., Submitted). In color in digital version.

enable spontaneous switching from one state to the other (Figure 1.3 C) (Gardiner, 2008; Van Kampen, 2007). It was observed by biologists as early as ten years ago (Acar et al., 2005), usually deduced by looking at whole populations due to the limitations in resolution of experimental techniques, although more recently it has been observed at the single-cell level (Singer et al., 2014). In the first case, one of the two peaks in a population is selected. Then, if the distribution of concentrations in the population is measured at different times, it can be seen how the eliminated peak is gradually repopulated, as cells switch back and forth, until the steady state is reached again (Figure 1.3 B). From the evolution of this repopulation, dynamical information about the switching can be gleaned (Acar et al., 2005).

1.5 Challenges in network motifs and stochasticity

In the last 15 years, genetic networks have been extensively studied to try to unravel the function their subnetworks or motifs do (Tyson et al., 2003; Barabasi and Oltvai, 2004; Alon, 2007; Lim et al., 2013), to try to fix or manipulate them, as well as to design genetic circuits with specific functions (Hasty et al., 2002; Khalil and Collins, 2010; Estrada and Guantes, 2013; Lim et al., 2013), among others. Many of these studies were deterministic or, as a first step, added noise in naive ways, without much information of the source or nature of this noise.

However, at the same time, the enormous improvement in space and time resolution of experimental techniques has allowed to measure cell dynamics and, with them, stochastic behaviours (Eldar and Elowitz, 2010; Munsky et al., 2012; Levine et al., 2013). This has allowed us to distinguish between different sources of noise (Elowitz et al., 2002; Singh et al., 2012), with different properties and even to use these measurements to infer the details of the underlying network (Munsky et al., 2009, 2012).

It has long been known in physics that noise can have nontrivial effects, beyond a simple perturbation of the deterministic system, and that these nontrivial effects depend strongly on the type and origin of the noise (Horsthemke and Lefever, 1984; San Miguel and Toral, 2000; Sagués et al., 2007). Only in the last years have these nontrivial effects started to be studied in biological systems. And indeed, it seems that noise in biological systems can interact with gene architecture and they can significantly affect its design or function (Süel et al., 2006; Kittisopikul and Süel, 2010), differently depending on the nature of noise (Morelli et al., 2008; Frigola et al., 2012; Jaruszewicz et al., 2013). However, comparisons between different types of noise or explanations for specific biological examples remain infrequent, if not rare. In chapter 2 we compare a bistable Positive Feedback Loop under a noise that generates a simple perturbation from the deterministic state, and under a more complex and realistic noise, and qualitatively reproduce an experimentally observed phenomenon, asymmetric switching, in which the stability of each of the states is differently affected by noise.

Although quite a few studies have already concentrated on studying how specific circuits behave under noise (Lipshtat et al., 2006; Cheng et al., 2008; Strasser et al., 2012; Weber and Buceta, 2013), not many have compared the effect of different types of noise (Tao et al., 2007; Morelli et al., 2008; Li and Li, 2008; Jaruszewicz and Lipniacki, 2013; Jaruszewicz et al., 2013; Caravagna et al., 2013), even less have compared differences of deterministically similar architectures under noise (Süel et al., 2006; Kittisopikul and Süel, 2010) and, to our knowledge, none have done a two-level comparison between the effects of different noise types on different circuit architectures. In chapter 3, we perform one such comparison, of five different motifs that can be assimilated to a Positive Feedback Loop and generate bistability, under noise coming from five different biochemical origins.

Rather than a general study of network motifs and other gene circuits that is then linked to specific functions, we can also approach them from specific realizations, i.e. by modelling small circuits that are found to do specific functions in biological systems, or by trying to find out which minimal circuit is responsible for a certain function. These specific circuits have been often studied in the context of cell decisions which, in multicellular organisms, often consist of cell type specification (Perkins and Swain, 2009; Graham et al., 2010; Garcia-Ojalvo and Martinez Arias, 2012). This study of specific circuits is complementary to the more general, theoretical approach, as focusing on actual biological circuits may clear up what parts of the theoretical studies are more biologically relevant, as well as bring to light unexpected aspects of the problems.

In the second part of results of this thesis we take this approach, studying a specific plant system. Not many of the examples of modelling of specific gene regulatory circuits are in plant biology (see for instance Jönsson et al. (2005); Cruz-Ramírez et al. (2012); Pokhilko et al. (2013)), despite the Stem Cell Niches of *Arabidopsis thaliana* (a very popular plant model) being a subject of intense experimental study (Aichinger et al., 2012). In chapters 4, 5 and 6 we tackle some aspects of the problem of the regulation of quiescence, a state of arrested progression of the cell cycle, of a group of stem cells in the root of *Arabidopsis thaliana*. A standing collaboration with the plant developmental biology group led by Dr. Ana I. Caño-Delgado at the Center for Research in Agricultural Genomics (CRAG) (CSIC-IRTA-UAB-UB) allows us to work with problems of biological significance that need a modelling approach to be more

completely solved. In particular, in Chapter 4 we bring together in a model the experimental results of our collaborators to predict the behaviour of a gene recently discovered by them to be regulating quiescence. In chapter 5 we extend this model to add another gene, and make new predictions.

There are not many studies of stochastic behaviour in plants yet (Walther et al., 2012; Meyer and Roeder, 2014), and some of these do not explicitly account for noisy dynamics but just consider probabilistic behaviour in cell decisions (Roeder et al., 2010). This is possibly because precise dynamical information, with resolution at the cellular level, is still not abundant enough. For this same reason, in chapter 6 we do a small study of the synchronization in the spontaneous division of slow-dividing Quiescent Centre that simply considers stochastic cell decisions phenomenologically, without considering the mechanism that generates them.

All these studies go in the direction of trying to understand both dynamics and function of small regulatory circuits in biology, from different perspectives, with the ultimate goal of unveiling some of the principles behind the functioning of living cells.

Part II

Noise in bistable gene circuits

Chapter 2

Autoactivating loop under intrinsic noise

In this chapter we begin our investigation on the effects of noise on positive feedback loops by studying the simplest loop possible, the self activation presented in the previous section, under the effects of the most obvious noise source, the intrinsic noise due to finite molecule number. To this end, we derive the stochastic model that accurately represents intrinsic noise, and compare it to a model that only has additive noise, which allows phenomenology such as stochastic switching but disables the specific features of our noise source. We also compare our results to experimental data on the stochastic phenomenon of stochastic switching, to see whether the properties of intrinsic noise are capable of explaining some of the particularities in the observations.

Most of the work presented in this chapter was published in the form of a research article in 2012 (Frigola et al., 2012).

2.1 The model

2.1.1 Deterministic description

We use the same simple chemical kinetic model that was presented in section 1.4 of the introduction. We take the deterministic equation there formulated for such a system, already reduced to dimensionless variables (equation (1.2)). The equation is, then

$$\frac{dx}{dt} = R + r\frac{x^n}{1+x^n} - x = -\frac{dU(x)}{dx}, \tag{2.1}$$

where

$$x = \frac{x_{dim}}{\sqrt[n]{K_d}}\ , \quad t = k_{deg}t_{dim},$$

$$r = \frac{r_{dim}}{k_{deg}\sqrt[n]{K_d}}\ , \quad R = \frac{R_{dim}}{k_{deg}\sqrt[n]{K_d}},$$

and $U(x) = \int_0^x \frac{dx}{dt}dx$ is the energy potential, which for $n = 2$ reads:

$$U(x) = r\,arctan(x) + \frac{x^2}{2} - (r+R)x. \tag{2.2}$$

This potential describes the evolution of the system after a perturbation, and when the system is bistable, it allows us to compute the energy barrier that needs to be overcome to escape from one stable state, over the unstable state, to the other stable state:

$$\Delta U = U(x^{unstable}) - U(x^{stable}) \tag{2.3}$$

This deterministic description is independent of the cell volume V. However, when this framework is related to stochastic kinetic reactions, the dependence on the cell volume becomes evident. We therefore need a value for V, as well as for all other parameters. We use the parameter values from Cheng et al. (2008), who previously studied this model with intrinsic noise: $K_d = 10$ nM^n, $R_{dim} = 0.4$ nM min^{-1}, $k_{deg} = 2$ min^{-1}, and $n = 2$. In order to satisfy $Vx = N$, where N is the number of molecules, then the dimensionless cell volume shall be $V = V_{dim}\frac{x_{dim}}{x} = V_{dim}\sqrt[n]{K_d}$,which, using the value $V_{dim} = 30$ nM^{-1}, is $V = 94.9$.

2.1.2 Stochastic description I: Multiplicative noise model

When the molecular species are present in small numbers, the stochasticity of chemical reactions becomes more evident and the deterministic description no longer describes accurately the real dynamics. A stochastic description is then required. Biochemical reactions can be described by birth-death processes governed by chemical Master equations (Kepler and Elston, 2001). To model the autoactivation circuit dynamics we have considered two one-step processes $N \to N+1$ and $N \to N-1$. The Master equation will then be (Gardiner, 2008):

$$\frac{\partial P(N,t)}{\partial t} = W_1(N-1)P(N-1,t) + \tag{2.4}$$
$$+W_2(N+1)P(N+1,t) - (W_1(N)+W_2(N))P(N,t),$$

where $P(N,t)$ is the probability distribution at time t. The transition probabilities per unit time are, as formulated in (Cheng et al., 2008):

$$W_1(N) = \left(R + r\frac{N^n}{N^n+V^n}\right)V, \tag{2.5}$$

$$W_2(N) = N. \tag{2.6}$$

N stands for the number of molecules and V for the nondimensional cell volume (properly adjusted for the dimension transformation described above). Rather than a full description of the biochemical system, this Master equation is a translation of the deterministic system where we consider the effective rates of production and degradation generated by all the underlying reactions.

Rewriting the Master equation with continuous variables (i.e. concentrations), the corresponding Fokker-Planck equation for the system can be (Bialek, 2000; Van Kampen, 2007)

$$\frac{\partial P(x,t)}{\partial t} = -\frac{\partial}{\partial x}A(x)P(x,t) + \frac{1}{2V}\frac{\partial^2}{\partial x^2}B(x)P(x,t), \tag{2.7}$$

$$A(x) = \frac{rx^2}{x^2+1} - x + R, \tag{2.8}$$

$$B(x) = \frac{rx^2}{x^2+1} + x + R, \tag{2.9}$$

where $P(x,t)$ is the probability of having a concentration x at time t. The Fokker-Planck equation is amenable to theoretical stochastic analysis. This equation can be readily solved in the stationary regime (Van Kampen, 2007), obtaining the steady state probability

$$P_s(x) = Ce^{-2V\phi(x)}, \tag{2.10}$$

where C is a normalization constant and $\phi(x)$ is the effective stochastic potential (as opposed to the deterministic potential in Eq (2.2))

$$\phi(x) = \frac{1}{2V}\ln\left(\frac{B(x)}{V}\right) - \int_0^x \frac{A(s)}{B(s)}ds. \tag{2.11}$$

For $A(x)$ and $B(x)$ as in equations (2.8) and (2.9), this stochastic potential has been studied in (Cheng et al., 2008).

An equivalent description to the Fokker-Planck equation, which provides actual individual stochastic trajectories as opposed to probability distributions, is the Langevin equation. The Langevin equation corresponding to Eq (2.7) in the Itô interpretation (Gardiner, 2008) is

$$\frac{dx}{dt} = A(x) + \sqrt{B(x)}\xi(t) \tag{2.12}$$

where $\xi(t)$ is a Gaussian white noise with

$$\langle\xi(t)\rangle = 0, \qquad \langle\xi(t)\xi(t')\rangle = \frac{1}{V}\delta(t-t'). \tag{2.13}$$

This corresponds to the so-called chemical Langevin equation (Gillespie, 2000). This description identifies $B(x)/V$ with the square power of the noise intensity. The noise becomes reduced as the cell volume V increases. For $V \to \infty$, we recover the deterministic description of Eq (2.1).

Notice that the noise term appears in the Langevin equation with a state-dependent term, $\sqrt{B(x)}$, multiplying it. Therefore, the intrinsic noise coming

from the biochemical reactions arises naturally in this equation as a multiplicative noise. Hereafter we refer to this dynamics (either in the Langevin, Fokker-Planck or Master equation description) as the multiplicative noise scenario.

The Langevin description enables the time-integration of the dynamics, obtaining simulated stochastic trajectories. The Gillespie algorithm also allows to simulate the time evolution of the number of molecules according to conditional probabilites related to the transition probabilities of the Master equation (Gillespie, 1977). In contrast with the Master equation description, the Langevin approach focuses on a continuous variable, the concentration of the molecular species.

2.1.3 Stochastic description II: Additive noise model

For comparison, we also studied the states and dynamics of a description that takes constant noise regardless of the protein concentration x. This corresponds to analyzing the autoactivation circuit in a thermal bath. It does not correspond to a description based on the stochastic chemical equations, and the noise term does not account for intrinsic fluctuations.

We constructed this dynamics from the Langevin equation by setting the deterministic dynamics plus a noise term which is state-independent:

$$\frac{dx}{dt} = A(x) + \sqrt{B_0}\xi(t), \tag{2.14}$$

with $\xi(t)$ as in Eq (2.13) and with $A(x)$ given by Eq (2.8). Notice that the difference with the multiplicative noise scenario (Eq (2.12)) relies on the use of B_0, a constant, instead of the function $B(x)$. Hereafter we call this approach the additive noise case, since the noise enters in an additive way. The stationary solutions and the bifurcation diagram for the average concentration $\langle x \rangle$ are the same as for the deterministic model.

The Fokker-Planck equation corresponding to the above Langevin equation (2.14) reads (Gardiner, 2008):

$$\frac{\partial P(x,t)}{\partial t} = -\frac{\partial}{\partial x}A(x)P(x,t) + \frac{B_0}{2V}\frac{\partial^2}{\partial x^2}P(x,t). \tag{2.15}$$

From this Fokker-Planck equation we can obtain the stochastic potential for the additive case, $\bar{U}(x)$

$$\bar{U}(x) = \frac{1}{2V} \ln\left(\frac{B_0}{V}\right) - \int_0^x \frac{A(s)}{B_0} ds = C_1 + C_2 U(x), \tag{2.16}$$

where $C_1 = \frac{1}{2V} \ln\left(\frac{B_0}{V}\right)$ and $C_2 = \frac{1}{B_0}$ are constant factors that only depend on B_0 and V i.e. on the noise intensity. These shift and scale factors are the only difference between $\bar{U}(x)$ and $U(x)$ (Eq (2.2)). Accordingly, the relative stability of the states provided by this function is the same as the one derived from the energy potential $U(x)$.

For a good comparison between the additive and multiplicative noise cases, we chose a value of B_0 such that the stochastic potential $\phi(x)$ and the potential $\bar{U}$ coincide at the OFF state value of the multiplicative noise dynamics. For each r, a B_0 value can be evaluated. However, we observed no significant differences if the same value of B_0 was used for all r values. Thus in all figures, unless indicated otherwise, we have used $B_0 = 0.09$ which corresponds to $r = 1.5$.

2.1.4 Mean First Passage Time (MFPT)

The MFPT gives the average time to switch from one state to another one. For the Fokker-Planck equation of Eq (2.7), the MFPT $T(x)$ satisfies the following differential equation (Gardiner, 2008),

$$A(x)\frac{\partial T(x)}{\partial x} + \frac{1}{2V} B(x) \frac{\partial^2 T(x)}{\partial x^2} = -1, \tag{2.17}$$

which can be solved with the proper boundary conditions: an absorbing boundary at the potential maximum separating both stable states and a reflecting boundary either at 0 or ∞ , depending on which transition is studied (Gardiner, 2008), where we define the OFF state as the one with lower $\langle x \rangle$, which

is always close to zero, and the ON state as the one with larger $\langle x \rangle$:

$$T_{OFF \to ON} = 2V \int_{x_{OFF}}^{x_{max}} \frac{dy}{\psi(y)} \int_{0}^{y} \frac{\psi(z)}{B(z)} dz, \tag{2.18}$$

$$T_{ON \to OFF} = 2V \int_{x_{max}}^{x_{ON}} \frac{dy}{\psi(y)} \int_{y}^{\infty} \frac{\psi(z)}{B(z)} dz, \tag{2.19}$$

where

$$\psi(x) = exp \left\{ \int_{x_0}^{x} \frac{2VA(x')}{B(x')} dx' \right\}. \tag{2.20}$$

with $x_0 = 0$ for the $OFF \to ON$ transition, and $x_0 = x_{max}$ for the $ON \to OFF$ transition.

The MFPTs (Eqs (2.18) and (2.19)) were computed both for the multiplicative noise case, with $A(x)$ and $B(x)$ given by Eqs (2.8) and (2.9), and for the additive noise case, with $A(x)$ given by Eq (2.8) and $B(x) = B_0$.

2.1.5 Numerical integration and simulations

Due to the difficulty of solving equations (2.18),(2.19) analitically, in particular in the multiplicative noise scenario, we have used different complementary (and, for additional certainty in the results, redundant) numerical strategies.

We computed stochastic trajectories of the system through two different methods. Langevin equations (2.12) and (2.14) have been simulated using an extension of Heun's method (García-Ojalvo and Sancho, 2012). Heun's method uses a predictor of the evolution of x,

$$\bar{x} = x(t) + f(x(t))\Delta t + g(x(t))\sqrt{\Delta t} Rnd. \tag{2.21}$$

Where Rnd is a number obtained from a random number generator that follows a gaussian distribution of mean zero and variance one, and that we generated using the method from (Toral and Chakrabarti, 1993). The formula for the final value of x is (Carrillo et al., 2003)

$$x(t+\Delta t) = x(t) + \frac{f(x(t)) + f(\bar{x})}{2}\Delta t + g(x(t))\sqrt{\Delta t}Rnd. \tag{2.22}$$

We also simulated the discrete system represented by the Master equation (2.4) (which only represents the multiplicative noise system) by using the Gillespie algorithm (Gillespie, 1977). This algorithm uses two uniformly distributed random numbers at each step to exactly reproduce a statistically correct time evolution of the discrete stochastic variables, that follows the same distribution as the Master equation. To do this, it chooses the time of the next reaction according to an exponential distribution the parameter of which is related to the total probability per unit time that a reaction (or change in the system) happens, and which next reaction happens proportionally to the probability of each of them.

These two methods were used both to compute the steady states and their fluctuations, and to compute the MFPTs. To compute the states and their fluctuations, we computed $500 \leq N \leq 1000$ trajectories of the system with initial conditions normally distributed around each deterministic stable state for a time $t = 100$, pruning those that crossed the unstable state into the opposing stable state, and computed the statistics on the final state of every trajectory, both for the Langevin and Gillespie dynamics. To compute the MFPTs, $100 \leq N \leq 500$ trajectories were initiated also around each of the deterministic stable states. To be consistent with the theoretical definition of MFPTs, we stopped each trajectory when it reaches the the unstable state, and saved this time as its First Passage Time. In the case of Langevin dynamics, we took $\delta t = 5.0 \times 10^{-3}$.

Finally, we also numerically integrated MFPTs from their theoretical expressions (2.18),(2.19) and the steady state probability distributions from expression (2.10) (combined with the potentials (2.11) and (2.16)) repeatedly using a Romberg algorithm (Press et al., 1993), with tolerance $\varepsilon = 10^{-6}$, initial number of subintervals $n_0 = 100$ and maximum iterations of trapezoidal estimates $7 < n_{max} < 10$, depending on the integral.

2.2 Results

2.2.1 Bistability

As explained in section 1.4 of the Introduction, it is well known that positive feedback loops formed by autoactivation exhibit bistability. Specifically, both the deterministic and stochastic models presented in subsections 2.1.1, 2.1.2 and 2.1.3 have been shown to have a bistable regime (Becskei et al., 2001; Cheng et al., 2008). However, no detailed comparison of both descriptions had been performed at the time of doing this work, as far as we know. In this section we are interested in evaluating the effect of intrinsic fluctuations in the steady states. Accordingly, we compare the bifurcation diagrams for the stochastic multiplicative noise and for the deterministic models. From a biophysical point of view, by doing so we are comparing the features of the same autoactivation circuit in two cells with very different volumes. The autoactivation circuit in the cell with a small volume would be described by the stochastic multiplicative noise model, whereas it would be well approximated by the deterministic description in the cell with a very (extremely) large volume.

The bifurcation diagram for the control parameter r, related to the maximal molecular production rate, is shown in Fig. 2.1. The steady state solutions of the bifurcation diagram have been obtained by computing numerically (Mathematica Software (Wolfram Research, 2010)) the minima and maxima of the potentials, Eqs (2.2) and (2.11), for the deterministic and stochastic multiplicative noise models. The results for the deterministric model are the same as those shown in Figure 1.2 but are repeated here for comparison with those of the intrinsic noise case. As it is shown, both descriptions show a very similar bifurcation diagram with a bistable regime for intermediate values of r in which two stable states, a low-concentration state (OFF) and a high-concentration (ON) state, can coexist. The steady state concentrations are very similar in the two descriptions. A difference between the bifurcation diagrams is an enlargement of the bistability region for the stochastic multiplicative noise model. However, when stochastic switching between the states is taken into account, this enlargement becomes not relevant for the parameters here used, and it has been shown that for this region it is extremely easy to escape from the OFF state and to switch (irreversibly, for very long time scales) to the ON state (Cheng et al., 2008). Hence, bistability is not expected to be observed in this

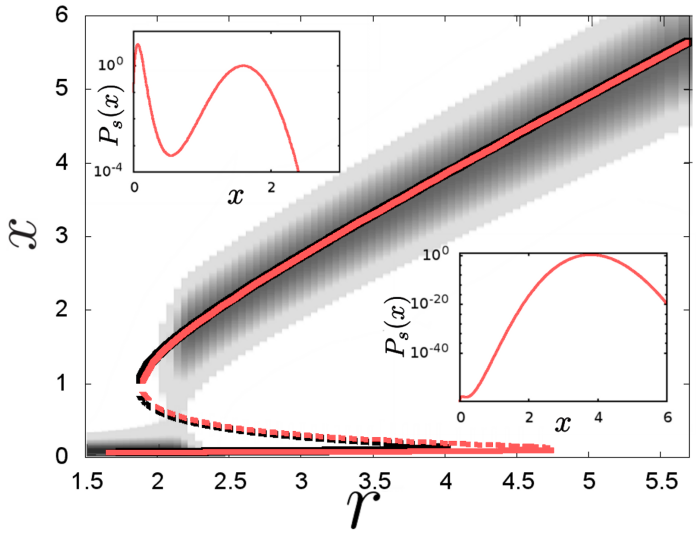

Figure 2.1 Steady state values do not change significantly when intrinsic noise is included. Bifurcation diagram for the deterministic model (black) and the multiplicative noise model (gray, light red in digital version). Stable steady states (continuous lines) and unstable steady states (dashed lines) are minima and maxima, respectively, of the potentials. The bifurcation diagram of a stochastic description with a thermal bath (additive noise) is necessarily the same as the one of the deterministic model. The stationary probability distribution for the multiplicative noise model, Eq (2.10), for different r values is shown in grey scale. Insets: Stationary probability distributions for the multiplicative noise model for $r = 2.15$ (top) and $r = 4.00$ (bottom). Figure adapted from (Frigola et al., 2012). In color in digital version.

region, precluding the observation of differences between the deterministic and the stochastic descriptions (compare insets in Fig. 2.1). In fact, bistability is especially obvious in a narrow region ($r \approx 2$, see grey areas in the figure). However, a more general study of this effect done by others (Weber and Buceta, 2013) has shown that, while the steady state concentrations may not change much in the common bistable region of the deterministic and stochastic systems, this enlargement of the bistable region due to intrinsic noise can be larger than we show here and, more importantly, it can be relevant in the sense that the states can be stable enough against stochastic switching that they are expected to be observable.

2.2.2 Fluctuations

Intrinsic stochasticity of the biochemical reactions of the autoactivation circuit result in state-dependent multiplicative noise (see section 2.1.2, (Cheng et al., 2008)). Fluctuations are expected to be larger in the ON state than in the OFF state (Fig. 2.2A) because the noise intensity increases with the concentration according to the function $B(x)$ (Eq (2.9)). Since dynamics such as MFPTs depend on absolute fluctuations we have computed the standard deviation of concentrations in each stable steady state.

We can approximate these fluctuations by doing a linear approximation of the steady state. If we define a new variable for the system

$$x = x^{st} + \delta x, \tag{2.23}$$

where x^{st} is the deterministic steady state, such that $A(x^{st}) = 0$, and we expand $A(x)$ and $B(x)$ around x^{st} to their first nonzero terms, the Fokker-Planck equation (2.7) becomes (Van Kampen, 2007)

$$\frac{\partial P(\delta x,t)}{\partial t} = -A'(x^{st})\frac{\partial}{\partial \delta x}\delta x P(\delta x,t) + \frac{1}{2V}B(x^{st})\frac{\partial^2 P(\delta x,t)}{\partial \delta x^2}, \tag{2.24}$$

where $A'(x)$ stands for $A'(x) = \frac{dA(x)}{dt}$. Then, it can be shown that the intensity of the fluctuations, represented by the variance, is (Van Kampen, 2007)

$$\langle \delta x^2\rangle - \langle \delta x\rangle^2 = \langle \delta x^2\rangle = \frac{1}{2V}\frac{B(x^{st})}{-A'(x^{st})} = \frac{1}{2V}\frac{B(x^{st})}{1-\frac{2rx^{st}}{({x^{st}}^2+1)^2}}. \tag{2.25}$$

The denominator of this expression does not vary much for our values of x^{st}, except very close to the bifurcation points, where $\langle \delta x^2\rangle$ diverges. Due to this, the fluctuations $\sigma = \sqrt{\langle \delta x^2\rangle}$ mostly follow $B(x^{st})$ and, since it is a monotonically increasing function, the fluctuations will be larger in the ON state than in the OFF state (save for a very small region near one of the bifurcation points). Indeed, numerical simulations of the stochastic multiplicative noise dynamics corroborate that absolute fluctuations are larger in the ON state than in the OFF state (Fig. 2.2B).

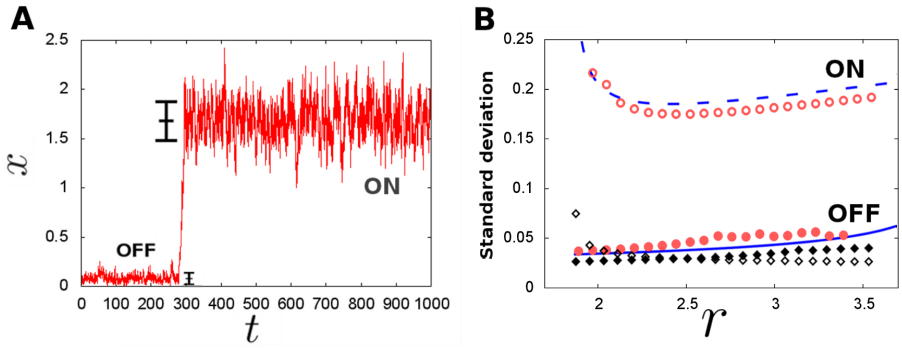

Figure 2.2 Intrinsic multiplicative noise drives larger absolute fluctuations in the ON state. **A** Time evolution of the concentration x for $r = 2.18$. Error bars denote the fluctuations size in each state, which is much higher in the ON state. **B** Fluctuations in the OFF steady state (filled symbols and solid line) and in the ON steady state (empty symbols and dashed line) for the multiplicative noise model (grey symbols, light red in digital version), its linear approximation from Eq (2.25) (blue lines) and for the additive noise model (black symbols). Fluctuations are measured as the standard deviation from the steady state. For the multiplicative noise model, fluctuations in the ON state are larger than in the OFF state. For the additive noise model, fluctuations in the OFF and ON states are similar. Standard deviations have been computed over samples of sizes ranging from 100 to 1000 repetitions of the corresponding Langevin dynamics at time t=100. For the additive noise model, B_0 has been recalculated for each point. However, the results are qualitatively identical to those with a constant B_0. Figure adapted from (Frigola et al., 2012), where theoretical lines of panel B have been added. In color in digital version.

The coefficient of variation (*i.e.* relative fluctuations, defined as the standard deviation over the mean) is larger in the OFF state and slowly decreases for larger volumes (see Table 2.1) (Paulsson, 2004), in agreement to the linear approximation which states that $\frac{\sigma}{x^{st}}$ scales with $\frac{1}{\sqrt{V}}$ (from Eq (2.25)). According to the linear approximation the ratio of the coefficients of variation should stay constant when changing volume, since both coefficients scale equally. However, simulations show that it very slowly decreases as volume increases. This effect is small, and the larger coefficient of variation in the OFF state is still preserved. In any case, it is important to notice that the coefficient of variation is not the relevant magnitude in our analysis as we will show below.

Fluctuations in an energy potential well depend on the shape of the potential.

	OFF	ON	OFF/ON
$V = 94.9$	0.474	0.131	3.62
$V = 474.5$	0.208	0.062	3.33

Table 2.1 The ratio between fluctuactions in the OFF and ON states is mantained at larger volumes. Relative fluctuations in each steady state for two different nondimensional cell volumes V for $r = 2.13$ for the multiplicative noise model. Relative fluctuations have been computed as the ratio between the standard deviation over the mean steady state. Standard deviations and mean values have been extracted from Langevin dynamics as in Fig. 2. As shown, relative fluctuations decrease with cell volume, but are always larger in the OFF state. The ratio between the relative fluctuations in the two states is indicated in the last column. This ratio is little sensitive to the cell volume, staying close to the theoretical value of 3.77 (from eq. (2.25)) for this r.

Since the energy potential corresponding to autoactivation dynamics is asymmetric, we can expect the ON and OFF states to exhibit different standard deviations even if the noise intensity is the same in both cases. To corroborate that the differences in standard deviation observed in Fig. 2.2B are driven by intrinsic noise and are not just the result of an asymmetric energy potential, we computed the standard deviation for each steady state for the additive noise model, in which noise stands for a thermal bath and not for intrinsic fluctuations. In this additive noise model, the noise intensity is the same for all states and the dynamics are subjected to the energy potential of autoactivation. As shown in Fig. 2.2B, fluctuations in the additive noise model are very similar in the OFF and ON states. This result indicates that the asymmetry of the energy potential does not drive a significant difference in the fluctuations around each steady state, and thus is not responsible for the large differences observed in the multiplicative noise model with intrinsic noise.

Altogether we have shown that intrinsic noise in the positive feedback loop of autoactivation creates larger absolute fluctuations in the ON state than in the OFF state.

2.2.3 Stochastic switching

Stochastic switching dynamics depend on the energy potential and on fluctuations. Since intrinsic noise drives different fluctuations in the ON and OFF states we may expect different switching dynamics from each state. To evaluate the role of intrinsic noise on the switching dynamics, we measured the escape or switching rates as the inverse of the MFPT (section 2.1.4) for the multiplicative noise dynamics. When plotting these rates as a function of the energy barrier (Eq (2.3)), we see that the switching becomes asymmetric: for the same energy barrier height, it is more probable to switch from the ON state than from the OFF state (Fig. 2.3A).

To corroborate whether this asymmetry is driven by intrinsic noise, we measured the escape rates for the additive noise model. For this model, the asymmetric effect is absent (Fig. 2.3B). Together, our results show that state-dependent intrinsic noise in autoactivation dynamics drive an asymmetric switching.

Importantly, the differences in fluctuations among the ON/OFF states arising from intrinsic noise are preserved for different cell volumes and are little sensitive to changes in the cell volume (Table 1). Hence, we can expect that the phenomenology of asymmetric switching rates holds for a wide range of cell volumes. Fig. 2.4 shows this is indeed the case. For larger cell volumes the switching rates decrease overall (since the switch becomes more stable (Bialek, 2000)), but they still show a similar relative asymmetry. It is still more probable to switch from the ON state than from the OFF state for equal energy barrier height values. This result stresses the importance of intrinsic fluctuations at a fundamental level.

The asymmetry can be also observed by analyzing the behaviour of the value of r at which the switching rates from the OFF states and from the ON states are the same. This value is larger when intrinsic noise is taken into account than when only additive noise is present ($r_c^{add} = 1.99$, $r_c^{mult} = 2.16$, see Fig. 2.5). This shift indicates that intrinsic fluctuations enlarge the region of values of the control parameter r for which it is less frequent to switch from the OFF state than from the ON state.

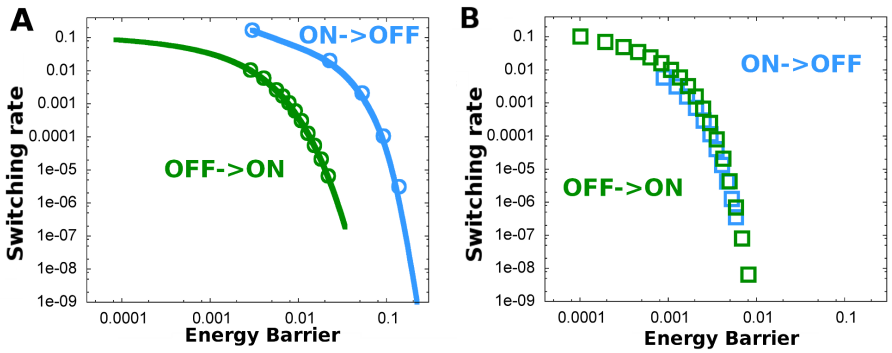

Figure 2.3 Intrinsic multiplicative noise generates an asymmetry in switching rates. A Switching rate versus energy barrier for the stochastic system with intrinsic multiplicative noise. The lines represent the values obtained through theoretical MFPT calculations, Eq (2.17), and the circles represent the values obtained through simulation (Gillespie and Langevin are identical). In both panels, the energy barriers were calculated from Eq (2.2). Light grey color (blue in digital version) corresponds to switching from ON to OFF and dark grey color (green in digital version) corresponds to OFF to ON switching. **B** Switching rate versus energy barrier for the additive noise case. Notice how the rates for both states keep the same relation with the energy barriers. Colour code is as in previous panel. Symbols correspond to theoretical MFPT calculations. Simulations are in perfect agreement, but are not represented for clarity. In both panels, the nondimensional cell volume is $V = 94.9$. Figure adapted from (Frigola et al., 2012). In color in digital version.

This shift is preserved even at larger volumes: when the volume is increased 5-fold, the region still remains enlarged. r_c shifts a little, but still stays far away from the value for the additive noise system (Fig. 2.6).

Our results show that intrinsic fluctuations in autoactivation dynamics introduce a state-dependent noise which consistently drives larger absolute fluctuations in the ON state and elicit a faster switching rate from this state than from the OFF state for the same energy barrier height.

2.2.4 Stochastic potential

We compared the stochastic potential of the multiplicative noise model Eq (2.11) with the energy potential Eq (2.16). Note we used Eq (2.16) which is, up to scale and shift factors, the deterministic energy potential Eq (2.2).

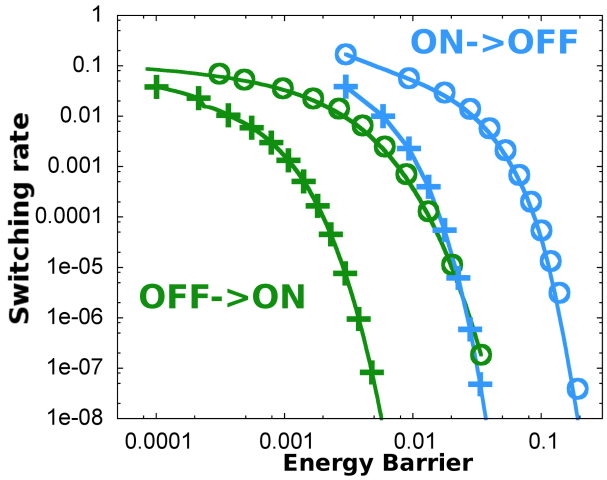

Figure 2.4 The asymmetry of switching rates does not disappear at larger volumes. Switching rates for different cell volumes as a function of the energy barrier. Switching rates (computed from Eq (2.17)) of the stochastic system with intrinsic multiplicative noise for an adimensonal cell volume $V = 94.9$ (circles) and for a larger volume $V = 5 \times 94.9$ (crosses). Light grey color (blue in digital version) corresponds to ON to OFF switching and dark grey color (green in digital version) corresponds to OFF to ON switching. The asymmetry of the switching rates is observed for both volumes. Figure adapted from (Frigola et al., 2012). In color in digital version.

The two potentials are shown in Fig. 2.7. The stochastic potential for the multiplicative noise scenario has been previously reported in (Cheng et al., 2008). As shown in Fig.2.7, the multiplicative noise affects drastically the ON state, reducing the barrier height and decreasing the curvature of the potential at the ON state. Moreover, the fact that the well potential in the ON state becomes flattened due to the intrinsic multiplicative noise implies larger fluctuations in the copy number which, in turn, will induce faster transitions. These two changes favor the transition rate from the ON state to the OFF one, thus reducing the stability of the ON state.

These results show that intrinsic fluctuations from finite molecule numbers can drive large changes in a positive feedback loop based on autoactivation which could reduce the differences in the stability of the steady states. Hence, the

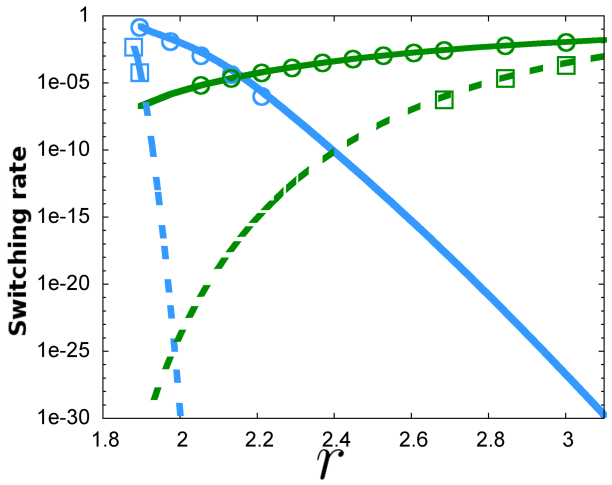

Figure 2.5 Intrinsic multiplicative noise increases the domain where the OFF state predominates. Switching rates for stochastic transitions from ON to OFF (light grey, blue in digital version) and viceversa (dark grey, green in digital) for the additive (dashed lines) and for the multiplicative (continuous lines) systems, computed from Eq (2.17). The critical value r_c at which the switching rates for the two transitions are equal is shifted from $r_c^{add} = 1.99$ in the additive case to $r_c^{mult} = 2.16$ for the multiplicative noise scenario. Results for Langevin simulations of the additive noise model (squares) and for Gillespie simulations of the multiplicative noise model (circles) are depicted. For the multiplicative noise case, the dimensional MFPT as a function of the dimensional maximal production rate of the autoactivation r_{dim} was previously reported by Cheng et al. (2008), with our results in agreement with them. Figure adapted from (Frigola et al., 2012). In color in digital version.

relative stability of the bistable states is a dynamical phenomenon which is very sensitive to the noise characteristics.

2.3 Discussion

We have presented a theoretical and numerical analysis of the role of intrinsic noise in a bistable switch with autoactivation dynamics. Our theoretical approach is consistent and independent of a particular scenario either using Master or Langevin equations, and is complemented with numerical integrations and stochastic simulations. Our results exemplify that intrinsic noise in

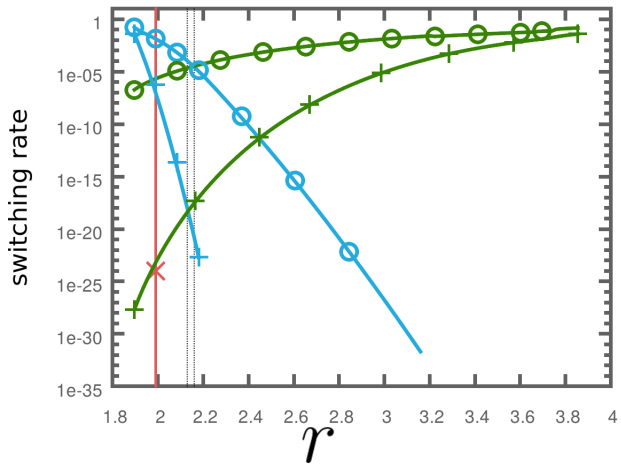

Figure 2.6 At larger volumes the increased domain where the OFF state predominates is preserved. Switching rates for stochastic transitions from ON to OFF (light grey, blue in digital version) and viceversa (dark grey, green in digital) the multiplicative system with adimensional cell volumes $V = 94.9$ (circles) and $V = 5 \times 94.9$ (crosses). We see how r_c shifts from $r_c^{V0} = 2.16$ to $r_c^{Vx5} = 2.13$ (marked with dashed lines), but still stays far away from the critcal value for the additive noise scenario, $r_c^{add} = 1.99$ (marked with red continuous line). The red cross marks the point at which the lines for the additive system in Fig. 2.5 cross. Symbols are only guides to distinguish different curves, all data from numerical integration of equations (2.18) and (2.19). In color in digital version.

autoactivation dynamics, which result in multiplicative noise (state-dependent fluctuations), are a relevant ingredient for the dynamics. Specifically, while in the conditions of our study the bifurcation diagram is mostly unchanged when intrinsic noise is taken into account, the switching dynamics and the relative stability of the states are very sensitive to state-dependent fluctuations.

It has been previously shown that noise can be different in the ON and OFF states of feedforward loop genetic circuits (Kittisopikul and Süel, 2010). For a genetic circuit involving positive and negative feedbacks it also has been shown that intrinsic noise can stabilize a deterministically unstable state (Turcotte et al., 2008). Herein, we show that intrinsic noise in autoactivation dynamics makes the ON state less stable. Specifically, intrinsic noise drives larger absolute fluctuations in the ON state which elicit a faster switching rate from this state than from the OFF state for the same energy barrier height. Remarkably,

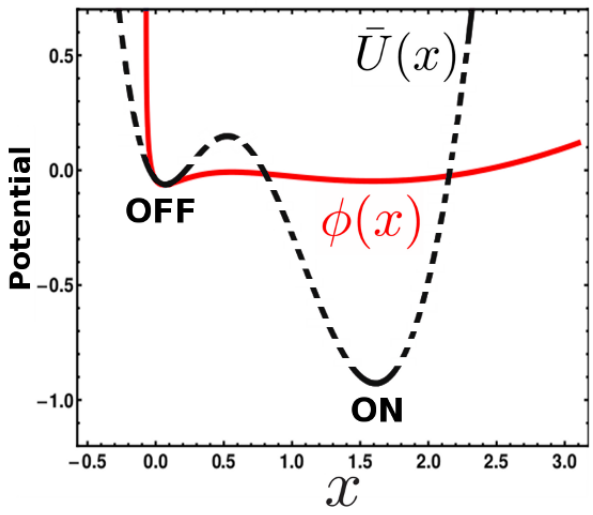

Figure 2.7 Intrinsic multiplicative noise changes the relative stability of the ON state. Stochastic potential of the additive noise model (black dashed line, Eq (2.16)) and of the multiplicative noise scenario (red continuous line, Eq (2.11)) for $r = 2.15$. As shown, the ON state is clearly destabilized by multiplicative noise. This is also observed for different values of r. Figure from (Frigola et al., 2012). In color in digital version.

this phenomenology holds for different cell volumes, and accordingly for different noise intensities. We have termed this phenomenon asymmetric stochastic switching.

Asymmetric stochastic switching has been observed in the gallactose signalling network in yeast (Acar et al., 2005). In this network, a positive feedback loop involving the cytoplasmic molecule Gal3p drives bistability of low (OFF) and high (ON) pathway activity states in which GAL3 expression is low and high respectively (Acar et al., 2005). For a specific parameter regime, yeast cells can switch spontaneously and stochastically between these states during the time period being analyzed. When comparing the switching rates from each (OFF/ON) state for the same value of the energy barrier height, Acar et al. obtained that it is more probable to switch from the ON to the OFF state than viceversa (Acar et al., 2005) (Figure 2.8), similarly to our own results (Figure 2.3). Moreover, they measured the fluctuations of GAL3 expression in each state and concluded that fluctuations are larger in the ON state than in the OFF state

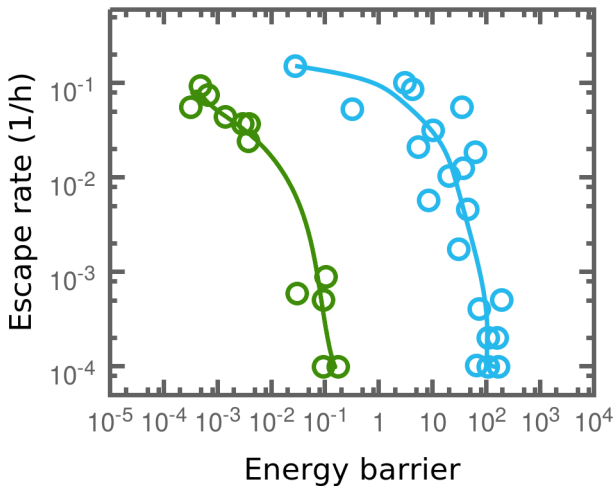

Figure 2.8 Experimentally observed switching rates are also asymmetric Experimental data vs modeled potential barrier extracted from (Acar et al., 2005). The results are qualitatively similar to ours, showing a similar asymmetry in the same direction. As in previous figures, light grey (blue in digital version) color corresponds to switching from ON to OFF and dark grey (green in digital) color corresponds to OFF to ON switching. Circles are experimental data, and lines are only guides to the eye. All datapoints were extracted from (Acar et al., 2005). In color in digital version.

(Acar et al., 2005). These two features, larger probability of switching from the ON state and larger fluctuations in the ON state, are analogous to the ones we obtain by theoretical and numerical means for the stochastic autoactivation switch with intrinsic noise (Fig. 2.9).

It remains to be elucidated which noise sources are present in this experimental system and how they are coupled with the specific circuit topology of the gallactose signalling network. Our results suggest that, for states where the amounts of protein are very distinct, intrinsic noise can be sufficient to drive asymmetric switching between them.

Together, our study explains that although the bistability phenomenon is rather independent of the noise characteristics, the relative stability of each state and stochastic switching dynamics are dynamical features very sensitive to the kind of noise: additive or multiplicative. A simplistic approach with an additive

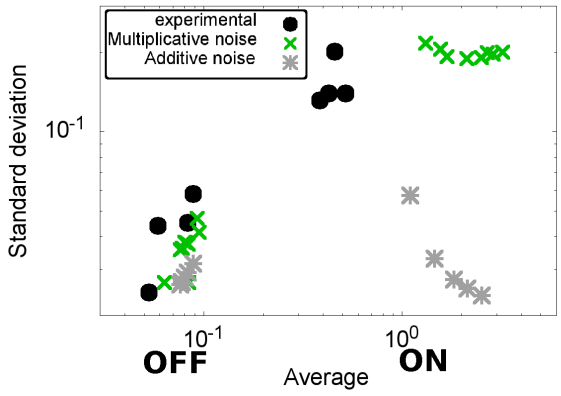

Figure 2.9 Intrinsic noise drives larger fluctuations in the ON state in agreement with experiments Larger fluctuations in ON state are seen experimentally (black dots), an effect that is reproduced when including intrinsic noise in the model (green crosses) but not with additive noise (grey stars). Experimental points extracted from (Acar et al., 2005). In color in digital version.

noise can not address all the possible phenomenologies and one has to resort to carefully considering noise as an intrinsic part of the system, which is relevant at a fundamental level and not as a correction.

Chapter 3

Noise sources and positive feedback loop architecture

3.1 Introduction

As shown in the Introduction and in Chapter 2, fluctuations have been known to be both beneficial and detrimental to biological systems. In particular, when they affect a bistable system, they have been experimentally shown to enable stochastic switching (Acar et al., 2005) and population heterogeneity (Dubnau and Losick, 2006). Both these effects have been theorized but also experimentally supported to be beneficial to the cell (Acar et al., 2008; Veening et al., 2008). On a more theoretical level, noise in biochemical systems has been shown to enhance the bistability range of positive feedback loops (Weber and Buceta, 2013) and even enable bistability in deterministically monostable systems (To and Maheshri, 2010; Strasser et al., 2012), results that had been shown in generic contexts much earlier (Horsthemke and Lefever, 1984) but not in genetic circuits. Furthermore, in genetic circuits these effects have been theoretically shown to depend on the specific origin of the noise: be it noise due to low molecule numbers, gene state switching, or noise due to the timescales involved in specific chemical reactions (such as dimerization or protein-gene binding and unbinding) (Jaruszewicz et al., 2013; Jaruszewicz and Lipniacki, 2013).

On the other hand, noise is known to interact with genetic circuit architecture in such a way that it generates different functions on otherwise equivalent circuits (Süel et al., 2006), going as far as allowing for classifications that are entirely different to the deterministic, classical ones (Kittisopikul and Süel, 2010).

Herein we do an extensive comparison of the effect of different noise types on different circuits that enable bistability. In particular we consider the motifs that are most recurrent in generation of bistability: different simple architectures that lead to a transcriptional Positive Feedback Loop (Autoactivation, Mutual activation and Mutual inhibition), which are known to generate bistability when the transcriptional regulations are nonlinear enough. Beyond these, we consider other topologies that have also been shown to be capable of bistability through a mechanism that, in the end, is also a feedback coupled to a strong enough nonlinearity. In this case, however, both the nonlinearity and part of the feedback come from a post-transcriptional interaction in the form of molecular titration (François and Hakim, 2004; Buchler and Louis, 2008). These circuits have two proteins X and Y that form a complex that is degraded, and achieve bistability through two different transcriptional interactions: the AutoActivation with Complex (AAC) has a transcriptional activation of protein X by itself that, importantly, is linear, whereas the Mixed Feedback Loop (MFL) has a transcriptional repression of protein X by protein Y that is again linear. The MFL has been shown to be over-represented in statistical analyses of gene-protein interaction databases (Yeger-Lotem and Margalit, 2003; François and Hakim, 2005). A summary of all the circuits can be found in Figure 3.1.

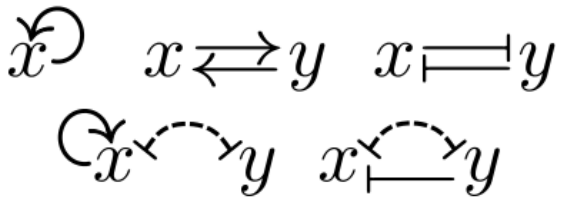

Figure 3.1 Schematic representation of the five circuits studied in this chapter. Top row: Autoactivation, Mutual Activation, Mutual Inhibition. Bottom row: Autoactivation with Complex and Mixed Feedback Loop. Pointed arrows represent activations and blunted arrows repressions. Continuous lines are transcriptional interactions and dashed lines are post-transcriptional interactions.

3.2 Model and noise sources

To be able to represent different noise sources, we built a model in which DNA can be in one of three states: *off*, *on*, or TF-bound (Figure 3.2). In the *off* (inactive) state, the promoter has no transcriptional activity. In the *on* state, transcription occurs at a basal level r, and in the TF-bound state, the transcription rate is ε times the basal one.

The promoter can switch from *off* to *on* and back at constant rates (k_{on},k_{off}). We termed this gene switching, and it represents different biological processes such as chromatin remodelling or necessary activation by a third protein that does otherwise not participate in our small network. When the promoter is in the *on* state, the molecule TF (for Transcription Factor, representing whichever molecule is doing the transcriptional regulation) can bind to it with a rate proportional to the concentration of TF ($k_+ \times TF$), and unbind from the TF-bound state at a constant rate (k_-). We have called this reaction protein-promoter binding. Transitions from the *off* to the TF-bound state and back are forbidden: the promoter must be *on* for TF to bind to it (Figure 3.2).

Notice that gene switching and protein-promoter binding can and oftentimes have been lumped in a single process, if the transcriptional regulation completely enables or disables promoter activity (Morelli et al., 2008; Jaruszewicz et al., 2013). In our case, however, they are separate and give rise to two different noise sources: one affects whether the promoter is active at all, and the other one affects the regulatory feedback.

The transcriptional activity from the *on* and the TF-bound promoter produces mRNA molecules m at rates r and εr respectively. These mRNA molecules can degrade with a rate d_m. Protein molecules X are translated from mRNA with a rate t_x, and also degrade with rate d_x (Figure 3.2). As explained later in the text, the inclusion of explicit mRNA gives rise to a specific noise source.

The transition probabilities per unit time for all these reactions, as they would be implemented in the corresponding Master Equations or in the Gillespie algorithm are

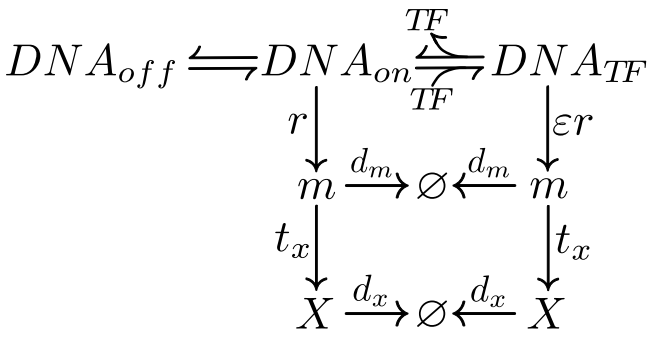

Figure 3.2 DNA regulation and gene expression model. The promoter (represented here as 'DNA') has an off state with no activity, which transitions to an on state and back with constant rates k_{on},k_{off}. In the on state, mRNA is expressed with rate r. When the promoter is in this state, a transcription factor TF can bind an unbind to it with rates k_+,k_-. The promoter with the transcription factor bound to it has a transcription rate εr. mRNA is always translated into protein at the same rate t_x. Both mRNA and protein are degraded with linear rates d_m and d_x respectively.

$$
\begin{aligned}
&W(DNA_{off} \to DNA_{on}) = k_{on} \\
&W(DNA_{on} \to DNA_{off}) = k_{off} \\
&W(DNA_{on} \to DNA_{TF};\, TF \to TF - 1) = k_+ \times TF \\
&W(DNA_{TF} \to DNA_{on};\, TF \to TF + 1) = k_- \\
&W(m \to m + 1) = r \times DNA_{on} + \varepsilon r \times DNA_{TF} \\
&W(X \to X + 1) = t_x \times m \\
&W(m \to m - 1) = d_m \times m \\
&W(X \to X - 1) = d_x \times X
\end{aligned}
\tag{3.1}
$$

Where DNA represents the promoter and its states, and between parenthesis for each reaction (i.e. transition) is the change in the system it produces. The cross $\times$ represents multiplication. This is the generic case that applies for all 5 systems and is shown in Figure 3.2. For Mutual Activation, Mutual Inhibition, AAC and MFL, there is a second promoter for protein Y, with equivalent reactions and transition probabilities. Furthermore, all systems have additional dimerization reactions. Autoactivation, Mutual Activation and Mutual Inhibition have a homodimerization reaction, with transition probabilities per unit time

$$W(X \to X-2;\, X_2 \to X_2+1) = k_{D+} \times X \times (X-1) \qquad (3.2)$$
$$W(X_2 \to X_2-1;\, X \to X+2) = k_{D-} \times X_2$$

In these cases, the dimer does the function TF. In Autoactivation X_2 regulates the promoter of X, whereas in Mutual Activation and Mutual Inhibition X_2 regulates the promoter of Y and vice versa.

The dimerization in AAC and MFL is different. In these cases, proteins X and Y form a heterodimer C (for 'complex') that degrades, providing additional nonlinearity that enables bistability. The transition probabilities per unit time for these are

$$W(X \to X-1;\, Y \to Y-1;\, C \to C+1) = k_{D+} \times X \times Y$$
$$W(C \to C-1;\, X \to X+1;\, Y \to Y+1) = k_{D-} \times C \qquad (3.3)$$
$$W(C \to C-1) = d_C \times C$$

This C does not perform the function of TF in these cases. Instead, in AAC the TF that regulates X is protein X itself (in monomeric form), and in the MFL the TF that regulates X is a monomer of Y. In both cases, protein Y is not transcriptionally regulated, and thus its promoter does not have access to the TF-bound state.

3.2.1 Noise sources

All these reactions give rise to different noise sources. The intensity of each noise is defined to be proportional to a parameter or parameters of the system. The exact dependence of this is unclear, and also unimportant: in all our analysis, we define a reference point and study noise as it varies from this reference point. Furthermore, we vary parameters with the constraint that the deterministic solutions of the system do not change. This usually means that equilibrium constants for each reaction are fixed.

The first noise sources have already been introduced in the previous section. They are the noises coming from the discrete states of DNA: gene switching and protein-promoter binding. We define, *a priori*, the noise arising from these sources as the inverse of their rate, either forward or backward, both are equivalent since they are changed together to keep the equilibrium constant (k_{on}, k_{off} for gene switching and k_+,k_- for protein-promoter binding). This is supported by previous studies (Morelli et al., 2008; Jaruszewicz et al., 2013), as well as by the reasoning that faster reactions are closer to an adiabatic approximation.

We have also considered the noise of the dimerization reaction. This is only possible in the states with cooperative transcriptional regulation (Autoactivation, Mutual Activation and Mutual Inhibition). With the same reasoning as in the case of DNA state changes, and also supported by previous studies (Jaruszewicz et al., 2013), we *a priori* consider this noise to be inversely proportional to the speed of the reactions k_{D+} and k_{D-}. In Autoactivation with Complex and Mixed Feedback Loop, since the Complex C degrades, the equilibrium solutions will change when k_{D+} and k_{D-} are varied, even if their ratio $K_D = \frac{k_{D+}}{k_{D-}}$ is kept constant (because the equilibrium of C depends on X and Y as $C = \frac{k_{D+}XY}{k_{D-}+d_C}$). Furthermore, in these systems C acts as a sink in a competetive degradation, so it is not trivial to change d_C and leave the deterministic system unchanged. For these reasons, we do not consider this noise source for these two systems.

The inclusion of separate mRNA and protein dynamics in our model also allows us to observe noise effects that may arise from this separation, such as bursting. In the last ten years, the burstiness of gene expression has been shown to be a very relevant source of biological noise, and a dominant mode of gene expression (Dar et al., 2012). Both mRNA and proteins can be expressed in bursts. Transcriptional bursting (i.e. mRNA expressed in bursts) only happens when gene switching is present and is slower than the degradation of mRNA (Golding et al., 2005; Munsky et al., 2012). Translational bursting (i.e. protein expressed in bursts) happens when the amount of mRNA molecules is very low and fluctuating (usually averaging less than 1) but several protein copies are expressed from each mRNA molecule (Ozbudak et al., 2002; Friedman et al., 2006; Raj and van Oudenaarden, 2008; Weber and Buceta, 2011). Both can and have been experimentally deduced to coexist in prokaryotes and eukaryotes (Golding et al., 2005; Raj and van Oudenaarden, 2008). As such, in our model we consider a joint noise source that we term simply 'bursting'. This is

proportional to the degradation rate of mRNA d_m, which generates a bursty mRNA transcription. But it will be also proportional to protein translation t_x, which will be varied equally so that the average protein levels do not change. At higher d_m, mRNA levels are lower, generating also a more bursty protein expression.

Lastly, we consider a more classical noise source, that is already studied in Chapter 2 of this thesis. This is volume (or 'finite molecule number'), that is known to scale intrinsic noise. This has oftentimes been considered as 'transcriptional noise' in literature (Jaruszewicz et al., 2013; Jaruszewicz and Lipniacki, 2013). Notice that although volume V does not appear in the transition probabilities (3.1) (3.2) and (3.3), the values of the parameters are properly rescaled so that the steady state numbers of molecules scale with volume (Table 3.1). This volume noise corresponds, in a way, with changing many noise sources at the same time: by increasing the number of molecules and keeping concentrations constant we are increasing the frequency of many reactions (even of those such as dimerization, which when working with numbers of molecules instead of concentrations have a rate divided by volume, because such scaling is precisely to keep the transition probabilities with dimensions of molecules/time: k_{D+} is scaled by V so that $W(X \to X-2; X_2 \to X_2+1) = k_{D+} \times X \times (X-1) = X \times (X-1) \times \frac{k'_{D+}}{V} \propto X$). For this reason we do not use the naming convention of 'transcriptional noise'.

All in all, we have five possible noise sources: Gene switching, protein-promoter binding, dimerization, bursting and volume.

Parameters were chosen so that there are two states with comparable stability (measured in terms of the Mean First Passage Time to escape each state), and so that many timescales are similar in many systems, as can be seen in table 3.1. AAC and MFL are based on the parameters from (François and Hakim, 2004). In all cases parameters have been chosen within biologically meaningful ranges (for a concise but complete summary of biological timescales for our reactions in eukaryotes and prokaryotes, see (Jaruszewicz et al., 2013)). Since gene switching and dimerization noises are inversely proportional to the timescale of the reactions, we chose relatively large values for these rates.

		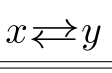	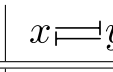	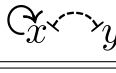	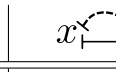
k_{on}	200	200	200	200	1000
k_{off}	200	200	200	200	1000
k_+	$\frac{200\,\mathrm{nM}^{-1}}{V}$	$\frac{200\,\mathrm{nM}^{-1}}{V}$	$\frac{200\,\mathrm{nM}^{-1}}{V}$	$\frac{200\,\mathrm{nM}^{-1}}{V}$	$\frac{89.44\,\mathrm{nM}^{-1}}{V}$
k_-	20	20	20	20	49.4
k_{D+}	$\frac{20\,\mathrm{nM}^{-1}}{V}$	$\frac{20\,\mathrm{nM}^{-1}}{V}$	$\frac{20\,\mathrm{nM}^{-1}}{V}$	$\frac{2000\,\mathrm{nM}^{-1}}{V}$	$\frac{528\,\mathrm{nM}^{-1}}{V}$
k_{D-}	200	200	200	20	0.016
V	$40\,\mathrm{nM}^{-1}$	$40\,\mathrm{nM}^{-1}$	$40\,\mathrm{nM}^{-1}$	$40\,\mathrm{nM}^{-1}$	$440\,\mathrm{nM}^{-1}$
r_x	$1\,\mathrm{nM} \times V$	$1\,\mathrm{nM} \times V$	$4\,\mathrm{nM} \times V$	$0.6\,\mathrm{nM} \times V$	$14.7\,\mathrm{nM} \times V$
r_y	-	$1\,\mathrm{nM} \times V$	$4\,\mathrm{nM} \times V$	$10\,\mathrm{nM} \times V$	$11.77\,\mathrm{nM} \times V$
ε	15	15.05	0.01	24	0.073
$t_{x,y}$	2	2	20	2	117.6
d_m	10	10	10	10	117.6
$d_{x,y}$	1	1	1	1	1
d_c	-	-	-	1.4	4

Table 3.1 Parameters for all reactions in each model. Parameters have been adimensionalized to a reference timescale of $d_x = 5 \times 10^{-4}\,\mathrm{s}^{-1}$. Some parameters in the table appear to have dimensions of concentration, but once they are rescaled by the volume, these dimensional units are lost in favour of molecule numbers. $k_{on,off}$,$k_{+,-}$,$k_{D+,-}$ are equal for X and Y when applicable. Volume $V = 40\,\mathrm{nM}^{-1}$ corresponds to a volume of about $67\,\mu\mathrm{m}^3$ which is of the order of the volume of eukaryotic cell nuclei and of some bacteria (Milo et al., 2010).

3.2.2 Measurements and definitions

To measure how each noise source affects stability of states, we measured how Mean First Passage Time (MFPT) of each transition changes with the different noise intensities. To this end, we chose a reference point in parameter space (the one shown in table 3.1) and varied each noise intensity individually, both increasing and decreasing it, in such a way that the deterministic states of the system remained unchanged as explained. Then, for each point, we computed the steady state distributions in the 2D X,Y plane (where X and Y are the number of protein monomers), to determine the actual steady states of the system when noise is considered.

To compute the MFPTs, we chose a set of coordinates so that transitions were mostly unidimensional for each system: we transformed the X,Y plane into a new plane with coordinates $X - Y$,$\frac{X+Y}{2}$ (which is a simple 45 degree rotation with a rescaling of one axis). These two axes are reasonably good reaction

coordinates for the transitions of each of our states: Autoactivation and Mutual Activation do their transitions along the $\frac{X+Y}{2}$ direction, whereas Mutual Inhibition, Autoactivation with Complex and the Mixed Feedback Loop have transitions mostly in the $X - Y$ direction (Figure 3.3). Thus, when plotting their steady state distributions for each of these coordinates, the states are well separated only in one of the directions (Figure 3.3).

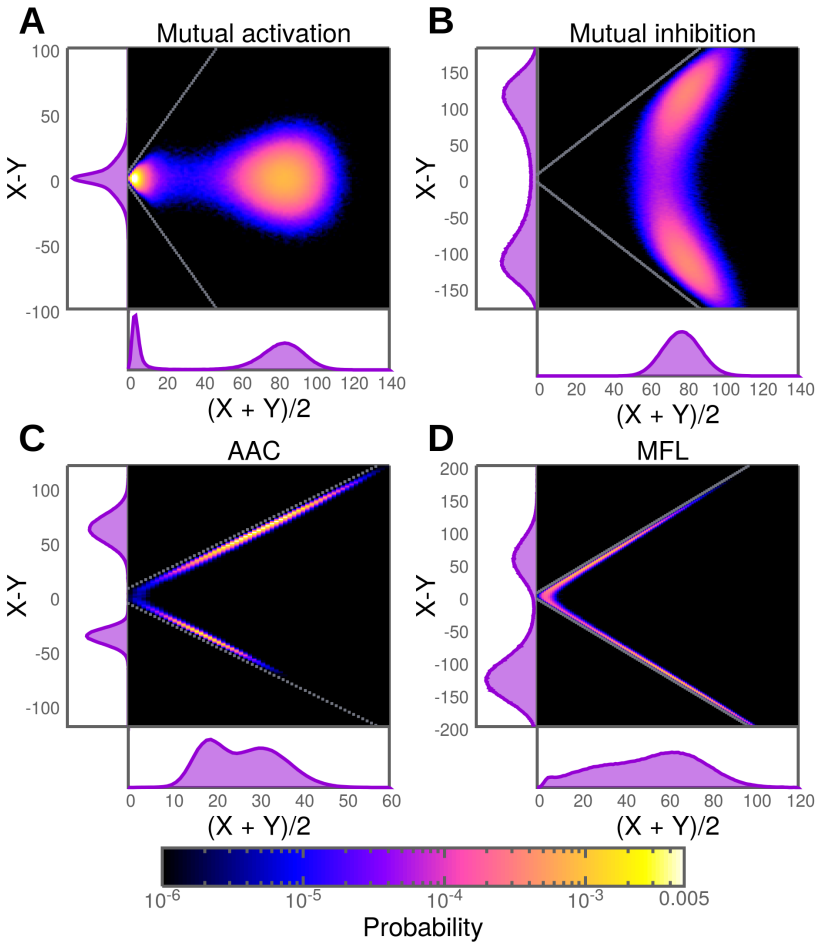

Figure 3.3 $X - Y, \frac{X+Y}{2}$ histograms and their projection onto each axis. Grey lines in the 2D plane mark the X,Y axes, and delimit regions inaccessible to the system because either $X < 0$ or $Y < 0$. (In color in digital version).

We then computed the analogue to the deterministic unstable state as the minimum in the steady state distribution as projected in whichever axis we considered the reaction coordinate for each system. To avoid false positives in the transition, however, we considered several First Passage Time definitions. The first is, obviously, to consider a successful transition when the trajectory first passes the minimum that separates the states. But since when this minimum is very flat it may not be very indicative of whether the trajectory has become trapped in the new state, we also considered going different distances into this arriving state.

If we name the reaction coordinate Z ($Z = \frac{X+Y}{2}$ or $Z = X - Y$, depending on the system as discussed earlier), and define Z_{min},$Z_{max_{1,2}}$ such that $p(Z_{min})$ is the local minimum between the states and $p(Z_{max_{1,2}})$ are the peaks of the distribution, the different distances are $Z_{1/10}$, $Z_{1/5}$ and $Z_{1/3}$ defined as $p(Z_{\{1/10,1/5,1/3\}_{2,1}}) = \frac{p(Z_{max_{1,2}})-p(Z_{min})}{\{10,5,3\}} + p(Z_{min})$. That is, we consider the distances that involve arriving at 1/10th, 1/5th or 1/3rd of the probability of the peak of the arriving state (Figure 3.4 A).

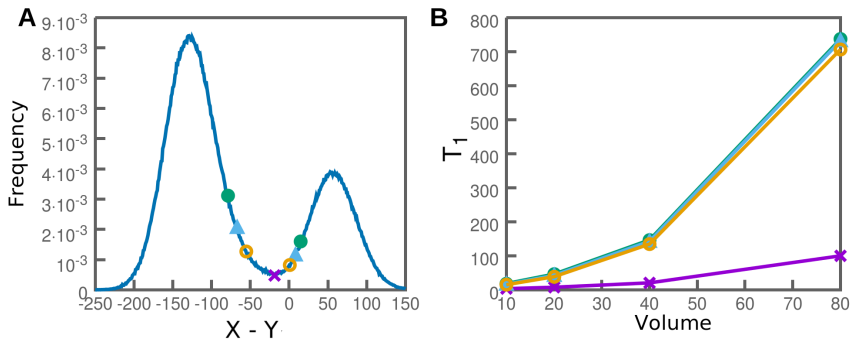

Figure 3.4 Thresholds for First Passage Time computation. **A** Steady state distribution in the $X-Y$ dimension for the reference point of the Mixed Feedback Loop. Points mark thresholds for transitions: purple cross marks de minimum of the distribution, yellow empty circle is 1/10th into the state, blue triangle 1/5th and green full circle is 1/3rd into the state. **B** Mean First Passage Times computed as detailed in the text, for the transition from the state on the right to the state on the left, for all 4 thresholds and for different volumes (the thresholds were computed independently for each value). Each line corresponds to the threshold with the same symbol and color in panel A. In color in digital version.

We computed these four MFPTs for each of our points by simulating $N = 500$ trajectories starting in each of the stable steady states (defined as the peak of

the distribution in X, Y space, with the other variables in equilibrium with it) using the Gillespie algorithm, and recording each FPT as previously defined. As it can be seen in the example shown in Figure 3.4 B, the MFPT when crossing the maximum is often much smaller than the other three definitions. For this reason, all following results use the threshold for transitions at 1/10th, since it seems to avoid false positives but is as close as possible to the separation of the states.

We also computed the First Passage Time histograms, to check whether the MFPT is a good measurement of stability. Figure 3.5 shows how the First Passage Time distributions for the reference point of each system fit an exponential quite well. Furthermore, we used Mathematica software (Wolfram Research, 2010) to apply different statistical tests and were unable to reject the hypothesis of an exponential distribution. In particular, the Cramér-Von Mises test (Darling, 1957) does not reject the exponential distribution hypothesis at the 5% level ($p = 0.05$) in any case. Therefore, we can safely assume that the MFPT captures the relevant information of the transition rates between states.

To see the effect on each system we would have needed to compare the MFPT from each state, T_1 and T_2 (where state 1 is always the state that has a higher concentration of X at the reference point, and T_1 is the MFPT to escape from it) and then compare the systems. For a much simpler comparison of each system, we defined two quantities that distill the information that interests us from these MFPTs. First, we defined Global Stability as $G = T_1 + T_2$, which gives information about how propense each system is to switching from any of the two states, for each noise value. We also considered Relative Stability as $R = \frac{T_1 - T_2}{G}$, which only shows how stable is each state compared to the other, regardless of how frequent switching is. These quantities make comparison of different systems much easier, at no information loss.

We then systematically varied each noise source, changing the relevant timescale or parameter without changing the deterministic solution for the protein concentration: in the case of gene switching, protein-promoter binding and dimerization, the timescale is changed keeping the equilibrium constant, and in the case of bursting the ratio $\frac{t_x}{d_m}$ is maintained constant. Each noise was reduced by a factor of 10 from the reference (2 for Volume noise) and increased by factors of 10 and 100 (2 and 4 for Volume noise), and Global and Relative stabilities were computed for each of these points. We also computed points outside this

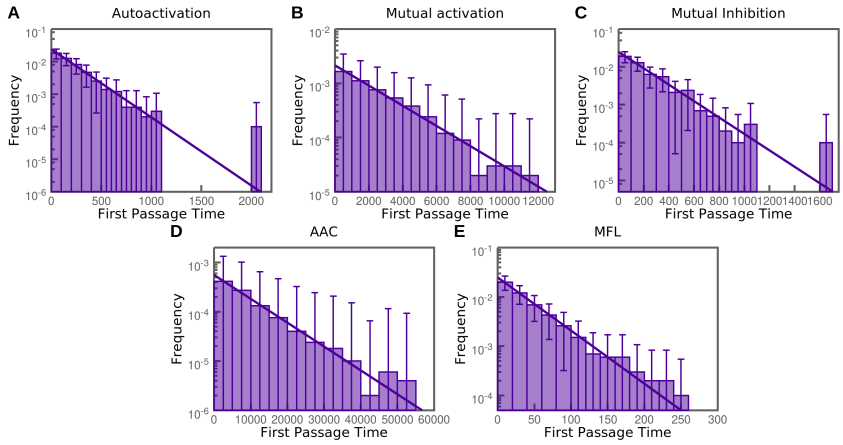

Figure 3.5 First Passage Time distributions. Boxes represent the histogram of $N = 500$ FPTs computed as specified in the text, for the transition from the state with higher amount of X (state 1) to the state with a lower amount (state 2), except for Mutual Inhibition, which is symmetric, in the reference point. Error bars are computed assuming a poisson distribution of errors, according to the formula $\sigma = \sqrt{\frac{p_i}{N}}$. Continuous line represents the exponential distribution $\lambda e^{-\lambda x}$ with $\lambda = \frac{1}{MFPT}$, as computed for each system. **A** Autoactivation, $MFPT = 207.15$. **B** Mutual Activation, $MFPT = 2333.3$. **C** Mutual Inhibition, $MFPT = 200.1$. **D** AAC, $MFPT = 8974.6$. **E** MFL, $MFPT = 40.3$.

range, or with a finer resolution of points within it, as needed to understand the effect of specific noises on some systems.

In all cases, noise was changed to the parameters of both X and Y, when applicable. In the case of Mutual Inhibition, since the states are completely symmetrical and therefore Relative Stability would always be 0, we also studied the case where noise only changed for the parameters of protein X. Only for Mutual Inhibition, then, in the following sections we refer as 'symmetrical' to the case with parameters changed for both X and Y and as 'asymmetrical' to the case where only parameters for X changed.

3.3 Results

3.3.1 Effect on steady states

Before computing the stability of the states through MFPT simulations, we used the information from the steady state distributions we computed to observe the effect of each noise source on the states themselves. Although, naturally, the height and width of the peaks of the distribution changes easily with noise, the position of the peaks themselves does not change for many noise values (Figure 3.6). Notably, when it does change, it sometimes changes dramatically. The noise sources that affect the states the most are the two DNA switching rates, k_{on} and k_{+}. These go as far as making the distribution trimodal, making one of the two states degenerate, when they are high enough (Figure 3.6 A,B,E).

3.3.2 Definition of dimerization noise

In section 3.2.1, we defined dimerization noise as the inverse of the dimerization rate timescale as is shown to behave in (Jaruszewicz et al., 2013) for the toggle switch. However, when we computed the MFPTs varying this noise, we found that the stability increased at large noise values for all three systems where it is applicable (Figure 3.7).

This is a puzzling result, as it goes opposite to previously reported results (Jaruszewicz et al., 2013) and also contravenes the *a priori* characterization related to adiabaticity. It does not dispute the results from previous studies at all, though. Rather, one could say that depending on model details and parameter values, dimerization noise has two regimes of dependence with the timescale of its reaction, at least for mutual inhibition. In agreement with this argument, dimerization noise was shown to be proportional to the dimerization rate (as we also find) in (Morelli et al., 2008) for a model identical to the one in (Jaruszewicz et al., 2013), although it was not interpreted this way, since they did not define such a quantity as 'dimerization noise'. In any case, in the following sections we redefine dimerization noise as proportional to the timescale of the reaction, since that is the behaviour found in our studies.

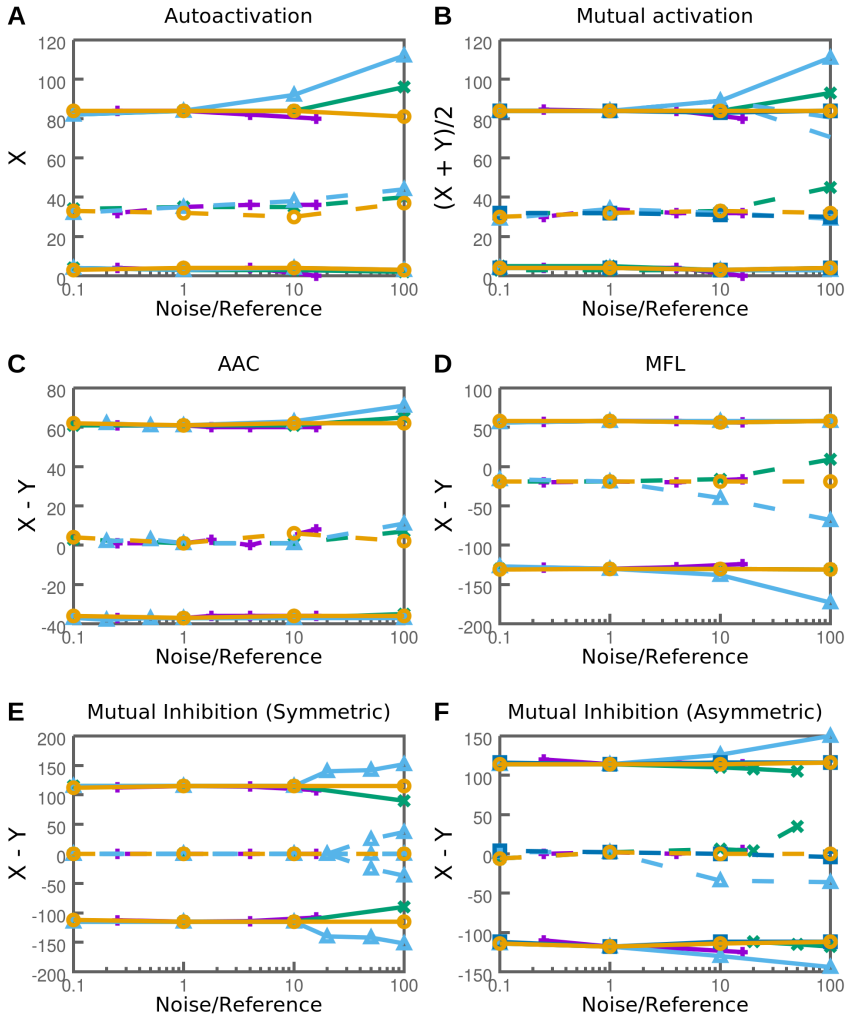

Figure 3.6 Effect of noise on steady states. Different symbols denote numerically computed maxima and minima of the distribution of the plotted variable for each noise type. Lines are a guide to the eye and denote stability of the state: continuous lines for stable states (maxima of distribution) and dashed lines for unstable states (minima of the distribution). Purple crosses correspond to volume (V). Green crosses correspond to gene switching (k_{on}). Light blue triangles correspond to protein-promoter binding (k_+). Dark blue squares correspond to protein dimerization (k_D). Gold, empty circles correspond to bursting noise (d_m). In the case of volume noise, X and Y do not show actual numbers of molecules and are instead rescaled back as $\tilde{X} = X \times \frac{V}{V_{Ref}}$.

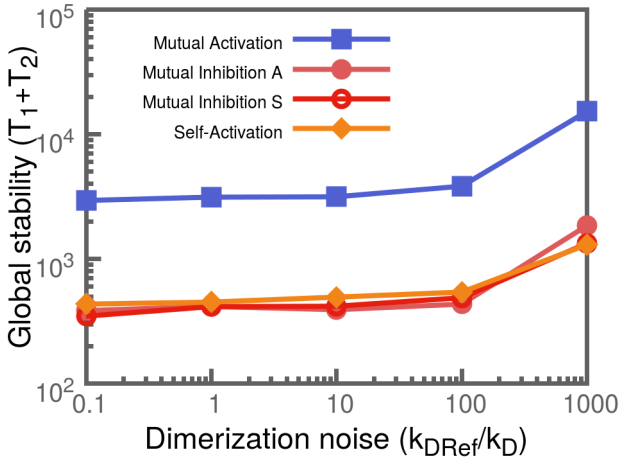

Figure 3.7 Global Stability vs Dimerization noise. Blue squares, mutual activation. Dark red, empty circles, Mutual Inhibition S, for Symmetrically changed parameters. Light red, full circles, Mutual Inhibition A, for Asymmetrically changed parameters. Orange diamonds, autoactivation. Symbols are numerical results computed as detailed in text, and lines are guides to the eye. In color in digital version.

3.3.3 Effect of Volume

We first see the effect, across all systems, of increasing the number of molecules. When we looked into the effect of increasing volume we found that, as expected, all systems behaved similarly, with decreased global stability as volume decreases (Figure 3.8 A). Regarding symmetry between states, although later sections explore this further, there is a somewhat general result: increasing volume increased the stability of the state with more protein in all circuits except for the Mixed Feedback Loop (State 1 is always the state with more amount of X, and in all cases that coincides with the state with more protein, except in the Mixed Feedback Loop, see Figures 3.3 and 3.6). This is a nice confirmation of our main result in Chapter 2 for an autoactivating loop: increasing intrinsic noise stabilizes the state with less protein (The 'OFF' state, in the notation of Chapter 2).

We then looked into the behaviour of each individual system.

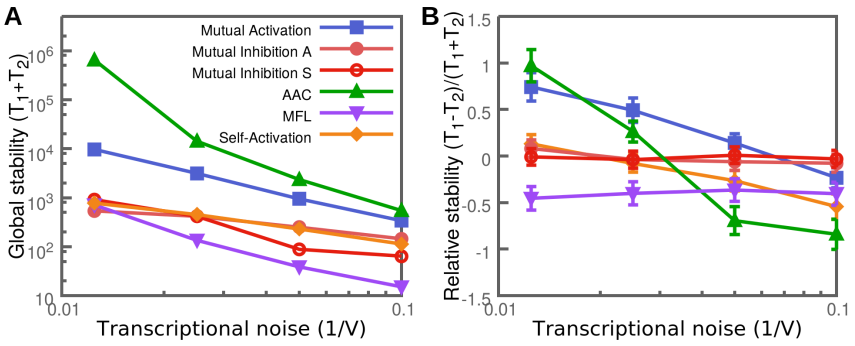

Figure 3.8 Blue squares, mutual activation. Red circles, Mutual Inhibition: Bright red, empty circles, noise changed symmetrically; light red, full circles, noise changed only for X. Green triangles, AAC. Purple, inverted triangles, MFL. Orange diamonds, autoactivation. Error bars in Relative Stability indicate error propagated from SEM. Error not shown in Global stability because its size is comparable to that of the symbols.

3.3.4 Purely transcriptional systems

3.3.4.1 Autoactivation and Mutual Activation

We started with Autoactivation, as the simplest circuit here that can generate bistability. The effects of noise on this circuit had also been studied by ourselves (see Chapter 2,(Frigola et al., 2012)) and by others (Cheng et al., 2008; Jaruszewicz et al., 2013). In particular, previous studies concentrated on volume and gene switching noise (Cheng et al., 2008; Jaruszewicz et al., 2013). Mutual Activation has very similar results, as shown further in this section, and has an equivalent deterministic behaviour (Figure 3.9), so we show them together.

In particular, Jaruszewicz et al. (2013) did a similar study to the one presented here, comparing the effect of number of molecules and gene switching on an autoactivating loop very similar to ours. We therefore compare our results to theirs here. These results can be summarized as follows: In a PFL driven by autoactivation, transcriptional noise (related to number of molecules, like our volume), favors (i.e. differentially stabilizes) the low concentration state (i.e. state 2 or 'OFF'), whereas gene switching noise favors the high concentration state (i.e. state 2 or 'ON') (Jaruszewicz et al., 2013). It is also worth it to briefly explain the model used in this previous study (Jaruszewicz et al., 2013): it also

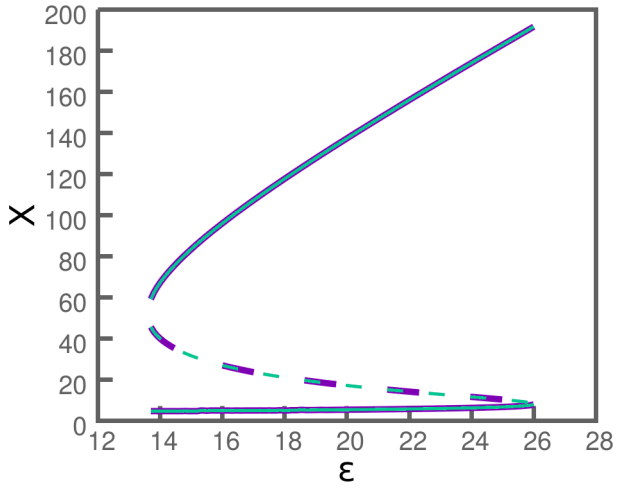

Figure 3.9 Deterministic bifurcation diagram of X vs ε for Autoactivation and $\frac{X+Y}{2}$ (or X, since they are equal) vs ε for Mutual Activation. Darker (purple in digital version), thick line represents Mutual Activation whereas lighter (green in digital version), thinner line represents autoactivation. Continuous lines represent stable states whereas the dashed line represents the unstable state. In color in digital version.

has DNA switching, although it only has two states to our three. Instead of having a constant switching rate and then a binding of protein to promoter, its states are equivalent, in terms of the transcriptional activity they drive, to our DNA_{off} and DNA_{on}, but their switching rate k_{on} scales with $(1 + k'X^2)$, incorporating a constant leaky term and an approximation for cooperative protein binding.

As explained in the previous section, volume noise destabilizes state 1, which has high levels of X. Figure 3.10 A and B show this more clearly. This result, also shown by Jaruszewicz et al. (2013), is preserved in Mutual Activation, with only changes in the specific stabilities and their slopes in relation to noise intensity.

Unlike volume noise, we found that the effect of gene switching noise saturated at decreasing noise values (Figure 3.10 C). In addition, gene switching noise is similar to volume noise, since it favors stability of the state with less protein, except at very high noises (Figure 3.10 D), which have an abnormal behaviour that we will analyze later. This result for the effect of gene switching noise

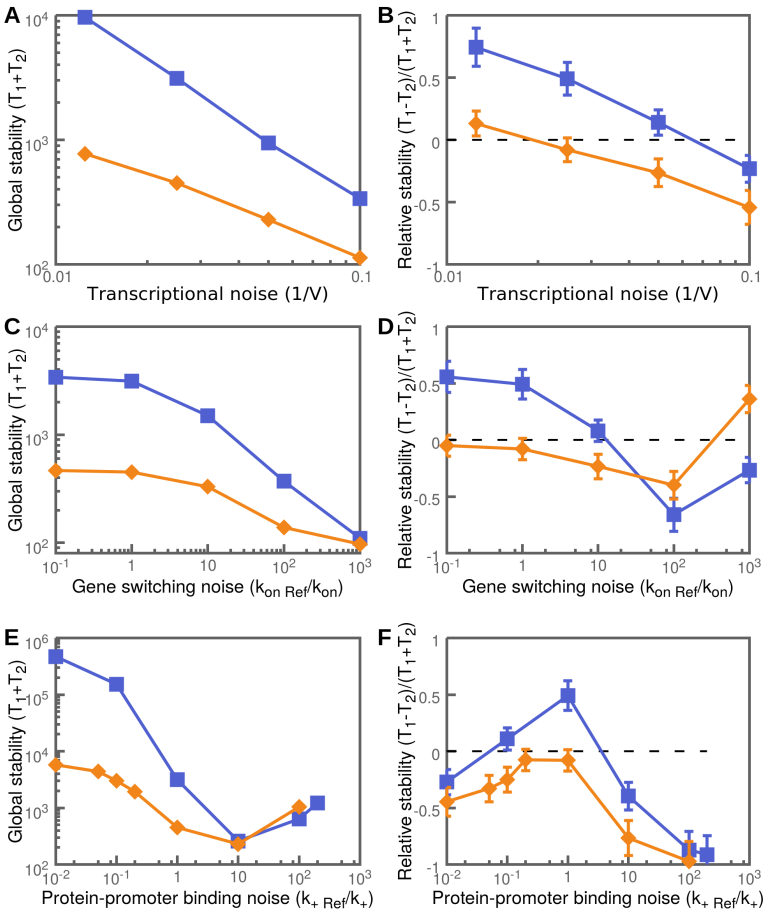

Figure 3.10 Global and Relative stability of Mutual Activation (blue, squares) and Autoactivation (orange, diamonds) as a function of (A,B) transcription noise, (C,D) gene switching noise, and (E,F) protein-promoter binding noise. Panels A,C,E represent global stability and panels B,D,F represent relative stability of the two states. Error bars in Relative Stability indicate error propagated from SEM. Error not shown in Global stability because its size is comparable to that of the symbols. Symbols are numerical results computed as detailed in text, and lines are guides to the eye. In color in digital version.

on Relative Stability does not agree with the reported findings of Jaruszewicz et al. (2013), which found that gene switching noise favored the state with more protein.

Contrary to gene switching, protein binding noise favored the high protein state at low noise values. This can be considered to be in agreement to Jaruszewicz et al. (2013), since their 'gene switching' corresponds to both our gene switching and our protein binding. Beyond a threshold, however, the behaviour reversed, like with gene switching (Figure 3.10 F). Furthermore, and even more surprisingly, global stability also changed slopes, increasing at very high protein-promoter binding noise values (Figure 3.10 F).

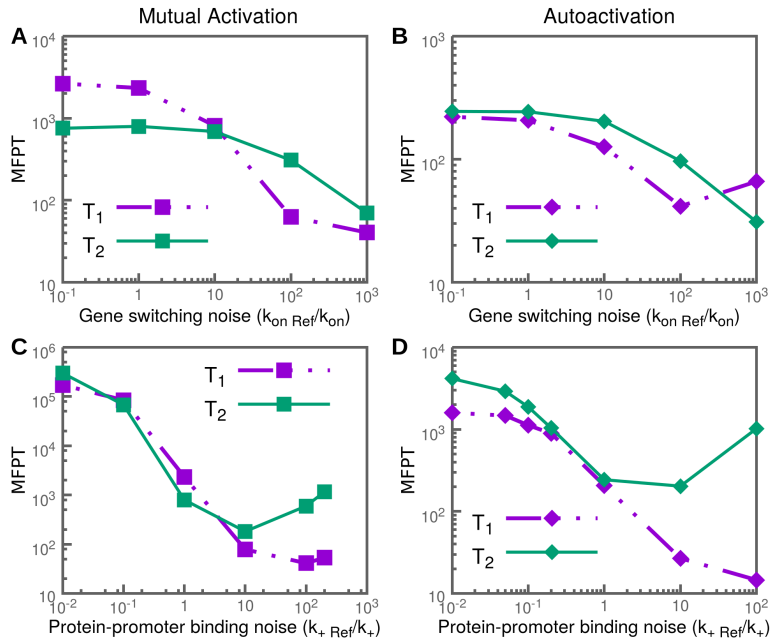

Figure 3.11 Mean First Passage Times as a function of gene switching and protein-promoter binding noises for (A,C) Mutual Activation, and (B,D) Autoactivation. Green, continous line is MFPT to escape from State 2 to State 1 ($OFF \rightarrow ON$) whereas purple, dot-dashed line is the time for the opposite transition. Symbols are numerical results computed as detailed in text, and lines are guides to the eye. In color in digital version.

This reversal of behaviour at high noises is puzzling, and worth trying to explain. To that end, we plotted both the separate Mean First Passage Times from each state (Figure 3.11) and the steady state distributions depending on

these two noise intensities (Figure 3.12). One thing that can be readily seen is that although global stability does not show it, there was also an increase in stability for high noise values in gene switching noise, for one of the states (Figure 3.11 B). Another effect that is observable is that the MFPT for both states evolves similarly in each case, but the escape time from the state that is most destabilized by each type of noise goes through this change at lower noise values (State 1, or ON, for gene switching noise and State 2, or OFF, for protein binding noise) (Figure 3.11).

Furthermore, although it seems that these thresholds are at different noise values for each noise type, they actually happen at similar timescales. Consider that the noise intensity of this transition for autoactivation $\frac{k_{onRef}}{k_{on}} = 100$ corresponds to rates of $k_{on} = k_{off} = 2$. A similar transition happens at $\frac{k_{+Ref}}{k_{+}} = 10$, which corresponds to $k_{-} = 2$ (Figure 3.10 D,F).

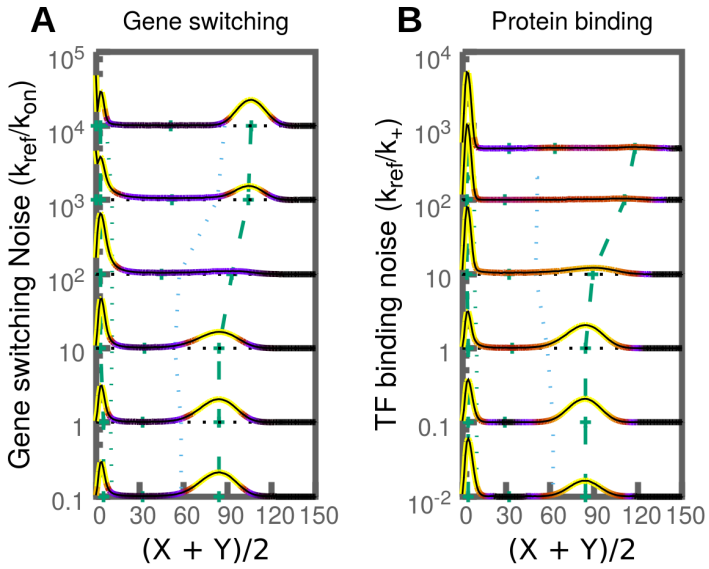

Figure 3.12 Steady state histograms for diferent gene switching and protein binding noise values in the Mutual Activation system. Color shows probability value in a logscale to better see the changes at very low probabilities. Crosses and dashed lines show the evolution of distribution maxima and minima depending on noise.

What happens is that at this slow timescales of gene state change, these reactions dominate switching: they happen rarely enough that, when they do,

they necessarily provoke a transition. This also helps understand which state is overall more affected by which noise: State 1, the high concentration state, is more affected by gene switching because if the gene turns off, the state is unsustainable. State 2, the low concentration state, is more destabilized by protein binding because when a dimer molecule binds to the promoter, production is enhanced and State 1 is favored.

When these timescales become slow enough, switching times start to go up with them, provoking this effect of nonmonotonic stability. This can also be seen in that the steady state concentrations themselves change at these limits and, at very high noise values, the distribution becomes trimodal, with two peaks at low concentrations for high gene switching noise and two peaks at high concentration for high protein binding noise (Figure 3.12). Thus, this effect is caused because we have, in a way, a mixture of bistability and bimodality due to the discrete gene states.

We also explored bursting and dimerization noise but found that, for these systems and for the ranges explored, they have relatively small effects (Figure 3.13). The effect that they do have, however, is quite similar. The effect of both noises on Global Stability saturates at high noise values (as opposed to the low noise saturation of gene switching). Furthermore they both, but dimerization in particular, have a small but non-negligible effect on Relative Stability, favouring the low concentration state like volume and gene switching noise.

In general, we can conclude that noise strongly tends to stabilize the low concentration state of the Autoactivation and Mutual Activation circuits, compared to the high concentration one, since we observed this effect for all noise sources, with the only exception of protein-promoter binding at low noise values. This can be considered a generalization of the main result of chapter 2.

3.3.4.2 Mutual Inhibition

We continued by studying Mutual Inhibition. As a classical motif underlying bistability, its relationship to noise has been studied many times, with different perspectives (Tian and Burrage, 2006; Morelli et al., 2008; Strasser et al., 2012; Jaruszewicz and Lipniacki, 2013). As such, many of our results in this section incrementally add on to the results of others, as well as confirm or clarify them.

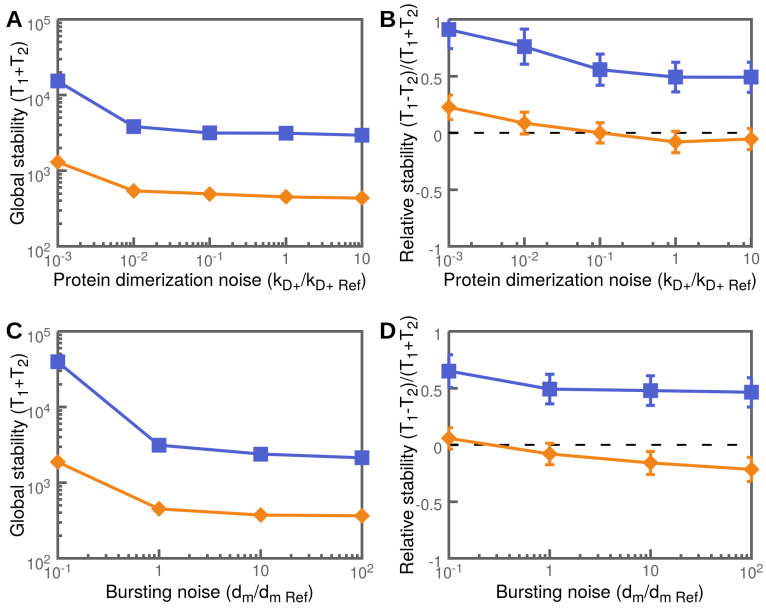

Figure 3.13 Global and Relative stability of Mutual Activation (blue, squares) and Autoactivation (orange, diamonds) as a function of (A,B) dimerization noise and (C,D) bursting noise. Panels A,C represent global stability and panels B,D represent relative stability of the two states. Error bars in Relative Stability indicate error propagated from SEM. Error not shown in Global stability because its size is comparable to that of the symbols. Symbols are numerical results computed as detailed in text, and lines are guides to the eye. In color in digital version.

We focused our comparison to previous results by Morelli et al. (2008) and Jaruszewicz and Lipniacki (2013). Both studies used an identical model of the toggle switch, which is very similar to ours. The only differences are that they do not have a DNA_{off} state and they both have a complete repression of expression when protein is bound to the promoter, i.e. $\varepsilon = 0$ in our notation, whereas we have a finite $\varepsilon = 0.01$. Both also studied the same noise sources as each other: protein-promoter binding and dimerization noise, but they each focused on different perspectives of the system. Morelli et al. (2008) changed noise symmetrically, providing results comparable to our Global Stability, whereas Jaruszewicz and Lipniacki (2013) focused on the effect of asymmetrically changed noise on the Relative Stability of the states.

Let us describe the main results of these studies that are of interest to us here (which are not by any means all their results). Morelli et al. (2008) found that

dimerization noise is directly proportional to dimerization and dedimerization rates (as anticipated in section 3.3.2) and protein-promoter binding noise is inversely proportional to its rates. When looking at their results, one also realizes that the system is quite insensitive to both noise sources (finding a change in switching rates of, at most, 1 order of magnitude for up to 4 orders of magnitude change in the timescales of the reactions), although they do not explicitly report this result (Morelli et al., 2008). The main results in Jaruszewicz and Lipniacki (2013) are that increasing protein-promoter binding noise in the promoter of X enhances the stability of the low X state, whereas increasing dimerization noise for X increases the stability of the state with high X (Jaruszewicz and Lipniacki, 2013). Recall from sections 3.3.2 and 3.2.2 that Jaruszewicz and Lipniacki (2013) considered (and showed) dimerization noise to be inversely proportional to the reaction timescale. Therefore, their result can also be read as saying that making the dimerization of X *slower* stabilizes the high X state.

When we measured how Global and Relative stabilities changed with noise we found that, overall, mutual inhibition was not very sensitive to noise changes (Figures 3.14 and 3.15). The noise source that affected the system the most is gene switching, both in Global Stability when it was changed symmetrically and in Relative stability when it was changed only for the promoter of X, dramatically favoring the state with lower X (Figure 3.14 C,D).

The noise that affected the system second most was the one that originates in dimerization. In particular, it had a large effect on relative stability when changed asymmetrically (Figure 3.15 A,B). However, we had to decrease the noise value further than initially intended to observe this effect. It is interesting to note that an increase of dimerization noise in X enhances the stability of the low X state. This result is the same shown by Jaruszewicz and Lipniacki (2013) and it makes intuitive sense: when we add noise to the dimerization of X, we are actually making the transcriptional repression of Y more noisy, thereby destabilizing the state that depends on Y being repressed (the low Y, high X state). However, notice that as explained earlier, the relationship of the dimerization timescale k_{D+} with dimerization noise in (Jaruszewicz and Lipniacki, 2013) remains opposite to ours. That is, if we consider how k_{D+} is changed instead of considering dimerization noise, our results regarding Relative Stability are no longer comparable.

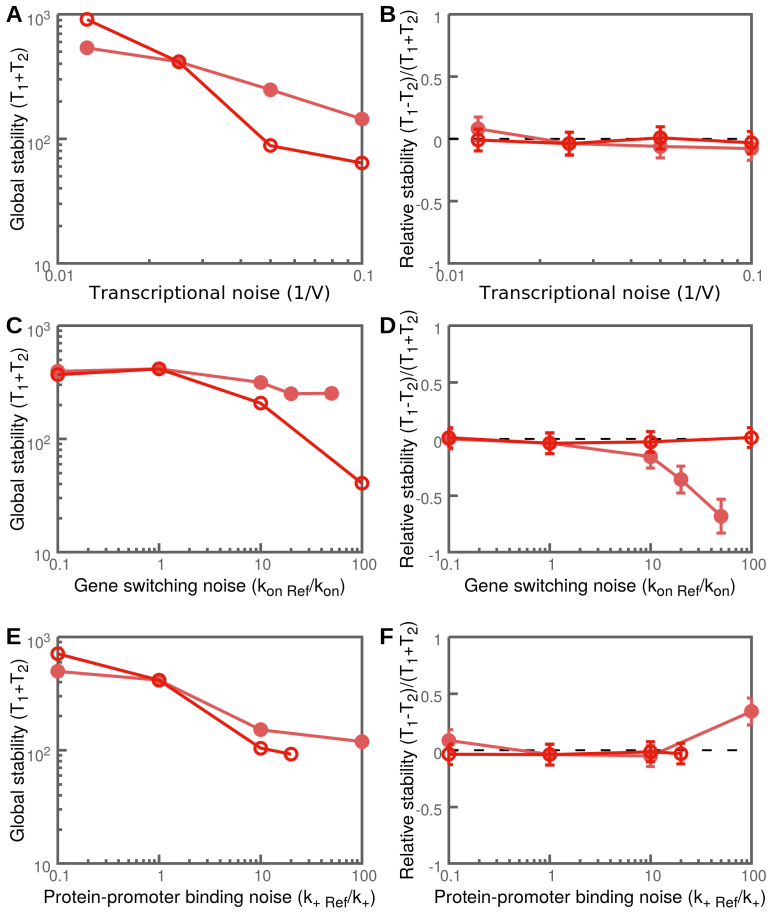

Figure 3.14 Global and Relative stability of Mutual Inhibition S (for Symmetrically changed noise, dark red, empty circles) and Mutual Inhibition A (for Asymmetrically changed noise, light red, full circles) as a function of (A,B) transcription noise, (C,D) gene switching noise, and (E,F) protein-promoter binding noise. Panels A,C,E represent global stability and panels B,D,F represent relative stability of the two states. Error bars in Relative Stability indicate error propagated from SEM. Error not shown in Global stability because its size is comparable to that of the symbols. Symbols are numerical results computed as detailed in text, and lines are guides to the eye. In color in digital version.

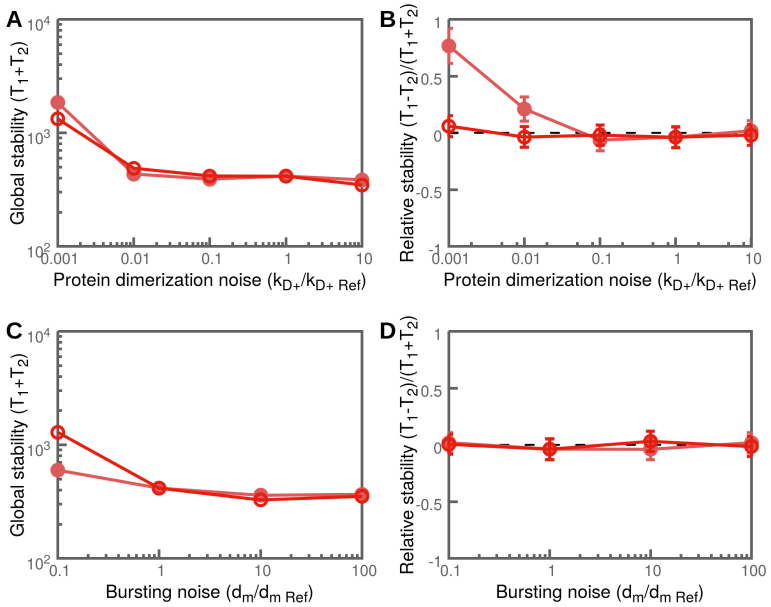

Figure 3.15 Global and Relative stability of Mutual Inhibition S (for Symmetrically changed noise, dark red, empty circles) and Mutual Inhibition A (for Asymmetrically changed noise, light red, full circles) as a function of (A,B) dimerization noise and (C,D) bursting noise. Panels A,C represent global stability and panels B,D represent relative stability of the two states. Error bars in Relative Stability indicate error propagated from SEM. Error not shown in Global stability because its size is comparable to that of the symbols. Symbols are numerical results computed as detailed in text, and lines are guides to the eye. In color in digital version.

When we checked the effect of protein-DNA binding, the result we obtained was the opposite to gene switching and dimerization noises: noise favors the high X state (Figure 3.14 F), although weakly. The intuitive explanation for this result is similar to that of dimerization: more noise in X repression enables the easier release of this repression and an increassed expression of X, destabilizing the low X state in favor of the opposite one.

In this case our result is opposite to the one obtained by Jaruszewicz and Lipniacki (2013). However, note that our gene switching noise result is similar to their protein-promoter binding result. Interestingly, the result that coincides in both cases is the one in which DNA is completely inactivated. This poses the question, then, of whether what defines our (and their) gene switching result is a DNA transition that brings transcription completely to a halt, rather

than a specific mode of DNA regulation (constant or mediated by protein binding). Furthermore, these results and their comparison to previous ones mirror the ones we obtained for autoactivation, suggesting some fundamental cause underlying them.

Like all other noise sources, volume and bursting noise affected Global Stability when changed both symmetrically and asymmetrically (Figures 3.14 A and 3.15 C) by a not very large amount. However, unlike with other noises, their effect on Relative Stability was completely negligible (Figures 3.14 B and 3.15 D).

The most relevant results in this section are, possibly, that Global Stability of Mutual Inhibition is not very sensitive to our noise sources (a result that is also extracted from the data in (Morelli et al., 2008) for dimerization and protein-promoter binding noises), and that the noise that affects relative stability the most is, by far, gene switching. Furthermore, like in Mutual Activation and Autoactivation, the only noise source that stabilizes state 2 (the high X state) is protein-promoter binding. In Mutual Inhibition, though, some noise sources did not strongly stabilize either state, unlike with Mutual Activation and Autoactivation, where all noises change Relative Stability.

3.3.5 Mixed motifs: AAC and MFL

Finally, we measured the effect of all different noise sources (except, as detailed in section 3.2.1, dimerization) on the Mixed Feedback Loop and the Autoactivation with Complex circuits. We put these two systems in a single category *a priori*, due to their particularity of needing post-transcriptional interactions of X and Y to yield bistability.

We found that the Global Stability of the AAC is, in general, much more sensitive than that of the MFL. However, the qualitative dependence of Global Stability with noise is remarkably similar in both circuits for transcriptional and gene switching noises, except for their different slopes (Figure 3.16 A,C). For bursting and protein-promoter binding noises, the dependence also seems qualitatively similar but the slope of the MFL Global Stability is so small that the similarity is hard to establish (Figure 3.16 E,G). The response of Relative Stability, however, is quite dissimilar for each motif in all cases.

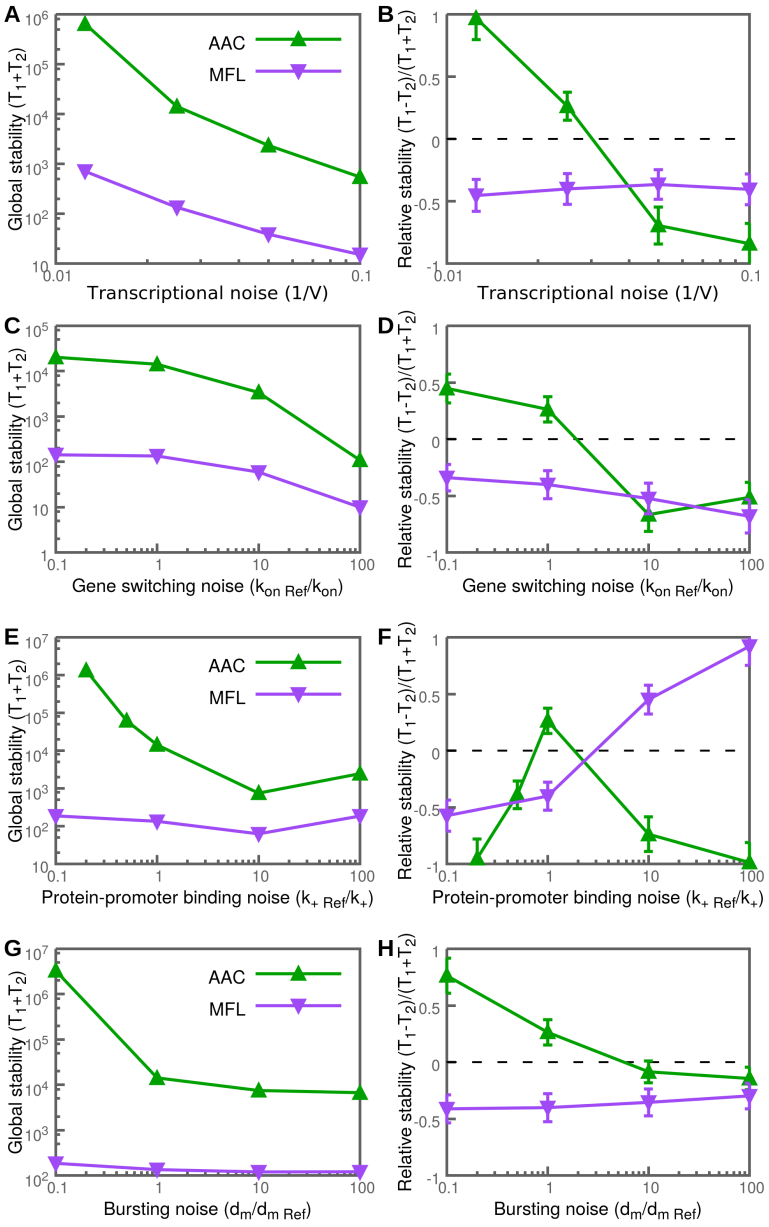

Figure 3.16 Global and Relative stability of AAC (green, triangles) and MFL (purple, inverted triangles) as a function of (A,B) transcription noise, (C,D) gene switching noise, (E,F) protein-promoter binding noise and (G-H) bursting noise. Panels A,C,E,G represent global stability and panels B,D,F,H represent relative stability of the two states. Error bars in Relative Stability indicate error propagated from SEM. Error not shown in Global stability because its size is comparable to that of the symbols. Symbols are numerical results computed as detailed in text, and lines are guides to the eye. In color in digital version.

Volume noise generates almost no effect on the relative stability of the MFL, whereas a change in volume of factor 8 is capable of almost completely changing states in the AAC (Figure 3.16 B). This is a remarkable difference given the similarity of their dependence of Global Stability with volume.

A similar thing happens for gene switching noise and bursting noises: AAC is very sensitive, with noise dramatically favoring the low X state, whereas the MFL Relative Stability is almost unaffected (Figure 3.16 D,H).

Both circuits are also very sensitive in their relative stability when protein-promoter binding noise is changed, and can go to complete asymmetry in only an order of magnitude change in the timescale of the reactions (Figure 3.16 F). They do it differently, though. MFL changes from one state to the other, whereas AAC shows a nonmonotonic behaviour more similar to Mutual activation and Autoactivation. In fact, when we compared AAC and Mutual Activation we saw that, like with Autoactivation, they are very similar (Figure 3.17). Notice that, although this is an 'asymmetric' system like Mutual Inhibition and MFL in that it has two species X and Y with opposed concentrations, it has a positive interaction in the form of an autoactivation, unlike these other two circuits.

Interestingly, in an analogous way to the AAC being similar to the purely-positive feedbacks, MFL is comparable to Mutual Inhibition. Like it, it is not very sensitive to noise, and the effect of volume and gene switching is remarkably similar in both circuits (Figure 3.18). The largest difference between Mutual Inhibition and the Mixed Feedback Loop can be found on the much larger effect of protein-promoter binding on the Relative Stability of MFL (Figure 3.18 F).

All in all, the classification according to bistability mechanism does not give a lot of information about the effect of noise on the circuit: AAC is much more stable and sensitive to noise than MFL and, although their global stabilities are qualitatively comparable, AAC is overall much more similar to Mutual Activation and MFL to Mutual Inhibition. It is worth it to highlight that the Relative Stabilities of both circuits are extremely sensitive to protein-promoter binding noise. If we focus on the differences of each circuit with the other circuits they seem to be similar to (i.e. if we compare AAC to the activation circuits and MFL to Mutual Inhibition), the Relative Stability of AAC is much more sensitive to Volume and bursting noises than Mutual Activation (Figure

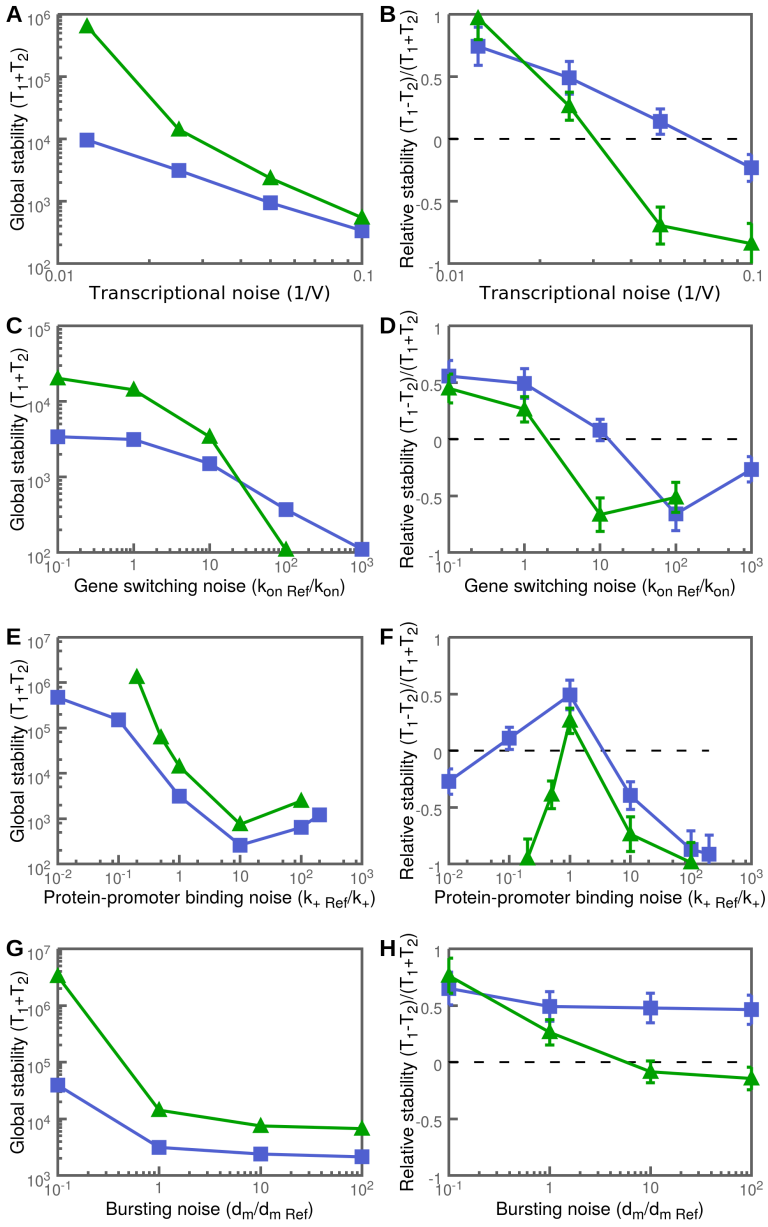

Figure 3.17 Global and Relative stability of AAC (green, triangles) and Mutual Activation (blue squares) as a function of (A,B) transcription noise, (C,D) gene switching noise, and (E,F) protein-promoter binding noise. Panels A,C,E represent global stability and panels B,D,F represent relative stability of the two states. Error bars in Relative Stability indicate error propagated from SEM. Error not shown in Global stability because its size is comparable to that of the symbols. Symbols are numerical results computed as detailed in text, and lines are guides to the eye. The data in this figure already appear in Figures 3.10, 3.13 and 3.16, but they are grouped and presented again for a better comparison. In color in digital version.

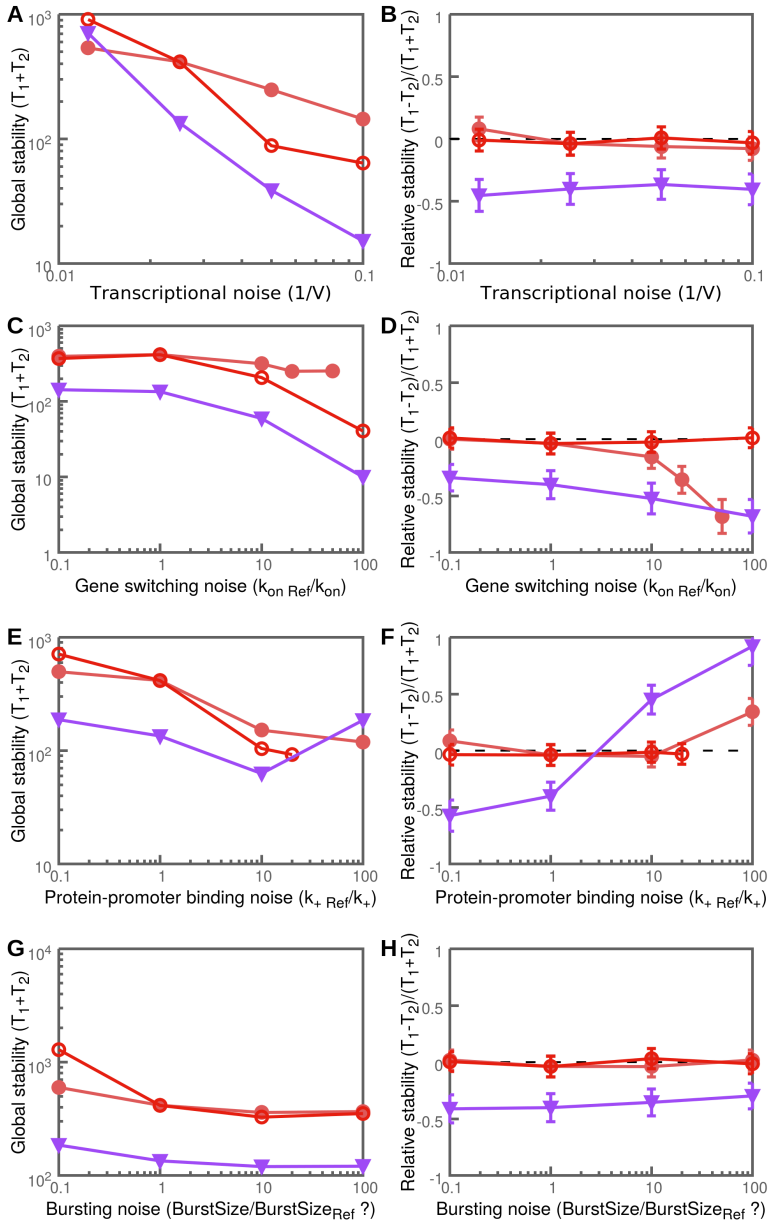

Figure 3.18 Global and Relative stability of AAC (green, triangles) and Mutual Activation (blue squares) as a function of (A,B) transcription noise, (C,D) gene switching noise, and (E,F) protein-promoter binding noise. Panels A,C,E represent global stability and panels B,D,F represent relative stability of the two states. Error bars in Relative Stability indicate error propagated from SEM. Error not shown in Global stability because its size is comparable to that of the symbols. Symbols are numerical results computed as detailed in text, and lines are guides to the eye. The data in this figure already appear in Figures 3.14, 3.15 and 3.16, but they are grouped and presented again for a better comparison. In color in digital version.

3.17), whereas MFL is much more sensitive than Mutual Inhibition to protein-promoter binding, but also much less sensitive to gene switching (Figure 3.18).

3.3.6 Five-way comparison of the circuits

To be able to compare all systems at a glance, we defined Global Stability Sensitivity and Relative Stability Sensitivity as how much the Stabilities changed when decreasing and increasing noise intensity by a factor 10 (2 for volume noise) above and below the reference point:

$$GSens_{Noise\,\lambda} = log\left(G_{Noise/10}\right) - log\left(G_{Noise\times 10}\right) \tag{3.4}$$

$$RSens_{Noise\,\lambda} = abs\left(R_{Noise/10} - R_{Noise\times 10}\right), \tag{3.5}$$

where $Noise$ stands for the reference value, and λ indicates that these expressions are computed for each noise source. That is, we computed the difference between the maximum and the minimum stabilities within this range of two orders of magnitude. When the relationship between noise and stability is monotonous, this quantity is an effective slope of that relationship at each reference point. In the case of G, we use logarithms to see the change in orders of magnitude, so that each system is within its own scale and they are all comparable. We also define Total Sensitivities as

$$TotalGSens = \sum_{\lambda\in\{NoiseTypes\}} GSens_{Noise\,\lambda} \tag{3.6}$$

$$TotalRSens = \sum_{\lambda\in\{NoiseTypes\}} RSens_{Noise\,\lambda}, \tag{3.7}$$

and the percentage contribution of each noise to this total,

$$\%GSens_{Noise\,\lambda} = \frac{GSens_{Noise\,\lambda}}{\sum_{\lambda \in \{NoiseTypes\}} GSensy_{Noise\,\lambda}} \tag{3.8}$$

$$\%RSens_{Noise\,\lambda} = \frac{RSens_{Noise\,\lambda}}{\sum_{\lambda \in \{NoiseTypes\}} RSens_{Noise\,\lambda}}. \tag{3.9}$$

Visually, Total Sensitivity is the total height of each system's bar in panels A and B of Figure 3.19 A,B.

Although this kind of representation eliminated qualitative details, and sensitivity to changes at extreme noise values, it allowed us to compare all five systems at a glance. The first thing we can see is that each system had different sensitivity overall, but Global Stability Sensitivity correlates well with Relative Stability Sensitivity (Figure 3.19 A,B). The effect of each noise source on the global stability, though, is not always indicative of its contribution to relative stability changes. That is, there are noise sources that do not affect Global Stability by much but have an important contribution to Relative Stability Sensitivity, and vice versa (Figure 3.19 C, D).

We also observed that, although the details of the percentual effect of each noise source on stability vary for each system, there is a certain generality in what are the most and least important noises. In particular, Volume and protein-promoter binding tend to be the main contributors to both Global and Relative Stability Sensitivity. For most systems, bursting also has an important effect on Global Stability, whereas gene switching tends to affect Relative Stability more.

If we focus on the main differences between systems, the clear outlier is the MFL, with a disproportionate Global Stability Sensitivity to Volume noise, and also a very large Relative Stability Sensitivity to protein-promoter binding.

Close observation of Figure 3.19 together with the figures of the previous sections, Figure 3.8 A in particular, also lead us to observe another result: it seems that the total Stability Sensitivity (that is, the total height of each bar in figure 3.19 A and B) is related to the Global Stability at the reference point. Indeed, when we plotted the Total Global Sensitivities against the logarithm of stability

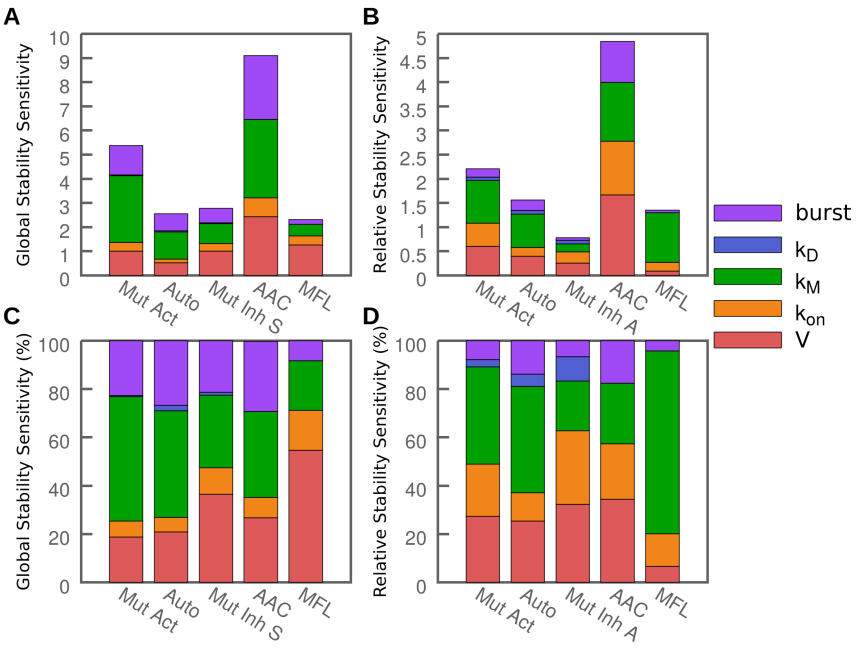

Figure 3.19 Contribution of each noise source to changes in stability for each circuit. Mut Act stands for Mutual Activation, Auto stands for Autoactivation and Mut Inh stands for Mutual Inhibition (S: with Symmetrically changed parameters and A: with Asymmetrically changed parameters) **A** Global Stability Sensitivity of each circuit to all noises. **B** Relative Stability Sensitivity of each circuit to all noises. **C** As panel A, but each system is normalized by its Total Sensitivity (the total height of its bar in panel A) **D** As panel B, but each system is normalized by its Total Sensitivity (the total height of its bar in panel B).

at the reference point, a linear relationship emerged (Figure 3.20 A). Interestingly, we were unable to uncover any relationship between average number of molecules and stability or sensitivity (Figure 3.20 B).

3.4 Discussion and perspectives

We have performed a study and comparison of the effect of five different noise sources on five different bistable circuits. This is, to our knowledge, the most extensive study of this type to date, and it hints at possible biological functions of each circuit, as detailed below. However, it has much room for improvement.

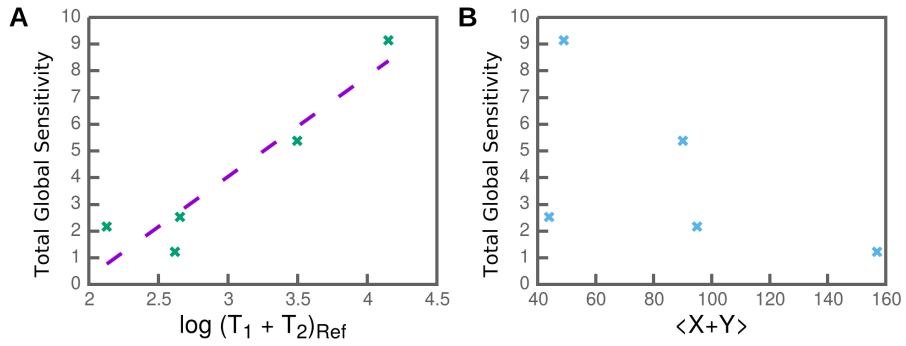

Figure 3.20 Total Global Sensitivity versus Stability at reference point and versus molecule number **A** Total Global Sensitivity versus stability at reference point. Crosses are values for each system, dashed line is a linear fit with $r^2 = 0.86$ **B** Global sensitivity of each circuit (as the sum of the sensitivities to all noise sources) versus average number of free X and Y molecules for each circuit computed as the average of the steady state X plus Y in both states of each system.

One of the novelties of our study is including post-transcriptional circuits that appear to exist in biological systems and can also enable bistability, and one of our main findings also relates to these circuits. We found that, although both post-transcriptional circuits involve two proteins that have strongly opposed states, the Autoactivation with Complex circuit is quite similar to Autoactivation and Mutual Activation, whereas the Mixed Feedback Loop is similar to Mutual Inhibition. This points toward an intrinsic characteristic depending on, for instance, the number of positive and negative transcriptional regulations (as was already found for the Feed Forward Loop (Kittisopikul and Süel, 2010)) that warrants further investigation but is beyond the scope of this type of study and possibly beyond the information it can yield. This opens a perspective of a systematic study of bistable circuits with different number of positive and negative interactions, and their relationship with noise.

Most of our results are in the specific dependency of Global and Relative Stability of each circuit. It is very interesting to see that all circuits have some noise source that, when tuned (only as a noise source, without changing the deterministic bistability of the system) can completely or almost completely switch extreme stability from one state to the other. Mutual Inhibition is quite insensitive to all noise sources, but strong gene switching noise in one of the

genes can completely destabilize its high concentration state. The MFL, instead, is very sensitive to noise in the protein-promoter binding reaction. In the AAC a change in molecule number without affecting concentration (i.e. a change in volume noise) completely changes the stability of the state, and protein-promoter binding does as well. For Mutual Activation and Autoactivation protein-promoter binding noise is also a key player, but this circuit is the one that is less clearly sensitive to a single noise source, being sensitive to volume and gene switching as well. This type of results could lead to the design of novel genetic circuits, with tunable properties according to the noise characteristics of the environment they are inserted in.

All these results are relevant, but they could depend on parameter values. Although the parameters were chosen so that molecule numbers are similar and the relevant timescales are relatively close to each other, an extensive parameter exploration should be performed to generalize these results. It was not performed here because our method is computationally expensive and does not allow for a wide exploration. We could have explored an additional parameter set for each system, but that would not have provided a lot more information. Instead, one of several methods available for fast computation of MFPTs or transition rates should be used. Two such methods that would be suitable for this are Weighted Ensemble (Kromer et al., 2013; Donovan et al., 2013) which allows for a fast computation of equilibrium distributions and of switching rates, and Forward Flux Sampling (Allen et al., 2009) which does not facilitate so much the computation of equilibrium distributions but, besides allowing for fast computation of transition rates, also yields information of the transition pathways, giving an additional dimension to compare the systems and the effect each noise source has on them.

One last point that needs to be addressed is the apparent dependency of Global Stability Sensitivity with Global Stability at the reference point. This may actually give information of the dependency of Global Stability with noise. In an exponential, for instance it is natural to find that the slope of this function at a given point is proportional to the value of the function at the point. In a way, exponentials that are equal except for an offset in the vertical axis can also be interpreted as having an offset in the horizontal axis. Our case is clearly not exponential, though: consider that our proportional slopes are after taking the logarithm in both axes.

One could still think that, for a fair comparison of all five systems, the MFPT curves and the sensitivity should be normalized in some way to eliminate this effect. We, however, think that this is not the case for several reasons. First and foremost, dividing by the value at the Global Stability at the reference point does not eliminate this dependency, because the slopes shown are in logarithmic scale, and any normalization would need to a more complex function than just dividing, and therefore would need to *a priori* assume some general dependency of Global Stability with the parameters.

Furthermore, the parameters were chosen to avoid at least some of this effect, and if it remains that is a result by itself. Also, the picture in which the different functions would line up with a displacement in the horizontal axis is patently false here: the functions are actually qualitatively different. Lastly, normalizing by rescaling the horizontal axis or moving the reference point would be similar to changing the definition of each noise so that, rather than changing the parameters or timescales as we do here, we were changing the noise itself. However this, again, eliminates some of the information provided by our results (namely, the relationship of each parameter with the noise it generates). Furthermore, it is not an approach that has been used in previous studies.

This discussion only justifies not normalizing the different Global Stability curves and Sensitivities. The more general study discussed earlier in this section would also help to clear this point up, which highlights the importance of performing it as a continuation of this work.

Part III

Regulation of quiescence in plant stem cells

Chapter 4

Modelling a stem cell regulation genetic module

4.1 Introduction

This Chapter presents the modelling contribution to a study of a regulatory circuit of a specific type of stem cells in the root of the plant model organism *Arabidopsis thaliana*. First the experimental data on which the model herein formulated relies is presented. Afterwards, the model and its analysis, together with the experimental evaluation of a prediction of the model is presented. This work has been done with the experimental collaboration of the plant developmental biology group of Ana I. Caño-Delgado at the Center for Research in Agricultural Genomics (CRAG). Most of the work in this chapter has been published in a research paper (Vilarrasa-Blasi et al., 2014).

4.1.1 The stem cell niche of the root of *Arabidopsis thaliana*

Dynamical systems theory, as well as stochastic processes, have been widely used as a paradigm to describe and understand developmental processes, and in particular the processes of pluripotency maintenance or stem cell differentiation (Rué and Garcia-Ojalvo, 2013). The differentiation process has been classically

viewed as the evolution through a changing multistable landscape (Ferrell, 2012; Huang, 2012), but there are also studies that show that stem cells may be an excitable system, rather than a multistable one (Kalmar et al., 2009).

In this chapter we study a specific system of stem cells, set in the root of model plant *Arabidopsis thaliana* (hereafter *Arabidopsis*). *Arabidopsis* has the usual properties of model systems such as a short life cycle and size (Koornneef and Meinke, 2010), and the added benefits of a simple anatomic structure and a small genome size. Furthermore, its root is a system particularly amenable to study, due to its very simple structure (Dolan et al., 1993) and its transparency, which allows observation of its inner cells and use of fluorescence techniques through relatively simple microscopy methods.

Arabidopsis has two stem cell niches, one at the tip of the shoot and one at the tip of the root. These stem cell niches consist of a small group of pluripotent stem cells named the organizing centre, surrounded by groups of stem cells that are precursors to specific cell types or lineages (see Figure 4.1 for the root stem cell niche) (Scheres, 2007). These precursors are continuously dividing to give rise to the different cell types, whereas the organizing centre cells have their cell cycle arrested and rarely divide, remaining in what is called a quiescent state (Aichinger et al., 2012; Cheung and Rando, 2013). Whenever any stress or damage compromises the function of the surrounding stem cells the organizing centre, also called Quiescent Centre (QC), divides and replaces the damaged cells to ensure proper root growth (Aichinger et al., 2012). The Quiescent Centre is also responsible for the preservation of the identity of its sorrounding cells: if it is destroyed, the stem cells around it differentiate, losing stemness (Van den Berg et al., 1997).

There are many questions of joint physical and biological interest within this context. From a more physical point of view, cell types are often interpreted as being different attractors for the cellular system, and stem cells, with their complex relationship to cell types, offer an opportunity to study the dependence and emergence of these attractors from a complex network, the dynamical behaviours such as multistability or excitability that can be found within them or, at the tissue level, the emergence of patterns (Garcia-Ojalvo and Martinez Arias, 2012). These problems have their biological counterpart in how is cell differentiation regulated, how it can be controlled, and so on. Regarding the Quiescent Centre specifically, common biological questions are how its position

is determined, how it helps establish the order that sorrounds it, or how its quiescense is maintained and released when necessary. In this collaborative work, we seek to tackle these questions of biological interest and also to highlight their physical aspect.

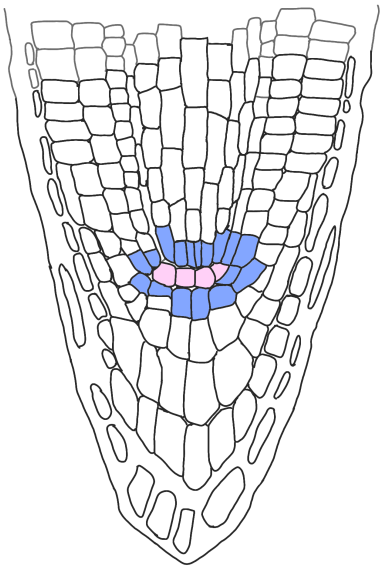

Figure 4.1 Root tip and stem cell niche of *Arabidopsis*. The light grey (pink in digital version) cells are the Quiescent Centre, and the dark grey (blue in digital version) cells sorrounding it are different types of stem cells.

4.1.2 BRAVO: A Brassinosteroid regulated cell specific repressor of divisions in the quiescent centre

All the work presented in this chapter is done in collaboration with the previously mentioned research group in *Arabidopsis thaliana* development, specialized in Brassinosteroid signaling. Hereby we summarize the research done by our collaborators which is the basis of our study as published in (Vilarrasa-Blasi et al., 2014). Brassinosteroids (BRs) are plant steroid hormones, analogue to animal steroids, that have been shown to be key regulators of plant growth and development (Caño-Delgado et al., 2010). Brassinosteroid signaling activates plasma membrane proteins such as BRI1, which trigger a cascade that promotes the dephosphorilation of transcription factors BES1 and BZR1, allowing them to

enter the nucleus and regulate DNA expression (Vert et al., 2005; Zhu et al., 2013). This pathway is well known, but how it regulates specific developmental events is an intense field of research.

It has been shown by our collaborators, and later confirmed by others, that BRs promote the division of the QC cells (González-García et al., 2011; Heyman et al., 2013). Since BR signaling components are expressed ubiquitously in the plant, it stands to reason that a mechanism exists in QC cells to counteract this signaling and preserve the low division rates of quiescence. A transcriptomic approach done by our collaborators identified a single protein of a known family of transcription factors (the MYB proteins), BRAVO (BRASSINOSTEROIDS AT VASCULAR AND ORGANIZING CENTER) that is expressed specifically in the QC (and in neighbouring vascular initial stem cells) and is transcriptionally regulated both by BES1 and BZR1 (Figure 4.2 A)(Vilarrasa-Blasi et al., 2014). Analysis of *bravo* loss-of-function mutants showed that QC divisions are dramatically increased when BRAVO is not functional, and no other phenotype is observed, indicating that BRAVO is a negative regulator of QC divisions (Vilarrasa-Blasi et al., 2014). These increased divisions are similar to those of plants treated with Brassinolide (BL), the most active BR compound, or of BES1 gain-of-function mutants (*bes1-D*), but these other plants also show altered cell cycle progression and differentiation in other parts of the root such as the meristem (González-García et al., 2011) (the region of rapidly dividing cells that is responsible for root growth). Furthermore, BL treated plants show QC divisions and a decrease in BRAVO expression (Vilarrasa-Blasi et al., 2014). Altogether, these data show that BRAVO, a target of BR signaling, is a QC specific repressor of cell division (Vilarrasa-Blasi et al., 2014).

The QC phenotype of the double mutant *bravo/bes1-D* indicated that BRAVO and BES1 regulation of QC divisions are not completely dependent on each other (i.e. they are at least partially independent), since double *bravo/bes1-D* mutants have increased divisions compared to both single mutants. The question arises then of how the BR signals and the effect of BRAVO are integrated into the final regulation of QC divisions. Transactivation assays show that BES1 strongly and directly represses BRAVO transcription, whereas BRAVO enhances its own production (Figure 4.2 B).

BES1 has been shown to heterodimerize with proteins of the MYB family,

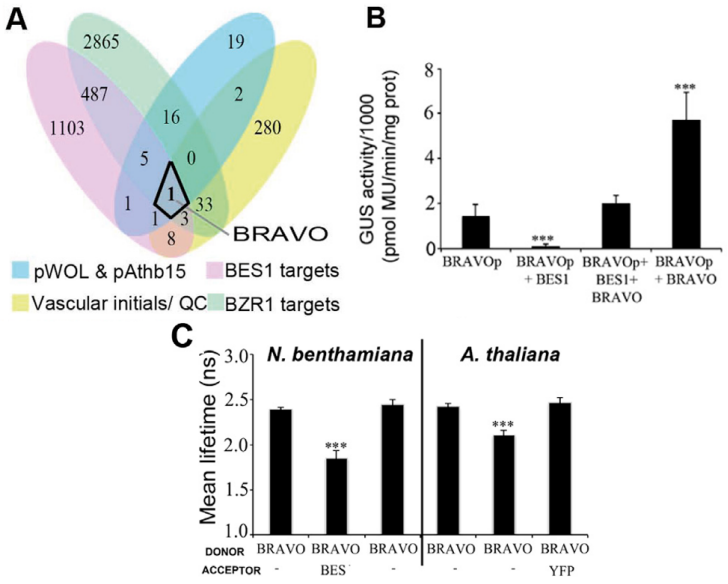

Figure 4.2 Experimental information about BRAVO and its interactions. **A** Venn diagram of up- or down- regulated genes in the QC and vascular initials according to different markers (yellow and blue) and of genes targeted by BES1 and BZR1 (pink and green) **B** Transactivation assays. GUS activity measures the transcription of the BRAVO promoter (BRAVOp) depending on what proteins are added. Notice how BES1 strongly represses activity, whereas BRAVO strongly activates it. **C** FRET-FLIM results. Bars show mean CPF lifetime. When BRAVO-CFP is coexpressed with BES1-YFP, the mean lifetime is reduced. In all cases, triple asterisks show that difference with control is statistically significant with $p < 0.001$. All panels and data are by our collaborators, and can be found in (Vilarrasa-Blasi et al., 2014). They are all also part of the Ph.D. thesis of Josep Vilarrasa-Blasi, (Vilarrasa-Blasi, 2014).

to which BRAVO belongs. Indeed, Fluorescence Resonance Energy Transfer-Fluorescence Lifetime Imaging Microscopy (FRET-FLIM) showed that BRAVO and BES1 interact, forming a heterodimer (Figure 4.2 C). Furthermore, in transactivation assays with both BES1 and BRAVO, BRAVO is expressed at the basal level, not affected by the repression by BES1 nor the activation by BRAVO (Figure 4.2 B). This may be due to dimerization of both proteins or due to how the joint transcriptional regulation is integrated. This is explored further in section 4.2.

It is unclear how all these elements come together to regulate quiescence, in particular how the apparently conflicting signals from BES1 and BRAVO are

integrated. We have participated in unraveling these questions with a continuous exchange with our collaborators, and one of its results is a mathematical model that sheds some light on the features of the BRAVO-BES1 mutual regulation and that we present in the following sections.

4.2 The BRAVO-BES1 module

4.2.1 Model derivation

To understand how the cross-regulations between BES and BRAVO integrate BR signaling to control QC divisions, we built a mathematical model that takes into account BRAVO-BES1 dimerization, BRAVO transcriptional control by BRAVO and BES1, and other details such as BES1 phosphorilation and dephosphorilation to represent BR signaling. However, we do not include details of how QC divisions are regulated downstream BRAVO and BES1. We also make one approximation: for simplicity, we consider only one binding site for BRAVO and another, non interfering one for BES1, despite there being more than one candidate site for each protein (Vilarrasa-Blasi, 2014). Our approximation is justified in the fact that BES1 seems to bind preferentially to one of these binding sites (Vilarrasa-Blasi, 2014), and in the assumption that more binding sites would not change results significantly. A cartoon of our model is shown in figure (Figure 4.3). All this can be represented by the following 17 chemical reactions:

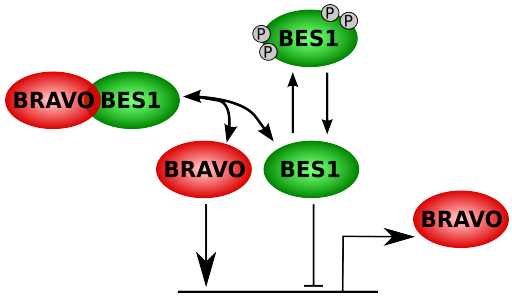

Figure 4.3 Cartoon of the elements included in our model: transcriptional repression of BRAVO by BES1, transcriptional autoactivation of BRAVO, BRAVO-BES1 dimer formation and BES1 dephosphorilation according to a signal. All degradations have been omitted for simplicity.

$$
\begin{aligned}
& D_1 + M \underset{k_{M+}}{\overset{k_{M-}}{\rightleftharpoons}} D_{1M} \quad ; \quad D_2 + B \underset{k_{B+}}{\overset{k_{B-}}{\rightleftharpoons}} D_{2B} \\
& D_1 + D_2 \xrightarrow{\alpha} D_1 + D_2 + M \\
& D_{1M} + D_2 \xrightarrow{\varepsilon_1 \alpha} D_{1M} + D_2 + M \\
& D_1 + D_{2B} \xrightarrow{\varepsilon_2 \alpha} D_1 + D_{2B} + M \\
& D_{1M} + D_{2B} \xrightarrow{\varepsilon_3 \alpha} D_{1M} + D_{2B} + M \\
& B \underset{k_{P-}}{\overset{k_{P+}}{\rightleftharpoons}} B_d \\
& M \xrightarrow{d_M} \varnothing \\
& \varnothing \xrightarrow{\beta} B \xrightarrow{d_B} \varnothing \\
& B_d \xrightarrow{d_{B_d}} \varnothing \\
& M + B_d \underset{k_{D+}}{\overset{k_{D-}}{\rightleftharpoons}} C \xrightarrow{d_C} \varnothing
\end{aligned}
\tag{4.1}
$$

Where M represents BRAVO (M stands for MYB, the family of proteins to which it belongs), B represents BES1, B_d is dephosphorilated (active) BES1 and C is the BES1-BRAVO heterodimer. We have also assumed independent binding sites for BRAVO and BES1 in the BRAVO promoter (D_1 and D_2 respectively). Explicit mRNA dynamics with linear mRNA degradation and protein production proportional to mRNA concentration have been omited for simplicity, and are included in the parameter α which includes all these steps in protein production. α is the basal rate of production when no transcriptional regulation occurs, and the different ε parameters represent the ratio between basal and regulated production. Therefore, ε will be $\varepsilon > 1$ when transcription is activated and $\varepsilon < 1$ when transcription is repressed.

Using mass action kinetics, we can translate these reactions into the following six ordinary differential equations, where $\dot{x}$ stands for the time derivative of x:

$$
\begin{aligned}
\dot{D}_1 &= k_{M-}D_{1M} - k_{M+}MD_1; \quad D_1 + D_{1M} = D_{tot1} \\
\dot{D}_2 &= k_{B-}D_{2B} - k_{B+}B_dD_2; \quad D_2 + D_{2B} = D_{tot2} \\
\dot{M} &= \alpha\left(D_1D_2 + \varepsilon_1 D_{1M}D_2 + \varepsilon_2 D_1 D_{2B} + \varepsilon_3 D_{1M}D_{2B}\right) + k_{M-}D_{1M} \\
&\quad - k_{M+}MD_1 - k_{D+}MB_d - d_M M \\
\dot{B}_d &= k_{p-}B + k_{B-}D_{2B} + k_{D-}C - k_{P+}B_d - k_{B+}B_dD_2 - k_{D+}MB_d - d_{B_d}B_d \\
\dot{B} &= \beta + k_{p+}B_d - k_{p-}B - d_B B \\
\dot{C} &= k_{D+}MB_d - k_{D-}C - d_C C
\end{aligned}
\tag{4.2}
$$

Assuming that binding and unbinding of proteins to DNA is much faster than the other reactions of the system, it is straightforward to reduce equations (4.2) to four equations, obtaining:

$$
\begin{aligned}
\dot{M} &= \alpha D_{tot1}D_{tot2}\frac{1 + \varepsilon_1 K_M M + \varepsilon_2 K_B B + \varepsilon_3 K_M K_B MB}{1 + K_M M + K_B B + K_M K_B MB} + k_{D-}C - k_{D+}MB_d - d_M M \\
\dot{B}_d &= k_{p-}B + k_{D-}C - k_{P+}B_d - k_{B+}B_dD_2 - d_{B_d}B_d \\
\dot{B} &= \beta + k_{p+}B_d - k_{p-}B - d_B B \\
\dot{C} &= k_{D+}MB_d - k_{D-}C - d_C C
\end{aligned}
\tag{4.3}
$$

where $K_M = \dfrac{K_{M+}}{K_{M-}}$ and $K_B = \dfrac{K_{B+}}{K_{B-}}$ are the equilibrium constants of BRAVO and BES1 binding to the BRAVO promoter. Although we have dynamic equations, we only studied the steady states, by setting all derivatives $\frac{dx}{dt} = 0$ and solving the corresponding system of equations numerically, through Mathematica software (Wolfram Research, 2010).

4.2.2 Parameter determination

For most of the parameters in this model, we had little information about their values, so we needed to choose them somehow arbitrarily. However, the transactivation data shown in Figure 4.2 B contains information about the relative

rates of BRAVO transcription depending on the different regulation modes. Therefore, we first tried to extract numerical information from this experiment.

In this assay, purified BRAVO and/or BES1 proteins are introduced in Tobacco (*N. benthamiana*) leaves containing the BRAVO promoter copied from *Arabidopsis*, and its transcription is measured through the activity of the GUS reporter (Froidure et al., 2010). We modeled the behaviour of this measured GUS activity, to be able to fit it to the parameters of our model. We assumed a linear degradation of Gus activity, and assumeed negligible degradations of B_d (active BES1), M (BRAVO) and their heterodimer (their total amounts are therefore constant). Gus production is proportional to that of M. Therefore, the set of equations we used is:

$$\begin{aligned} \dot{D_1} &= k_{M-} D_{1M} - k_{M+} M D_1; \quad D_1 + D_{1M} = D_{tot1} \\ \dot{D_2} &= k_{B-} D_{2B} - k_{B+} B D_2; \quad D_2 + D_{2B} = D_{tot2} \\ \dot{Gus} &= \alpha \left(D_1 D_2 + \varepsilon_1 D_{1M} D_2 + \varepsilon_2 D_1 D_{2B} + \varepsilon_3 D_{1M} D_{2B} \right) - deg_{Gus} Gus \end{aligned} \tag{4.4}$$

According to this, the stationary value of Gus concentration, Gus^{st}, would be

$$Gus^{st} = \frac{\alpha D_{tot}^2}{deg_{Gus}} \frac{1 + \varepsilon_1 K_M M^{st} + \varepsilon_2 K_B B^{st} + \varepsilon_3 K_M K_B M^{st} B^{st}}{1 + K_M M^{st} + K_B B^{st} + K_M K_B M^{st} B^{st}}, \tag{4.5}$$

where we have considered that $D_{tot1} = D_{tot2} = D_{tot}$. Now, for the basal activity of the assays (first column in Figure 4.2), we take eq. (4.5) with $M^{st} = B^{st} = 0$, and we obtain

$$Gus^{st}_{basal} = \frac{\alpha D_{tot}^2}{deg_{Gus}} = A_0, \tag{4.6}$$

where $A_0 = 1500 \pm 400$. Now we can compare this basal Gus to each of the transcriptionally regulated values, by substituting M^{st} and B^{st} by 0 or M_{tot}, B_{tot} in equation (4.5) according to the experimental conditions of each datapoint:

$$\frac{Gus^{st}_{M}}{Gus^{st}_{basal}} = \frac{1+\varepsilon_1 K_M M_{tot}}{1+K_M M_{tot}} = A_1 \tag{4.7}$$

$$\frac{Gus^{st}_{B}}{Gus^{st}_{basal}} = \frac{1+\varepsilon_2 K_B B_{tot}}{1+K_B B_{tot}} = A_2 \tag{4.8}$$

Where $Gus^{st}_{M,B}$ is Gus^{st} when only M (BRAVO) and B (BES1) are present, respectively, and Gus^{st}_{basal} corresponds to the control, without introduction of any protein. We therefore obtain $A_1 = 3.9 \pm 1.9$ by comparing the last and first columns in Figure 4.2 B. Notice that this sets the dependence between two parameters ε_1 and $K_M M_{tot}$, with the lower bounds $\varepsilon_1 \geq 3.9$ and $K_M M_{tot} \geq 0$. If $K_M M_{tot} \geq 10$ then $\varepsilon_1 \approx 3.9$. Something similar happens with $A_2 = 0.07 \pm 0.18$. We obtain the bounds $\varepsilon_2 \leq 0.07$ and $K_B B_{tot} \geq 13.28$. When $K_B B_{tot} \geq 100$, $0.06 \leq \varepsilon_2 \leq 0.07$.

When both *BES1* and *BRAVO* are present, we obtain

$$\frac{Gus^{st}_{M+B}}{Gus^{st}_{basal}} = \frac{1+\varepsilon_1 K_M M^{st} + \varepsilon_2 K_B B^{st} + \varepsilon_3 K_M K_B M^{st} B^{st}}{1+K_M M^{st} + K_B B^{st} + K_M K_B M^{st} B^{st}} = A_3 \tag{4.9}$$

where

$$B^{st} = \frac{B_{tot}}{1+\dfrac{k_{D+}}{k_{D-}} M^{st}} \quad ; \quad M^{st} = \frac{M_{tot}}{1+\dfrac{k_{D+}}{k_{D-}} B^{st}} \tag{4.10}$$

and $A_3 = 1.4 \pm 0.6$. Here we assumend that M_{tot} and B_{tot} are the same for all datapoints. But because the system is overdetermined, there is a wide range of values for the system parameters compatible with this A_3. To choose one set of parameter values we defined an Euclidean norm for the distance between de results of this simple model for GUS activity and the measured values (as shown in (Ashyraliyev et al., 2009)):

$$V_{MLE} = \sum_{i=1}^{n} \frac{\left(Gus^{st}(parameters, M_{tot}, B_{tot}) - Gus_i^{measured}\right)^2}{\sigma_i^2} \tag{4.11}$$

Because information about the exact quantities M_{tot}, B_{tot} used in the experiments was unavailable, but were known to be large, we chose $B_{tot} = M_{tot} = 100\,\mathrm{nM}$. We then minimized this norm using Mathematica Software (Wolfram Research, 2010), obtaining $\varepsilon_1 = 3.9$, $\varepsilon_2 = 0.068$, $\varepsilon_3 = 1.353$, $K_M = 72.66\,\mathrm{nM}^{-1}$, $K_B = 82.06\,\mathrm{nM}^{-1}$, $K_D = k_{D+}/k_{D-} = 164.76\,\mathrm{nM}^{-1}$, with $V_{MLE} = 1.85 \times 10^{-5}$. Since eqs. (4.3) depend also on k_{D+} and k_{D-} we set them as $k_{D+} = 329.52\,\mathrm{h}^{-1}\,\mathrm{nM}^{-1}$ and $k_{D-} = 2\,\mathrm{h}^{-1}$ which satisfies the equilibrium constant determined by the fitting.

Due to the overdetermination of the system, this is still only one of the large number of parameter sets that can reproduce the experimental values and yield small values of $V_{MLE} < 10^{-4}$ (Figure 4.4). Furthermore, our arbitrarily chosen M_{tot}, B_{tot} also give an additional constraint to the parameters, in particular to the binding constants K_M and K_B, which could take many values. However, the parameters yielded by the fitting mean that both binding sites are close to their saturation regime, meaning that our results are valid as long as the actual binding constants are large enough.

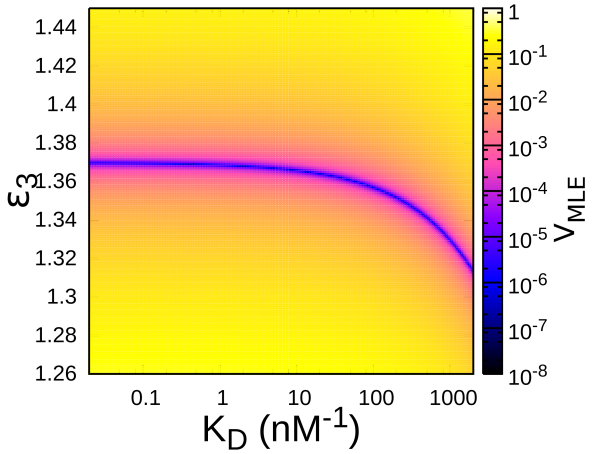

Figure 4.4 Value of V_{MLE} (colormap) as a function of ε_3 and $K_D = k_{D+}/k_{D-}$, for the other parameters as obtained by the fitting. Notice how there is a very large number of ε_3,K_D pairs that yield similarly low values. In color in digital version.

The rest of the parameters were chosen within biologically reasonable ranges, and are: $D_{tot1} = D_{tot2} = 0.6\,\mathrm{nM}$, $\alpha = 3\,\mathrm{nM\,h}^{-1}$, $\beta = 3\,\mathrm{nM\,h}^{-1}$, $d_M = d_B = d_C = 0.02\,\mathrm{h}^{-1}$, $d_{B_d} = 0.002\,\mathrm{h}^{-1}$, $k_{P+} = 0.01\,\mathrm{h}^{-1}$ and $k_{P-} = 0.002\,\mathrm{h}^{-1}$.

4.3 Results

4.3.1 Model results

When we analyzed the steady states of the system for these parameters, we found that it is bistable (Figure 4.5 A) . This is not surprising, since our module can be interpreted as a combination of the AAC and MFL circuits explored in Chapter 2. Furthermore, the circuit robustly drives two distinct states where the amounts of free BRAVO and free dephosphorilated BES1 are strongly opposed (Figure 4.5 A) and are either [HIGH BRAVO, LOW BES1] or [LOW BRAVO, HIGH BES1] that are preserved for total BRAVO (Figure 4.5 C) but not so much for total BES1 (Figure 4.5 D). At very low values of BR signaling, represented by the dephosphorilation rate k_{P-}, only the [HIGH, LOW] state exists, whereas at high values of it only the [LOW, HIGH] state is stable. This allows the system to sharply switch from one state to the other. Since apparently, as we explained in section 4.1.2, BRAVO and BES1 regulate QC divisions somewhat independently, this makes biological sense: strongly opposed states, together with a sharp transition, would ensure that there is a clear signal telling the QC whether it should divide or not, avoiding harder to interpret intermediate signaling levels.

To evaluate robustness of these results and see the relevance of the different reactions and parameters, we explored parameter spaces, varying parameters pairwise. These show that, while the right combination of values for the different transcriptional regulations ε is important, dimerization is key both for bistability and for the strongly opposed states (Figures 4.5 B and 4.6 A,C,D). This indicates that dimerization is the main element driving nonlinearity in this system. Beyond this, bistability and two distinct, opposed states are quite robust to changes of several orders of magnitude in several parameters (Figure 4.6).

We also performed a sensitivity analysis by varying several parameters in the same proportion (1%) and measuring the change in the BRAVO steady state. We found that for high phosphorilation values, the state is sensitive to several parameters. This is not expected to be very relevant, though, since this state has negligible amounts of BRAVO and therefore changes to it are not expected to be important (Figure 4.7).

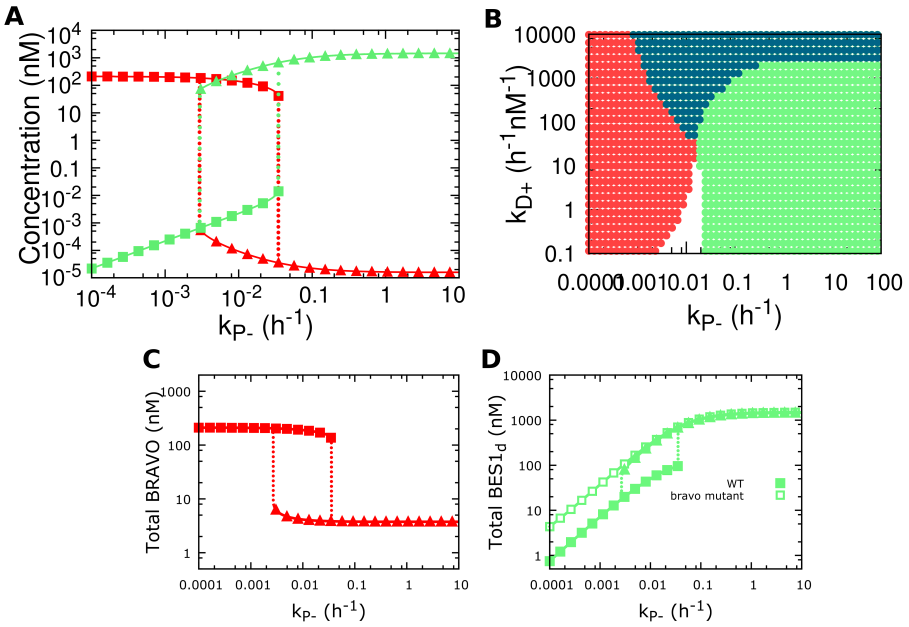

Figure 4.5 The BRAVO-BES1 model enables bistability. **A** Amounts of BRAVO (dark grey, red in digital version) and free dephosphorilated BES1 (light grey, green in digital version) as a function of BES1 dephosphorilation rate k_{P-}. When free BRAVO is at high amounts, free dephosphorilated BES1 is almost absent. This [HIGH,LOW] state is represented by squares. Similarly, when free dephosphorilated BES1 is in high amounts, free BRAVO is almost absent. This [LOW, HIGH] state is represented by triangles. Lines with symbols represent the stable steady states of the system. Dotted lines only represent the sharp transition that occurs when one state disappears. **B** BRAVO and BES1 as a function of k_{P-} and dimerization rate k_{D+}. Colored regions correspond to where BES1 and BRAVO that differ by at least one order of magnitude. The light grey (green in digital version) region corresponds to the [LOW,HIGH] state, darker grey (red in digital version) region corresponds to the [HIGH,LOW] state, and darkest grey (blue in digital version) region is bistable. **C** As **A** but with total amounts of BRAVO. Notice how sharp transition and opposed states are maintained but are separated by less than 2 orders of magnitude, whereas in panel **B** there is a separation of 7 orders of magnitude. **D** As panel **B** but with total amounts of dephosphorilated BES1. Empty squares represent total dephosphorilated BES1 when there is no BRAVO production. In color in digital version.

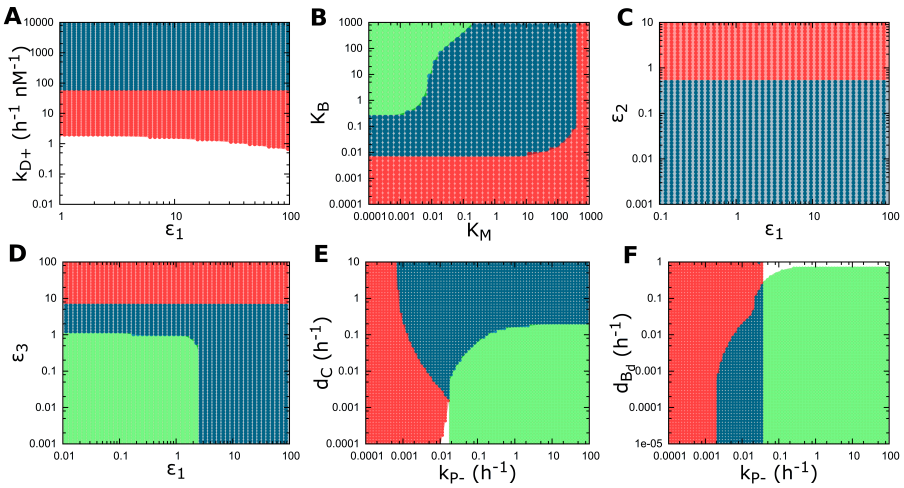

Figure 4.6 Strongly opposed states and bistability are compatible with large ranges of parameter values. Colored areas (red, green and blue) correspond to those parameter regions where the free BRAVO and free dephosphorylated BES1 stable stationary amounts differ in one or more orders of magnitude (i.e. their ratio is 10 or larger). In these regions we can define the stable states of (free BRAVO, free dephosphorylated BES1) as (HIGH,LOW) (dark grey areas,red in digital version) and (LOW,HIGH) (light grey areas, green in digital version). Bistable parameter regions with two stable states (HIGH, LOW) and/or (LOW, HIGH) are denoted in darker grey (blue in digital version). White stands for those regions where the amounts of free BRAVO and free dephosphorylated BES1 differ in less than one order of magnitude. Parameter space of **A** BRAVO auto-activation strength (ε_1) and dimerization rate (k_{D+}) of BRAVO with dephosphorylated BES1, **B** the equilibrium constants of binding/unbinding reactions of the BRAVO promoter with BRAVO (K_M) and with dephosphorylated BES1 (K_B), **C** strengths of BRAVO auto-production (ε_1) and dephosphorylated BES1-mediated production of BRAVO (ε_2), **D** strengths of BRAVO auto-production (ε_1) and production jointly regulated by BES1 and BRAVO(ε_3), **E** heterodimer degradation rate (d_C) and dephosphorylation rate (k_{P-}) and **F** dephosphorylated BES1 degradation rate (d_{Bd}) and dephosphorylation rate (k_{P-}). All remaining parameter values as specified in section 4.2.2. In color in digital version.

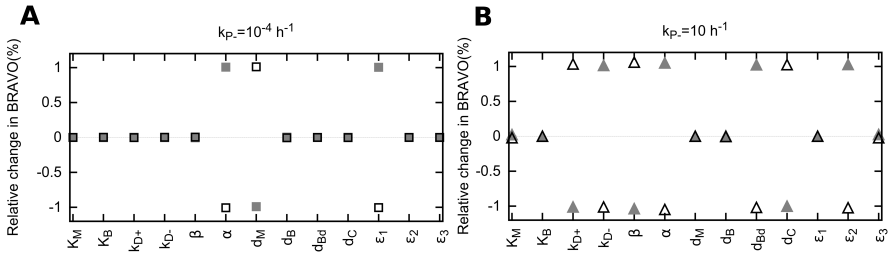

Figure 4.7 Sensitivity analysis measuring the relative change in the stable stationary amount of free BRAVO when a parameter is increased (filled symbol) or decreased (empty symbol) in 1% for **A** low dephosphorylation rates $k_{P-} = 10^{-4}h^{-1}$, i.e. in the (HIGH,LOW) state of (free BRAVO, free dephosphorylated BES1) and **B** higher dephosphorylation rates $k_{P-} = 10h^{-1}$, i.e. in the (LOW,HIGH) state of (free BRAVO, free dephosphorylated BES1). In B, free BRAVO amounts are rather sensitive to several parameter values. Yet, for this high dephosphorylation rates, the amount of free BRAVO is in all cases negligible compared to that in low dephosphorylation rates (see Fig. 4.5).

Finally, we explored whether our conclusions are robust to changing some of our initial assumptions. To this end, we challenge one of our implicit hypotheses, namely that the dimer is inactive and does not bind to DNA. So, instead, we include the possibility that the dimer binds either to the BRAVO or to the BES1 binding site in the BRAVO promoter. This is not unwarranted, since other MYB transcription factors have been shown to dimerize with BES1 and jointly regulate DNA (Li et al., 2009). We considered two variants of the model that extend it with three more reactions:

$$D_1 + C \underset{k_{1C+}}{\overset{k_{1C-}}{\rightleftharpoons}} D_{1C} \qquad (4.12)$$
$$D_{1C} + D_2 \xrightarrow{\varepsilon_{1C}\alpha} D_{1C} + D_2 + M; \quad D_{1C} + D_{2B} \xrightarrow{\varepsilon_3\alpha} D_{1C} + D_{2B} + M$$

when the complex binds to the *BRAVO* binding site, and

$$D_2 + C \underset{k_{2C+}}{\overset{k_{2C-}}{\rightleftharpoons}} D_{2C} \qquad (4.13)$$
$$D_1 + D_{2C} \xrightarrow{\varepsilon_{2C}\alpha} D_1 + D_{2C} + M; \quad D_{1M} + D_{2C} \xrightarrow{\varepsilon_3\alpha} D_{1M} + D_{2C} + M$$

when the complex binds to the *BES1* binding site. We did not explore the possibility of the complex being compatible with both sites.

The parameters are a straightforward analogue to the original model, and we also define the equilibrium constant of the binding and unbinding of the complex to DNA as $K_{C1} = k_{C1+}/k_{C1-}$ and $K_{C2} = k_{C2+}/k_{C2-}$, for each site respectively. Notice how, for simplicity, we have assumed that the production rate of BRAVO is always the same when the promoter is fully occupied, regardless of whether the complex binds to the BRAVO binding site D_1 or the BES1 binding site D_2, and regardless of the function done by the complex when it is alone.

This means that ε_3 is always the same for all cross terms of two different proteins bound to the promoter. Therefore, the only new parameters are K_{C1}, ε_{C1} in one case and K_{C2}, ε_{C2} in the other. All the other parameter values are as in section 4.2.2. We explored different values for the couples of free parameters $(K_{C\{1,2\}}, \varepsilon_{C\{1,2\}})$, and found that although the bistable region is diminished and in some cases destroyed, the properties of having a [HIGH,LOW] and a [LOW,HIGH] states with strongly opposed amounts of BRAVO and BES1 and a sharp transition between them holds (Figure 4.8).

4.3.2 Experimental testing of model predictions

Our model yields certain predictions. The strongest and more easily testable one is that there is a sharp transition from a high BRAVO to a low BRAVO concentration at a BR signaling threshold. We designed an experiment to test this prediction. For that, our collaborators planted *Arabidopsis* seeds in media containing different concentrations of Brassinolide (BL), which activates BR signaling and therefore has an indirect relationship to our activation parameter k_{P-}. Assuming a linear dependence between BL concentration and k_{P-}, the model predicts a sharp transition. These seeds contained the construct *pBRAVO:GFP*, meaning that Green Fluorescent Protein is expressed with the same regulations as BRAVO, but does not share its post-transcriptional regulations, such as dimerization with BES1, nor its degradation rate, which is much slower for GFP. It would therefore correspond to total BRAVO rather than free BRAVO in our model, but recall that total BRAVO also has a sharp transition, as can be seen in Figure 4.5 C. They then took confocal microscopy images of the root tips of these plants when the seedlings were 6 days old, and we quantified the fluorescence of each individual QC cell. This yielded an ultrasensitive curve (meaning that it fits a Hill function of cooperativity larger than 1) of

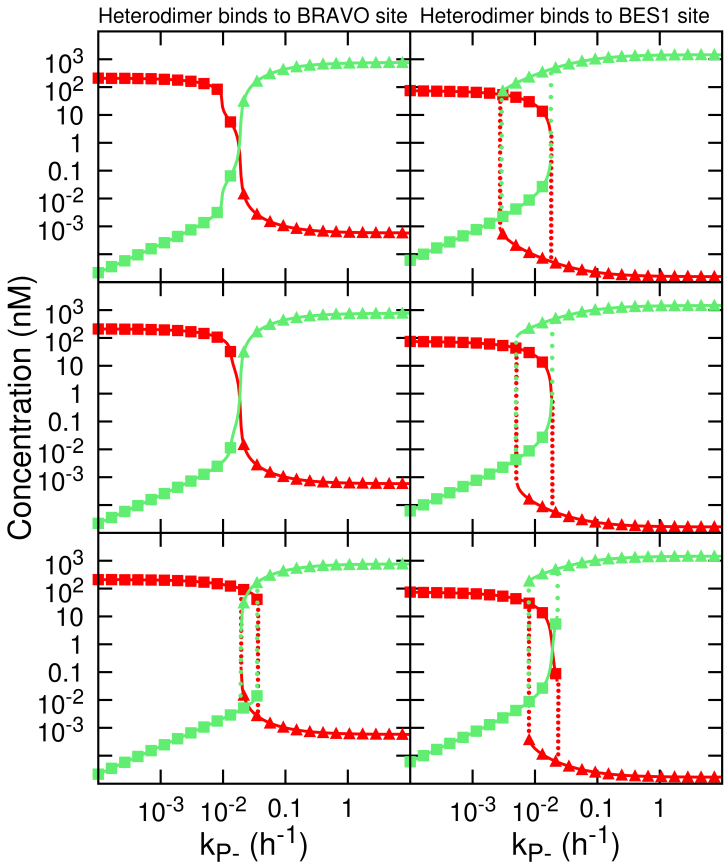

Figure 4.8 Bifurcation diagrams when complex is active. As in figure 4.5, squares represent the [HIGH,LOW] state and triangles represent the [LOW,HIGH] state.The different scenarios are: (Left) The heterodimer binds to the DNA at the BRAVO binding site [Eqs. (4.12)]; (Right) The heterodimer binds to the DNA at the BES1 binding site [Eqs. (4.13)]; The heterodimer (Top) represses, (Middle) drives at basal rate or (Bottom) activates BRAVO transcription when it is the only element bound to the promoter. In all cases, a switch is found. Parameter values as in B with (Left) $K_{C1} = K_M$ and (Top) $\varepsilon_{1C} = 0.1$, (Middle) $\varepsilon_{1C} = 1$, (Bottom) $\varepsilon_{1C} = \varepsilon_1 = 3.9$; (Right) $K_{C2} = K_B$ and (Top) $\varepsilon_{2C} = \varepsilon_2 = 0.068$, (Middle) $\varepsilon_{2C} = 1$, (Bottom) $\varepsilon_{2C} = 2$.

mean fluorescence versus BL concentration (Figure 4.9), with a threshold at an external BL concentration $BL = 2.7 \times 10^{-3}$nM.

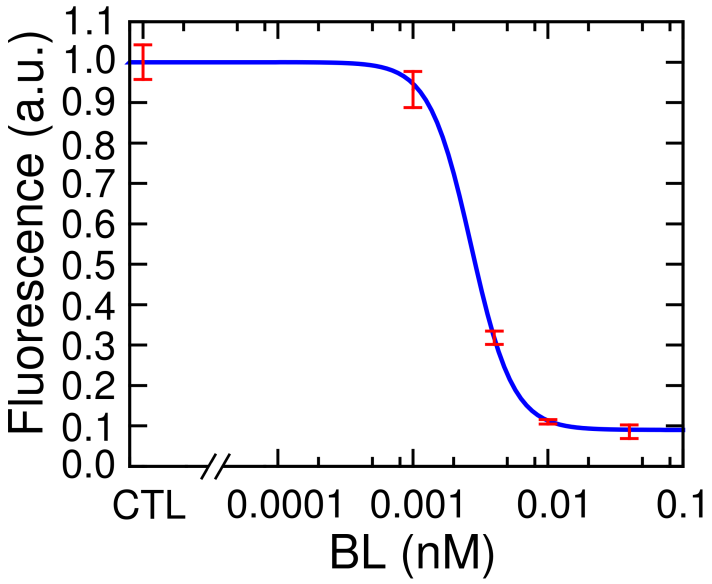

Figure 4.9 *pBRAVO:GFP* expression in QC cells as a function of BL concentration. Points stand for mean fluorescence per QC cell averaged over n ($18 < n < 100$) QC cells of 6-day-old seedlings continuously treated at each indicated concentration of BL. Data from two experiments. s.e.m is indicated as error bars. Fluorescence (in arbitrary units) has been normalized to the control (CTL) average fluorescence. The curved line represents the function $y = 1 - \frac{0.91x^h}{x^h + 0.0027^h}$ with $h = 2.8$ and x representing with and is the BL concentration, denoting the ultrasensitive response of *pBRAVO:GFP* response to BL.

4.4 Discussion

The experimental work of our collaborators, that discovered the novel transcription factor BRAVO and showed, for the first time, a gene that linked Brassinosteroids to regulation of quiescence, is extremely relevant and informative by itself. Nevertheless, it left some questions partly unanswered. Namely, what

are the key interactions between BES1 and BRAVO (among the ones experimentally observed) and how do they come together for BRAVO and BES1 to regulate quiescence with their antagonic functions of repressing and activating divisions.

Our mathematical model highlights that mutual repression through dimerization is key for a sharp transition between two states of strongly opposed BES1 and BRAVO, either through bistability or through ultrasensitivity. Furthermore, we showed that this holds under a variety of conditions, such as different regulation modes of BRAVO and for wide ranges of parameters.

Although we were unable to design an experiment to test the assertion that the dimer is essential for this sharp transition, we were able to test other predictions for the model. In particular, a signal-response curve of BRAVO production against BR signaling indeed showed a very sharp transition. However, since the relationship of the BR signaling in the experiment and our k_{P-} is not completely determined, further experiments are needed to test the predictions of the model, such as a precise measurement of this relationship.

To test the bistability predicted by the model, an experiment could be done to show hysteretic behaviour, which would mean that the response of the system is dependent on its history. This behaviour is particular to the bistability arising from our model. In our case, if at time $t = 0$ a QC senses a very high BR signaling and this signaling is decreased, the cells will only switch states if it is decreased further than a threshold (in Figure 4.5, at $k_{P-} \simeq 2\times10^{-3}$), whereas if at time $t = 0$ the QC cells sense a very low BR signaling that is then increased, the threshold that needs to be reached will be much higher (in Figure 4.5, at $k_{P-} \simeq 3 \times 10^{-2}$).

This could be done in our plants, in principle, with a setup similar to our previous experiment: plants could be grown at very high or very low BL concentrations, and then changed to media containing other, intermediate concentrations. If the system is bistable the fluorescence curve should mimic the free BRAVO curve in Figure 4.5. In reality, however, this experiment is technically complex, because there are different timescales involved, such as the response time of the observed GFP when changing the signal, the timescale of division, and so on, that complicate the specific design of the experiment. Furthermore, high BL concentrations affect the plant in many more ways than the division of the QC,

introducing a confounding factor. The first experimental design done by our collaborators and ourselves involved growing plants for 4 days in the starting medium, then changing them and measuring them two days later. The results were quite unclear, with part of a response that did not seem hysteretical but also with a memory effect at big signalling changes. In the future, the experiment design should be refined and new trials done to conclude whether this experimental approach is useful or must be discarded.

Altogether, our model answers the questions of how BRAVO and BES1 coordinate to act in concert and not give conflicting signals to the Quiescent Centre. However, it does not shed any light on how quiescence is regulated downstream this module, beyond the fact (concluded directly from experiments) that BRAVO signaling does not go through BES1 nor does BES1 signaling go through BRAVO. This has been, and will certainly be in the future, a matter of intense study.

Chapter 5

Regulation of quiescence by the WOX5 transcription factor

5.1 WOX5, another key player in quiescence regulation

The module shown in Chapter 4 showed how BES1 and BRAVO are always strongly opposed to not give conflicting signals to quiescence regulation. It remained to be elucidated how our module was related to transcription factor WOX5 (WUSCHEL HOMEOBOX 5), a QC marker which participates in the function of the Quiescent Centre as an organizer by preserving the stem cell identity of neighbouring cells (Haecker et al., 2004; Sarkar et al., 2007). In addition, showrt after our results were published, WOX5 was linked to quiescence maintenance through repression of Cyclin D, a protein responsible for the transition from G1 to S phase (Forzani et al., 2014). This shows an overlapping function of WOX5 and BRAVO. Furthermore, our collaborators had already shown in (Vilarrasa-Blasi et al., 2014) that BRAVO activates WOX5.

The common function and regulatory link between WOX5 and BRAVO suggests that WOX5 could also be a player in the BES1-BRAVO module, acting all

together to regulate quiescence. For this reason, we decided to study our module with the inclusion of WOX5.

5.1.1 Experimental evidences

We summarize here the first experimental evidences relating WOX5, BRAVO and BES1, obtained by our collaborators led by Ana I. Caño-Delgado. The first of these results is that BRAVO activates WOX5 (Vilarrasa-Blasi et al., 2014). This is known because when pWOX5:GFP is crossed with BRAVO mutant *bravo*, fluorescence goes down dramatically (Figure 5.1 A,B). It was also found by our collaborators that WOX5 promotes BRAVO expression. This is seen both by decreased expression of BRAVO in WOX5 mutants, and because WOX5 induced overexpression outside the QC (through specific lines, that allow to overexpress WOX5 upon treatment of hormone Dexamethasone) leads to BRAVO expression alongside it (Vilarrasa-Blasi, 2014).

Finally, BES1 also activates WOX5. This was shown by several results. The first of them is that BL treatment triggered WOX5 expression in cells that do not have it in normal conditions (i.e. non-QC cells) (González-García et al., 2011). The second of them is that, although BRAVO expression decreased in the gain of function mutant bes1-D, WOX5 expression did not (Figure 5.1 C-E) (Vilarrasa-Blasi et al., 2014). Lastly, an unpublished experiment by our collaborators showed, through Chromatin immunoprecipitation (ChIP) and PCR, that BES1 directly binds to the promoter of WOX5 and activates it.

5.1.2 The extended model

To analyze this system, we built on the model presented in section 4.2 to include all the additional experimentally deduced interactions between WOX5 and BRAVO or BES1. We made, however, additional assumptions to constrain the complexity of the model. Firstly, we did not assume independent binding sites for all transcription factors that regulate BRAVO (BRAVO itself, BES1, and WOX5), because that would generate seven parameters for the differential production rates, plus the three binding strengths. Instead, we considered a single binding site for all three proteins, thus restricting the number of parameters for the regulated production rates to three. Recall, from section 4.2, that

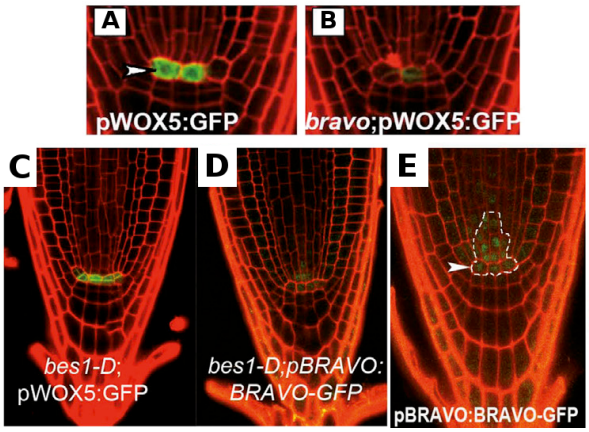

Figure 5.1 Experimental evidence of WOX5 interactions. **A-B** BRAVO mutant shows decreased WOX5 expression. **A** WOX5 promoter activity in wild type plant shown by fluorescence. Arrow indicates QC cells. **B** WOX5 promoter activity shown by fluorescence in BRAVO mutant. C-E. *bes1-D* shows decreased expression of BRAVO but not WOX5. **C** Wox5 promoter activity in gain of function mutant *bes1-D*. **D** BRAVO expression in plants with additional pBRAVO:BRAVO-GFP (These have double the amount of BRAVO, the one corresponding to the native promoter plus the BRAVO tagged with GFP) **E** pBRAVO:BRAVO-GFP in *bes1-D* gain of function background. All figures from (Vilarrasa-Blasi et al., 2014).

the original two independent binding sites were already an approximation. We are now making the alternative assumption that the two binding sites are interacting and exclusive. In any case, as it will be shown, our results suggest that this simplification is not crucial.

Regarding the regulation of WOX5, we made two different hypotheses. The fact that both increases of BES1 and BRAVO can lead to increased WOX5 can seem paradoxical, since free BES1 and free BRAVO are always strongly opposed. There are two possible explanations for this. Either both BRAVO and BES1 regulate WOX5 independently, and in the experimental data one regulator is a strong enough activator and in large enough quantities to compensate for the absence of the other, or both BES1 and BRAVO, together as a complex, activate WOX5 expression. The complex is a good candidate for regulation because, as explained in section 4.3.1, this type of complexes are already known to bind to DNA and regulate gene expression. In the first case, we made the same approximation as for the BRAVO promoter: there is a single binding site

for both transcription factors. In the second case, there is naturally only one binding site, as there is only one activator molecule.

With this, we can derive the set of differential equations for both systems. We omit the step of writing the chemical reactions, as they are analogous to (4.1), as is the derivation of differential equations from them. The equations for the system when WOX5 is regulated by BES1 and BRAVO independently read:

$$
\begin{aligned}
\dot{D_{MM}} &= k_{MM+}MD_M - k_{MM-}D_{MM}; \quad D_M + D_{MM} + D_{MB} + D_{MW} = D_{totM} \\
\dot{D_{MB}} &= k_{MB+}B_dD_M - k_{MB-}D_{MB}; \quad \dot{D_{MW}} = k_{MW+}WD_M - k_{MW-}D_{MW} \\
\dot{D_{WM}} &= k_{WM+}MD_W - k_{WM-}D_{WM}; \quad D_W + D_{WM} + D_{WB} = D_{totW} \\
\dot{D_{WB}} &= k_{WB+}B_dD_W - k_{WB-}D_{WB} \\
\dot{M} &= \alpha\left(D_M + \varepsilon_M MD_{MM} + \varepsilon_M BD_{MB} + \varepsilon_M WD_{MW}\right) + k_{D-}C + k_{MM-}D_{MM} \\
&\quad + k_{WM-}D_{WM} - k_{MM+}MD_M - k_{WM+}MD_W - k_{D+}MB_d - d_MM \\
\dot{B}_d &= k_{p-}B + k_{MB-}D_{MB} + k_{WB-}D_{WB} + k_{D-}C - k_{P+}B_d - k_{MB+}B_dD_M \\
&\quad - k_{WB+}B_dD_W - k_{D+}MB_d - d_{B_d}B_d \\
\dot{B} &= \beta + k_{p+}B_d - k_{p-}B - d_BB \\
\dot{W} &= \gamma\left(D_W + \varepsilon_{WM}D_{WM} + \varepsilon_{WB}D_{WB}\right) - d_WW \\
\dot{C} &= k_{D+}MB_d - k_{D-}C - d_CC.
\end{aligned}
\tag{5.1}
$$

And when it is regulated by the BRAVO-BES1 complex,

$$
\begin{aligned}
\dot{D_{MM}} &= k_{MM+}MD_M - k_{MM-}D_{MM}; \quad D_M + D_{MM} + D_{MB} + D_{MW} = D_{totM} \\
\dot{D_{MB}} &= k_{MB+}B_dD_M - k_{MB-}D_{MB}; \quad \dot{D_{MW}} = k_{MW+}WD_M - k_{MW-}D_{MW} \\
\dot{D_{WC}} &= k_{WC+}CD_W - k_{WC-}D_{WC}; \quad D_W + D_{WC} = D_{totW} \\
\dot{M} &= \alpha\left(D_M + \varepsilon_M MD_{MM} + \varepsilon_M BD_{MB} + \varepsilon_M WD_{MW}\right) + k_{D-}C + k_{MM-}D_{MM} \\
&\quad - k_{MM+}MD_M - k_{D+}MB_d - d_MM \qquad (5.2) \\
\dot{B}_d &= k_{p-}B + k_{MB-}D_{MB} + k_{D-}C - k_{P+}B_d - k_{MB+}B_dD_M \\
&\quad - k_{D+}MB_d - d_{B_d}B_d \\
\dot{B} &= \beta + k_{p+}B_d - k_{p-}B - d_BB \\
\dot{W} &= \gamma\left(D_W + \varepsilon_W D_{WC}\right) - d_WW \\
\dot{C} &= k_{D+}MB_d + k_{WC-}D_{WC} - k_{WC+}CD_W - k_{D-}C - d_CC.
\end{aligned}
$$

Where the only changes are in the binding and unbinding of C to D_W (which in (5.1) are binding and unbinding of M and B to D_W) and in the production term of W. In both systems, $K_{XY(+,-)}$ stand for (binding, unbinding) rates of molecule Y to promoter D_X of protein X, D_{XY} represent the promoter of X with Y bound to it, and ε_{XY} represent how upregulated or downregulated is production of protein X (in relation to its basal rate) when Y is bound to its promoter. As in equations (4.2), M stands for BRAVO (MYB56), B stands for phosphorilated, inactive BES1, B_d is dephosphorilated, active BES1 and C is the BRAVO-BES1 complex. The newly introduced variable W stands for WOX5, with basal production rate γ and degradation rate d_W. All other parameters are defined as in equations (4.2). Notice that ε_{MM} and ε_{MB} are equivalent to ε_1 and ε_2 of equations (4.2), but ε_3 has no analog here, because it is not possible for BRAVO and BES1 to be bound to the BRAVO promoter at the same time.

To simplify the analysis, we also considered DNA and inactive BES to have very fast dynamics and thus to be in equilibrium. We set the derivatives of the fast variables to zero, which is not a rigorous procedure (as the remaining equations lack the time-scaling factors that would appear in a proper adiabatic approximation), but which yields exactly the same steady states as the full system. Thus, we obtain 4 equations for our relevant proteins:

$$\begin{aligned}
\dot{M} &= \alpha\frac{1+\varepsilon_{MM}K_{MM}D_M M+\varepsilon_{MB}K_{MB}D_M B_d+\varepsilon_{MW}K_{MW}D_M W}{1+K_{MM}D_M M+K_{MB}D_M B_d+K_{MW}D_M W}+\\
&\quad +k_{D-}C-k_{D+}MB_d-d_M\\
\dot{B}_d &= \beta'+k_{D-}C-k_{D+}MB_d-d'_{B_d}B_d\\
\dot{W} &= \gamma\frac{1+\varepsilon_{WM}K_{WM}D_W M+\varepsilon_{WB}K_{WB}D_W B}{1+K_{WM}D_W M+K_{WB}D_W B}-d_W W\\
\dot{C} &= k_{D+}MB_d-k_{D-}C-d_C C,
\end{aligned} \tag{5.3}$$

for the system independently regulated by BES and BRAVO, and

$$\begin{aligned}
\dot{M} &= \alpha\frac{1+\varepsilon_{MM}K_{MM}D_M M+\varepsilon_{MB}K_{MB}D_N B_d+\varepsilon_{MW}K_{MW}D_M W}{1+K_{MM}D_M M+K_{MB}D_M B_d+K_{MW}D_M W}+\\
&\quad +k_{D-}C-k_{D+}MB_d-d_M M\\
\dot{B}_d &= \beta'+k_{D-}C-k_{D+}MB_d-d'_{B_d}B_d\\
\dot{W} &= \gamma\frac{1+\varepsilon_W K_{WC}D_W C}{1+K_{WC}D_W C}-d_W W\\
\dot{C} &= k_{D+}MB_d-k_{D-}C-d_C C.
\end{aligned} \tag{5.4}$$

Where $K_{XY}=\frac{k_{XY+}}{k_{XY-}}$, $\beta'=\beta\frac{k_{P-}}{k_{P-}+d_B}$ and $d'_{B_d}=d_B\frac{k_{P+}}{k_{P-}+d_B}+d_{B_d}$.

The fitting approach of section 4.2.2 is of limited application here. Because BES1 and BRAVO do not have a cross term in this model, the third datapoint A_3 only serves here to set the values K_{MM}, K_{MB} and the dimerization equilibrium constant $K_D=\frac{k_{D+}}{k_{D-}}$, which have large ranges of values compatible with experimental data and even the constrains of which strongly depend on the chosen M_{tot}, B_{tot}. Therefore, we only take the fitted $\varepsilon_{MM}=3.9$ and $\varepsilon_{MB}=0.068$, whereas for K_{MM}, K_{MB} and D_{eq} we only take the general result that they are of the same order of magnitude and ranging $10^{-1}-10^2$ for the binding constants and $10^{-3}-10^3$ for the dimerization constants given our chosen range of M_{tot}, B_{tot} $10-1000$nM.

5.2 Results

5.2.1 Bistability

We first analyzed the phenomenology that these models allow. To better understand this phenomenology, and other analyses that are explained in following sections, we first computed the nullclines of the system. A nullcline is a curve that shows for which values of the variables the derivative of one of them becomes zero, and they are helpful to qualitatively understand the dynamics of the system and how different regimes (such as monostability or bistability) are achieved.

Because there are four variables but we wanted to represent the nullclines in 2-D, we restricted ourselves to the dependence of two variables at a time. To this end, we assume the other two variables to always be in equilibrium and set their derivatives to zero. We numerically solved the nullclines of the two variables of the given phase space, using Mathematica software (Wolfram Research, 2010). Figure 5.2 summarizes the different qualitative behaviours of these nullclines.

For very wide ranges of parameter values, the nullclines $B\dot{E}S1 = 0$ and $BR\dot{A}VO = 0$ are qualitatively the same: when plotted against WOX5 concentration, they both show a highly nonlinear shape in which they almost mirror each other (Figure 5.2 A). In BRAVO-BES1 space, instead, they are monotonic decreasing curves, and parameters only regulate their curvature and relative position, depending on which they will intersect in one or three points, but always at high BRAVO when BES1 is low and viceversa (very much as in the BRAVO-BES1 module without WOX5) (Figure 5.2 C).

WOX5 has a very simple behaviour that changes with a few key parameters. In the model in which WOX5 is separately regulated by BES1 and BRAVO, $W\dot{O}X5$ is zero for two values of $WOX5$ for almost all values of BES1 and BRAVO, one higher and one lower, with a sharp transition in between. When $\varepsilon_{WM} > \varepsilon_{WB}$, the low value of WOX5 will be at high BES1 (and low BRAVO)(Figure 5.2 B), whereas when $\varepsilon_{WM} > \varepsilon_{WB}$, the low value of WOX5 will be at high BRAVO (and low BES1)(Figure 5.2 D). Notice how this is simply an effect of competition between BRAVO and BES1 to saturate the WOX5 promoter.

Something very different happens when WOX5 is regulated by the BRAVO-BES1 Complex. In this case, the $\dot{WOX5} = 0$ nullcline is at the same value of $WOX5$ for any BES1 and BRAVO beyond a threshold (that is very small) (Figure 5.2 E). Noticeably, and contrary to what happens in the case of separate regulation by BES1 and BRAVO, the WOX5 nullcline is very similar as a function of BES1 or BRAVO .

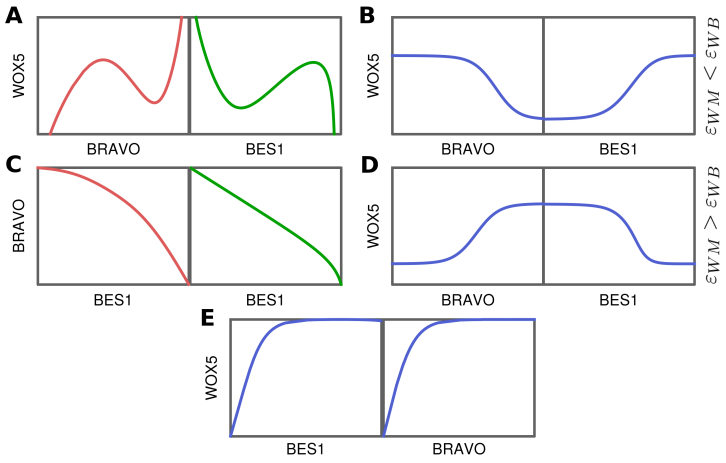

Figure 5.2 Nullclines for the WOX5-BES1-BRAVO module. **A,C** Nullclines for $\dot{BES1} = 0$ (green) and $\dot{BRAVO} = 0$ (red). All variables not shown are assumed to be in equilibrium. These nullclines are qualitatively the same regardless of choice of regulation for WOX5. **B,D** Nullclines for $\dot{WOX5} = 0$ when WOX5 is regulated by BRAVO and BES independently. **B** $\varepsilon_{WM} < \varepsilon_{WB}$**D** $\varepsilon_{WB} < \varepsilon_{WM}$ **E** $\dot{WOX5} = 0$ nullclines when WOX5 is regulated by the BRAVO-BES1 complex. Although no tics are shown, all axis are in logarithmic scale.

We first focused on the effect that including WOX5 has on bistability and sharp transitions, as the primary function of the BRAVO-BES1 module. To that end we chose parameters as close as possible to the original model, with minimal changes. These parameters are $d_M = d_B = d_C = d_W = 0.02\,\mathrm{h}^{-1}$, $d_{B_d} = 0.002\,\mathrm{h}^{-1}$, $K_{MM} = K_{WM} = 1\,\mathrm{nM}^{-1}$, $K_{MB} = 2\,\mathrm{nM}^{-1}$, $k_{D+} = 1\,\mathrm{h}^{-1}\,\mathrm{nM}^{-1}$, $k_{D-} = 1\,\mathrm{h}^{-1}$, $\beta = 4\,\mathrm{nM\,h}^{-1}$, $\alpha = 1\,\mathrm{nM\,h}^{-1}$, $\gamma = 0.15\,\mathrm{nM\,h}^{-1}$, $k_{P+} = 0.05\,\mathrm{h}^{-1}$, $k_{P-} = 0.1\,\mathrm{h}^{-1}$, and regulation rates for BRAVO $\varepsilon_{MM} = 3.9$, $\varepsilon_{MB} = 0.068$, $\varepsilon_{MW} = 5$. The only relevant changes from chapter 4 are in K_{MM}, K_{MB} and k_{P-}. However, recall from section 4.2.2 that the specific values of binding constants were hard to determine. Because this model increases the number of binding constants from 2 to 5, we chose small round values that simplify the

relationship between all of them. As for k_{P-}, we are now considering BES1 to be active by default, but will vary it throughout our analysis. These parameters are equal for both models (Eqs. (5.3) and (5.4)).

In the model for independently regulated WOX5 (Eqs. (5.3)), we set $K_{WB} = 3\,\mathrm{nM}^{-1}$, $K_{WM} = 1\,\mathrm{nM}^{-1}$, $\varepsilon_{WM} = 15$, $\varepsilon_{WB} = 2$.

In the model for jointly regulated WOX5 (Eqs. (5.4)), through BES1-BRAVO complex, we set $\varepsilon_{WC} = 2$ and $K_{WC} = 1\,\mathrm{nM}^{-1}$.

We then compared these two models with the same model with WOX5 production γ set to $\gamma = 0$. When plotting the bifurcation diagrams for all three systems we see that all three models preserve bistability as a mechanism for sharp transitions from high to low BRAVO states upon BR signalling, as well as a strong opposition of BES1 and BRAVO (Figure 5.3).

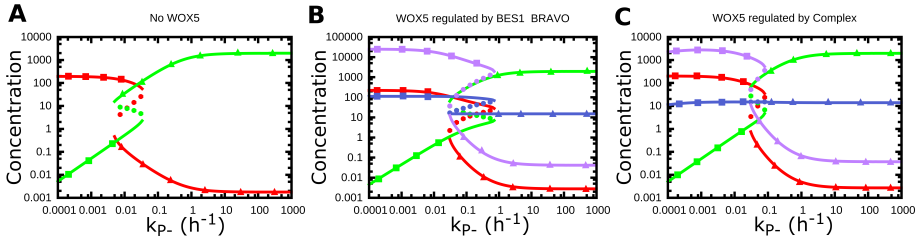

Figure 5.3 Bifurcation diagrams for all 3 models **A** Without WOX5. **B** WOX5 is regulated by BRAVO and BES1 separately. **C** WOX5 is regulated by BRAVO-BES1 complex. Continuous lines are stable states, and circles are unstable states. Green is BES1, red is BRAVO, blue is WOX5 and purple is WOX5×BRAVO. Squares mark the (High,Low) state whereas triangles mark the (Low,high) state.

WOX5, however, does not have such extremely low nor high values as BRAVO. However, notice how in the independently regulated WOX5 model (Figure 5.3 B), WOX5 still has a strong opposition with free BES1, even if at first look it does not look like it due to the very large range and logarithmic scale in the vertical axis. Therefore, these results suggest that the regulation of quiescence by BR signaling (in our model represented by BES1 dephosphorilation) could still be mediated by WOX5 thanks to its regulation by BRAVO, although it would be a poorer regulator than BRAVO itself.

When WOX5 is regulated by the BES1-BRAVO complex the situation is more complicated. Due to the joint regulation by BES1 and BRAVO, the [HIGH

BRAVO, LOW BES1] and the [LOW BRAVO, HIGH BES1] states produce similar effects on WOX5 (remember how the nullclines in Figure 5.2 E were very flat and behaved equally when increasing BRAVO or BES1, instead of being mirrored). Due to this, both stable states have very similar levels of WOX5. This means that, if the actual regulation of WOX5 is done by the BES1-BRAVO complex, WOX5 cannot be regulating quiescence. When we plotted the product $BRAVO \times WOX5$, which is proportional to the stable state concentration a BRAVO-WOX5 complex would have ($C_{BRAVO-WOX5} = \frac{k_{Dimerization}}{k_{Dedimerization}+deg_{C_{BRAVO-WOX5}}} BRAVO \times WOX5$), we observed that it has low and high values strongly opposed to BES1, like BRAVO. These results show that if WOX5 is activated only by the BES1-BRAVO complex, then WOX5 concentration becomes effectively independent of $BES1_d$ dephosphorilation and hence of BR signalling, while the WOX5-BRAVO complex does not. Therefore, in this scenario, WOX5 alone could not be mediating changes in quiescence induced by BR signalling and, instead, either the BRAVO-WOX5 complex would be mediating this regulation or BRAVO itself would be responsible of this BR-mediated function, with WOX5 regulating quiescence independently of BR signalling.

We also computed how different parameters affected bistability. We proceeded as in Figure 4.6 with all three systems. What is most noticeable is how the module becomes much less sensitive to the value of BRAVO autoactivation strength K_{MM} (Figure 5.4 A,D,G). This is natural, since now BRAVO does not have only one positive feedback loop through self activation but an additional one, indirectly through WOX5. Like in the original module, a minimum effect of the dimer, as measured both by k_{D+} and d_C is needed to obtain bistability (compare Figure 5.4 A,D,G to Figure 4.6 A and Figure 5.4 B,E,H to Figure 4.6 E).

Also with respect to d_C, the bistability range is greatly increased when including WOX5 (Figure 5.4 B,E,H). This, however, depends on the exact parameters chosen. For instance, when decreasing inactive BES1 production β the bistable region is enlarged, but in such a way that sharp transitions are impaired (see discussion for details). In contrast when increasing inactive BES1 production β, the inclusion of WOX5 actually decreases bistability, but preserves the capacity for sharp transitions (Figure 5.5). For other parameters, such as active BES1 degradation (d_{B_d}), WOX5 has no noticeable effect on the system (Figure 5.4 C,F,I).

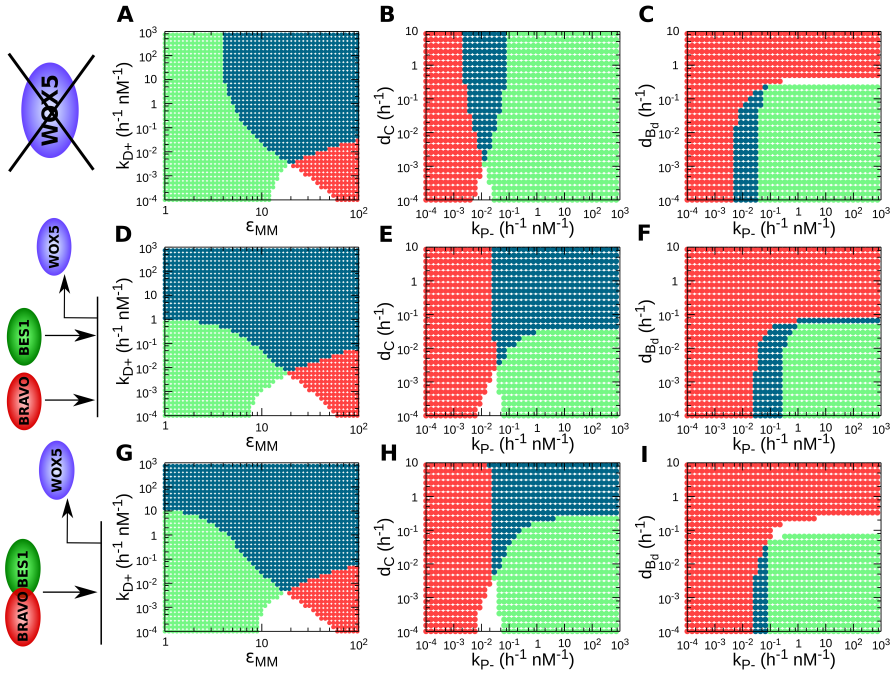

Figure 5.4 Bistability depending on different parameters for all 3 systems. **A-C** Model without WOX5. **D-F** Model with WOX5 independently regulated by BES1 and BRAVO. **G-I** Model with WOX5 regulated by BES1-BRAVO complex. As in figure 4.6, gray and black areas correspond to those parameter regions where the free BRAVO and free dephosphorylated BES1 stable stationary amounts differ in one or more orders of magnitude (i.e. their ratio is 10 or larger). Dark grey areas (in red in digital version) correspond to the (HIGH BRAVO,LOW BES1), light grey areas (in green in digital version) correspond to a (LOW BRAVO,HIGH BES1) state, and black areas (in blue in digital version) have two opposed stable states. White stands for those regions where the amounts of free BRAVO and free dephosphorylated BES1 differ in less than one order of magnitude.

5.2.2 Excitability and oscillations

The shapes of the nullclines in Figure 5.2 suggest that the system may be capable of other dynamic behaviours. Indeed, the system in which WOX5 is regulated by the BRAVO-BES1 complex only shows bistability, but the system with independent BRAVO and BES1 regulation shows Type II excitability for some sets of parameter values. Type II excitability is that which does not have a single sharp threshold above which there is a response of a fixed size but, instead, shows a response proportional to stimulus (Strogatz, 2014). If the

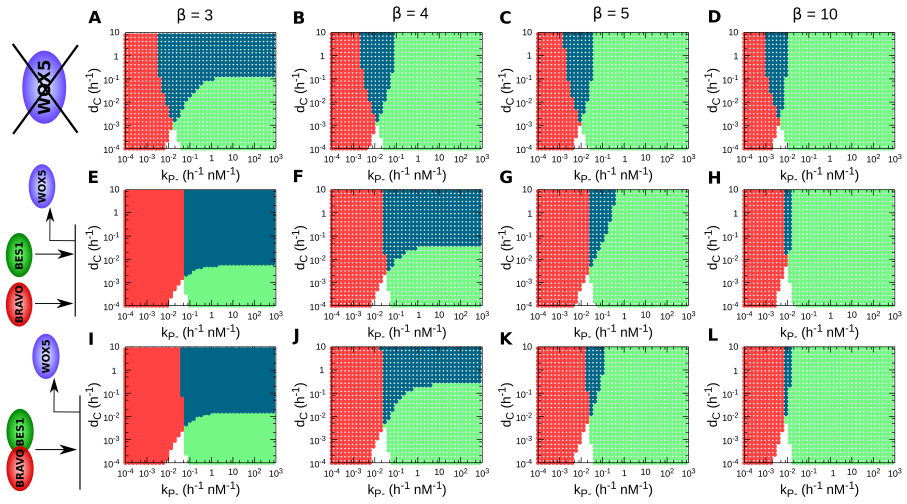

Figure 5.5 Bistability depending on d_C vs k_{P-} for different values of β. **A-D** Model without WOX5. **E-H** Model with WOX5 independently regulated by BES1 and BRAVO. **I-L** Model with WOX5 regulated by BES1-BRAVO complex. First column (panels **A,E,I**) has $\beta = 3$. Second column (panels **B,F,J**) has $\beta = 4$ and is equivalent to panels **B,E,H** of figure 5.4. Third column (panels **C,G,K**) has $\beta = 5$. Fourth column (panels **D,H,L**) has $\beta = 10$. Gray and black areas correspond to those parameter regions where the free BRAVO and free dephosphorylated BES1 stable stationary amounts differ in one or more orders of magnitude (i.e. their ratio is 10 or larger). Dark grey areas (in red in digital version) correspond to the (HIGH BRAVO,LOW BES1), light grey areas (in green in digital version) correspond to a (LOW BRAVO,HIGH BES1) state, and black areas (in blue in digital version) have two opposed stable states. White stands for those regions where the amounts of free BRAVO and free dephosphorylated BES1 differ in less than one order of magnitude.

system is perturbed far enough from the stable state, it does a large excursion along state space. When considering the stochastic version of the dynamics, fluctuations can drive these excursions spontaneously. We observed this by simulating the full system of reactions from which equations (5.1) were derived (22 reactions for 7 variables) using the Gillespie algorithm with a small volume (Figure 5.6) (that rescales the parameters with units of concentration, to obtain molecule numbers). The parameters that yielded excitability are the same as the ones that yield bistability as detailed in 5.2.1, with the only changes of $\beta = 3\,\mathrm{nM\,h^{-1}}$, $\gamma = 0.008\,\mathrm{nM\,h^{-1}}$, $d_W = 0.002\,\mathrm{h^{-1}}$, $\varepsilon_{MW} = 12$, $\varepsilon_{WM} = 2$, $\varepsilon_{WB} = 15$, $K_{MB} = 3\,\mathrm{nM}$-1 and $K_{WB} = 1\,\mathrm{nM}$-1 and $\alpha = 0.5\,\mathrm{nM\,h^{-1}}$. For a full description of the system, we also needed to choose values for protein-promoter binding and

unbinding rates $k_{XY+,-}$. To be consistent with our previous assumption that these reactions are fast, we took $k_{XY-} = 100\,\mathrm{nM\,h^{-1}}$ and $k_{XY+} = k_{XY-} \times K_{XY}$ in all cases.

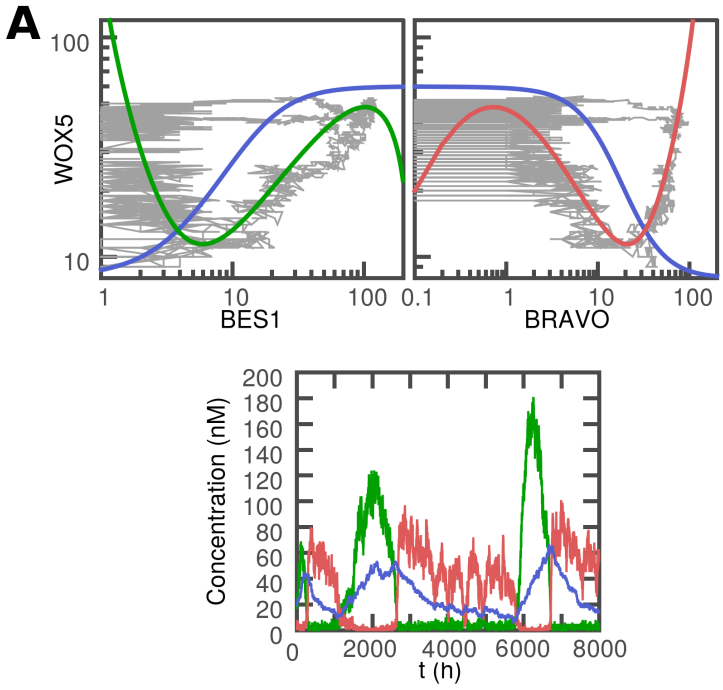

Figure 5.6 Excitability in the BRAVO-BES1 module. **A** Nullclines and excitable trajectory. Green nullcline corresponds to BES1, red to BRAVO and blue to WOX5. In grey is a trajectory with volume $V = 1\,\mathrm{nM^{-1}}$ that does two spontaneous excursions. **B** Same trajectory as in **A**, showing all three variables over time. Red corresponds to free BRAVO, green to free active BES1, and blue to WOX5.

The system is also capable of oscillations, that are also maintained under fluctuations with a remarkably constant period (Figure 5.7). We found oscillations to happen for parameters, again, very similar to those of section 5.2.1, with the only changes being $\beta = 3\,\mathrm{nM\,h^{-1}}$, $\gamma = 0.08\,\mathrm{nM\,h^{-1}}$, $\alpha = 0.5\,\mathrm{nM\,h^{-1}}$, $\varepsilon_{MW} = 9$, $\varepsilon_{WM} = 2$, $\varepsilon_{WB} = 25$ and $K_{WB} = 8\,\mathrm{nM\,h^{-1}}$ (with binding rates as for the excitable parameter set). Notice that both in this case in in that of excitatory behaviour, we did not change the parameters that were obtained or constrained by the fitting of experimental data.

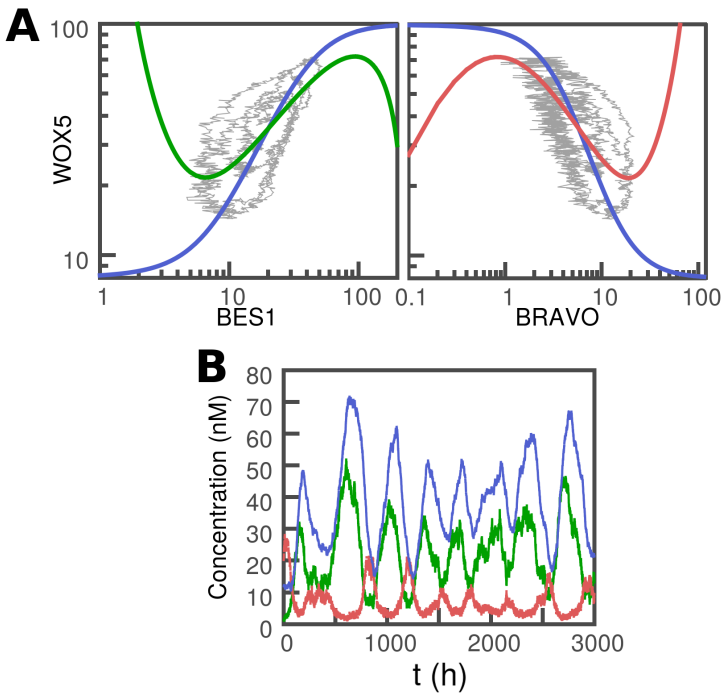

Figure 5.7 Oscillations in the BRAVO-BES1 module. **A** Nullclines and oscillating trajectory. Green nullcline corresponds to BES1, red to BRAVO and blue to WOX5. In grey is a trajectory with $V = 10\,\mathrm{nM}^{-1}$.**B** Same trajectory as in **A**, showing all three variables over time. Red corresponds to free BRAVO, green to free active BES1, and blue to WOX5.

Both dynamic behaviours are very suggestive as modes of regulation of quiescence. Unfortunately, neither of these two results are likely to be happening in the WOX5-BRAVO-BES1 module in QC cells. Since WOX5 inhibits QC division, and given that BRAVO also inhibits division (independently or through WOX5), these results, in which WOX5 and BRAVO oscillate in opposition or do excursions in opposite directions (WOX5 increases, BRAVO decreases, see Figure 5.6 A), are very hard to interpret. If this were happening in the biological realization of the module, there would need to be another complex step of integration of signals before regulation of quiescence, so we did not pursue these results further.

5.3 Discussion

We included a candidate gene for quiescence regulation, WOX5, in the BES1-BRAVO module assuming two different regulations for BRAVO and BES1 upon WOX5. The models used have certain simplifications with respect to the original model we studied for BRAVO and BES1, but reproduce most behaviour of the module when no WOX5 is present. Furthermore, including WOX5 can preserve bistability and sharp transitions and it increases the range of bistable behaviour for some sets of parameter values. This, however, is not always advantadgeous for sharp transitions: when bistability starts at a threshold dephosphorilation k_{P-} and is not lost even if k_{P-} is increased, there is no deterministic mechanism for sharp transitions: the high BRAVO state exists for all values of k_{P-} and so the system will not escape it when increasing BR signal. In these cases the transition, if it exists, must be stochastic. However, as we saw in previous chapters, the AAC regulatory circuit that is part of the BRAVO-BES1 module can be extremely stable. Indeed, in these cases where bistability persists for very high dephosphorilation rates k_{P-}, we were unable to observe stochastic transitions regardless of whether WOX5 was included or not.

Another feature that our modelling highlighted is that the fact that both BES1 and BRAVO regulate WOX5 positively lead to levels of free WOX5 that are much less opposed to active BES1 than those of free BRAVO (Figure 5.3). In the case of WOX5 regulated by the BES1-BRAVO heterodimer the states are almost identical, whereas in the case where BRAVO and BES1 regulate WOX5 independently WOX5 still has two different states, but their concentrations are closer to those of total BRAVO than to the more extreme values of free BRAVO (Figure 5.8). This led us to propose that WOX5 is not doing its quiescence regulation function by itself, but rather jointly with some other element. A good candidate for this is BRAVO itself, which may be dimerizing with WOX5 to do their joint function.

Further exploration of our models showed that this module is capable of excitability and oscillations only under the independent regulation hypothesis. It is unclear whether this excitability is relevant to the function of our circuit. Given that BRAVO and WOX5 repress QC divisions and BES1 activates them, the obvious picture for excitatory regulation of quiescence would be a state of

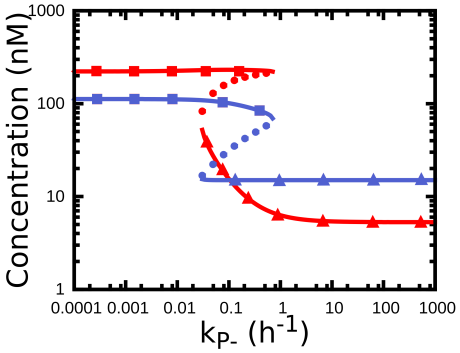

Figure 5.8 Bifurcation diagram of total BRAVO (free BRAVO plus BRAVO bound to BES1 and to DNA), in red, and total WOX5, in blue.

high BRAVO and WOX5 in which these two do an excursion to low concentrations concomitantly to an increase in active BES1. In our model, the stable state has high BRAVO and low BES1 (as expected) and BRAVO does an excursion to low values at the same time as BES1 doing an excursion to high values (also as expected). WOX5, however, increases its value with BES1 during the excursion, which is opposed to the expected behaviour (Figure 5.6). Therefore, if this module regulates quiescence through excitability it must do it through something a bit more convoluted, such as dimerization and joint regulation of quiescence by WOX5 and BRAVO.

The oscillations that our model yielded are even less believable to be happening in wild type plants. In the oscillations we observed through our model, BRAVO has very low concentrations over time, and is also opposed to WOX5 (Figure 5.6). In contrast, wild type roots show expression of both BRAVO and WOX5 in the QC (Vilarrasa-Blasi et al., 2014; Vilarrasa-Blasi, 2014). Therefore, we discard these oscillations as the behaviour of wild type QC cells. Since these oscillations require a threshold level of BES1 dephosphorilation k_{P-} to happen, below which there is a state of high BRAVO and low BES1, this may be the behaviour of QC cells under some induced BR signalling. Still, the hypothetical function of these oscillations is unclear.

Going to the more general interest of how our regulatory motifs are capable of certain dynamic behaviours it is worth noting that, to our knowledge, excitability has not been described with the exact same ingredients of this module.

In particular, minimal excitable circuits that have post-transcriptional interactions, such as the one shown in (Rué and Garcia-Ojalvo, 2011) have one protein repressing the other, whereas in our module nonlinearity comes from a mutual post-transcriptional repression in the form of molecular titration. This may only be a particular case of more general circuits. It remains to be seen, however, how this circuit can be reduced to a known, minimal, 2-element circuit.

Oscillations, on the other hand, had already been described for the Mixed Feedback Loop (François and Hakim, 2005), which is a motif included in the base BRAVO-BES1 module. The Mixed Feedback Loop that has oscillations, however, has a transcriptional activation instead of repression (in our case, that would happen if BES1 activated BRAVO instead of repressing it). This activation is provided in our circuit through the activation of WOX5 by BES1, and then of BRAVO by WOX5.

All in all, the most relevant results of our modelling here are the prediction that WOX5 levels do not change much in QC cells, the proposal that the regulation of Cyclin D3 by WOX5 is done jointly with BRAVO, and the observation of dynamic behaviours beyond sharp transitions of bistability that are enabled by the inclusion of WOX5 in the BRAVO-BES1 module.

Chapter 6

Synchrony of Quiescent Centre cell divisions

6.1 Introduction

As we saw in chapter 4, the mechanism through which the Quiescent Centre (QC) cells divide is unknown and a subject of intense research at the moment. Furthermore, although quiescence has long been defined as a reversible arrested state outside of the cell cycle, and therefore with no cell divisions (Cheung and Rando, 2013), *Arabidopsis* root Quiescent Centre cells are not defined by nondivision but by a slow infrequent division rate (Aichinger et al., 2012). Although it seems clear that this quiescent state is released to respond to stresses (Aichinger et al., 2012), it is unclear whether the slow division rate of wild type plants is due to spurious signals that mimic stresses or to a very slow progression in cell cycle (Aichinger et al., 2012). Moreover, how this release (or not) is regulated remains an open question. Although in previous chapters we showed a module that does regulate this, a separate question is how signalling is relayed to that module where it comes from, and whether there is some kind of feedback or cell-to-cell communication that shapes the decision. This topic of cell decision-making in stem cells and its relationship with stochasticity is one that has been intensely studied in the last years, both at the level of autonomous and collectives decisions, and more recently their interplay (Perkins

and Swain, 2009; Graham et al., 2010; Garcia-Ojalvo and Martinez Arias, 2012; Smith et al., 2015).

In this chapter we analyze quantified divisions of the QC, to find that these are not independent but synchronized within each plant, and compare different models that suggest that this synchrony is likely to come from cell-to-cell communication, rather than periodic or spurious signals. We also compare division data to fluorescence data already introduced in chapter 4, and find that although there is also synchrony in fluorescence, the relationship between measured fluorescence and measured division is not straightforward.

6.2 Results

6.2.1 Null hypothesis: QC cells divide independently

As part of the experimental work introduced in section 4.1, divisions were quantified in large numbers of plants of each mutant genotype or BR treatment. Divisions were observed morphologically: QC cells under no stress divide periclinally (in the direction in which the root points), and the 'bottom' cell (the one closer to the tip) differentiates as a Collumella Stem Cell and moves away to the next cell file (Cruz-Ramírez et al., 2013). During this process there is an undetermined period of time in which both QC cells remain in the QC cell file, in the space that the original cell occupied. This is what is considered as 'observing' a division.

This quantification of divisions was done to observe and quantify the raw effect of each molecular component on the quiescent state of cells (Vilarrasa-Blasi et al., 2014). This data, however, contain additional information. Plants were classified as None Divided (ND), Partially Divided (PD) and All Divided (AD), depending on whether no observed cells were divided in the QC, only some (but not all) cells were divided or all cells were divided (Figure 6.1). This granularity may contain indirect information on how QC divisions are regulated.

A small clarification should be done at this point: the (ND, PD, AD) states do *not* correspond to the whole QC, but to observed cells. The QC is a disk composed of about 10 cells but the typical direction of observation (and the one necessary to observe divisions clearly), from the side, can only put a maximum

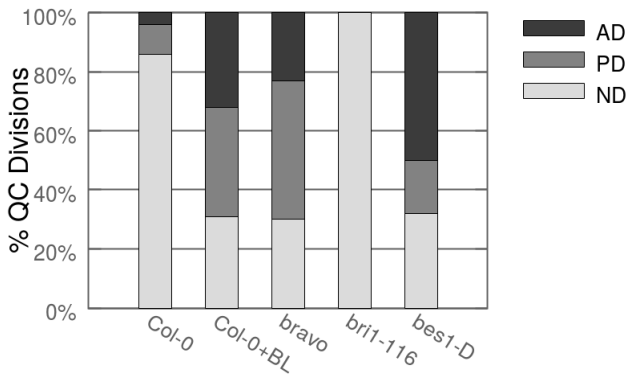

Figure 6.1 Experimentally measured QC divisions in different phenotypes and treatments. AD, PD and ND are as indicated in the text. Col-0 is the wild type plant. '+ BL' indicates a continuous treatment with Brassinolide. *bes1-D* is the gain-of-function mutant of BES1. *bri1-116* is a dominant mutant of Brassinosteroid receptor BRI1. *bravo-2* is a mutant of BRAVO. Data courtesy of Josep Vilarrasa-Blasi and Ana I. Caño-Delgado. Data were taken from $n > 50$ plants in each case.

of 4 or (rarely) 5 in one plane at the same time. So observations are of 2 to 5 cells in each plant, with almost all of them being of the central diametral file of 3 or 4 cells.

From the data in Figure 6.1, we can easily conclude that QC divisions are synchronized in some way. Consider a simple model in which each cell has a probability $p_d = a$ of being observed as dividing and a probability $p_{nd} = b = 1 - a$ of being observed as not dividing, in apparent quiescence. Then, if the probability for each cell is independent from the others, and assuming that 4 cells are observed, we can define the probability of the QC of a plant to be in the ND (0 divided cells), PD (1,2 or 3 divided cells) or AD (4 divided cells) as:

$$\begin{aligned} p_{ND} &= b^4 \\ p_{PD} &= 4a^3b + 6a^2b^2 + 4ab^3 = (a+b)^4 - a^4 - b^4 = 1 - ND - AD \\ p_{AD} &= a^4 \end{aligned} \tag{6.1}$$

Where the factors in p_{PD} correspond to the possible combinations in which each substate can appear (e.g., there are 4 possible combinations of 1 divided

and 3 nondivided cells). When trying to fit this model to the experimental data it becomes obvious that Partially Divided is extremely underrepresented in the actual plants (Figure 6.2). Or rather, the extreme states AD and ND are very overrepresented, indicating a synchrony in observable cell division.

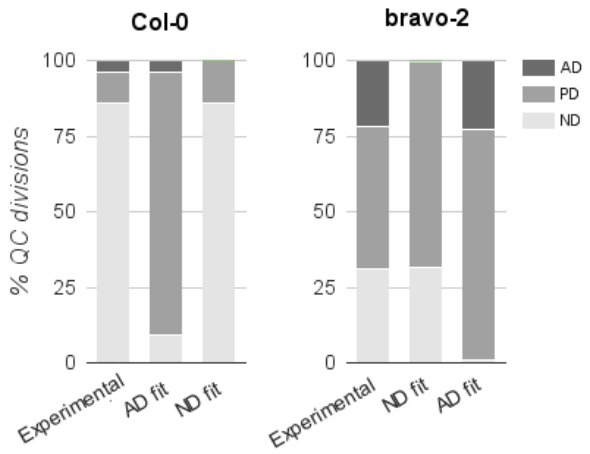

Figure 6.2 Experimentally measured divisions from figure 6.1 compared to possibilities of a model in which divisions of each cell are independent. Left panel is Col-0, the wild type, and right panel is *bravo* mutant bravo-2. AD/ND fit mean that rates a and b in equation (6.1) have been chosen so that the proportion of either AD or ND fit with the experimentally observed value, leaving the rest free. Observe how the independent divisions invariably yield larger PD than the experimental value.

The observation that divisions are synchronized is potentially relevant. However, this data should be able to provide more information on the origin of this synchronization.

6.2.2 Single cell model of non-independent division

To try to shed light on how divisions are synchronized, we can take the simple probabilistic model introduced in the previous section and generalize it. Now, the parameters a and b will be functions instead of constants. In particular, we will consider two simple hypotheses: that division is dependent on the number of cells that are already divided, and that it depends on time. The first hypothesis corresponds with the scenario that cells release a signal upon division, making other cells divide (this is also valid if the signal is released *before* division: what

matters is the cell decision itself), and the second can be made to represent spurious signals that trigger or enhance division in all cells or a division rate that depends on regular external factors that affect all cells at the same time.

We will have a process, then

$$nd \underset{a(n,t)}{\overset{b(n,t)}{\rightleftharpoons}} d \tag{6.2}$$

where nd is the nondividing state of a cell and d is its dividing state, and n is the number of cells that are dividing other than the one modeled. This is a master equation that can be written as

$$\dot{p_d} = a(n,t)p_{nd} - b(n,t)p_d \tag{6.3}$$

$$1 = p_d + p_{nd}, \tag{6.4}$$

which, in the case of constant a and b, is a telegraph process (Gardiner, 2008). This model can be analyzed by itself, but it is of little use to analyze the collective dynamics of the QC. For that, we can expand it into a model that includes the divisions of all 4 observed cells but preserves the information of single cell division transition probabilities per unit of time:

$$0d \underset{b_1(1,t)}{\overset{a_0(0,t)}{\rightleftharpoons}} 1d \underset{b_2(2,t)}{\overset{a_1(1,t)}{\rightleftharpoons}} 2d \underset{b_3(3,t)}{\overset{a_2(2,t)}{\rightleftharpoons}} 3d \underset{b_4(4,t)}{\overset{a_3(3,t)}{\rightleftharpoons}} 4d \tag{6.5}$$

Where $a_n(n,t) = (4-n)a(n,t)$ and $b_n(n,t) = nb(n,t)$ are obtained by multiplying the single cell transition probabilities per unit of time by the number of cells that can perform the transition in either direction. This collective model corresponds to the equations

$$
\begin{aligned}
\dot{p}_{0d} &= b_1(1,t)p_{1d} - a_0(0,t)p_{0d} \\
\dot{p}_{1d} &= b_2(2,t)p_{2d} + a_0(0,t)p_{0d} - (a_1(1,t) + b_1(1,t))p_{1d} \\
\dot{p}_{2d} &= b_3(3,t)p_{3d} + a_1(1,t)p_{1d} - (a_2(2,t) + b_2(2,t))p_{2d} \\
\dot{p}_{3d} &= b_4(4,t)p_{4d} + a_2(2,t)p_{2d} - (a_3(3,t) + b_3(3,t))p_{3d} \\
\dot{p}_{4d} &= a_3(3,t)p_{3d} - b_4(4,t)p_{4d}.
\end{aligned} \tag{6.6}
$$

The states of this model can easily be mapped onto the observed states (ND,PD,AD) as $p_{0d} \equiv p_{ND}$, $p_{4d} \equiv p_{AD}$ and $p_{1d} + p_{2d} + p_{3d} \equiv p_{PD}$.

We now make a symplifying assumption. Because we want to understand how division is regulated, we will consider that $b(n,t)$ is a constant, $b(n,t) = b$. This function represents the probability that a division that has happened stops being visible, i.e. the daughter cell migrates away from the QC. If we make the assumption that there is a fixed delay from division to differentiation, b should be a constant. This is only a working assumption, and not necessarily true, because synchrony in differentiation is also a possible cause for synchrony in observed divisions.

We also consider two different forms for $a(n,t)$, one dependent only on n, $a(n)$, and another dependent only on time, $a(t)$.

When the transition probabilities per unit of time do not depend on time, the steady state for equations (6.6) can be solved. We assumed that the probability to observe a given division state p_n^{obs} is equal to the steady state probability p_n^{st}. This probability is

$$
p_n^{st} = \frac{1}{C} \prod_{i=0}^{n-1} a_i(i) \prod_{i=n+1}^{4} b \tag{6.7}
$$

$$
C = \sum_{n=0}^{4} \left(\prod_{i=0}^{n-1} a_i(i) \prod_{i=n+1}^{4} b \right) \tag{6.8}
$$

Because we are in a steady state, we can rescale all timescales, and the specific value of b becomes irrelevant. Therefore we simplify the system and set $b = 1$.

Regarding the function $a(n)$, since we lack additional information to make a more complex or realistic assumption, we define the simplest possible function for the n-dependent $a(n)$:

$$a(n) = a + \alpha n \tag{6.9}$$

Notice that in this function, the probability to divide is proportional to the observed number of dividing cells n out of a total of 4 observed cells, which is not the real number N of dividing cells in the QC, out of about 10 cells. However, as explained in appendix A, the expected value of N depends linearly on observed n. Therefore, we can write a function of n and expect that the linear factors will be absorbed into α.

In the case where $a(n,t)$ does depend on t but not on n ($a(n,t) = a(t)$), given that the data that we have does not have dynamic information, and to simplify calculations, we considered the simplest possible time-varying function for $a(t)$, a periodic step function

$$a(t) = \begin{cases} a & 0 \leq t \leq \tau \\ \alpha & \tau \leq t \leq T \end{cases} \tag{6.10}$$

with two values a and α and a period T. Making the assumption that each time the division transition probability changes, the system reaches the steady state very fast (i.e. the transitory is negligible), the probability p_n^{obs} of observing each division state at a random point in time simply becomes the weighted average of the probability of the two regimes:

$$p_n^{obs} = \frac{\tau}{T}\left(\frac{1}{C}\prod_{i=0}^{n-1} a \prod_{i=n+1}^{4} b\right) + (1 - \frac{\tau}{T})\left(\frac{1}{C}\prod_{i=0}^{n-1} \alpha \prod_{i=n+1}^{4} b\right), \tag{6.11}$$

Where $\tau = \frac{\tau}{T}$ is the fraction of time spent in each regime. One could think that this representation, then, also represents the possibility that the cells are bistable and spend some time in each state, stochastically switching. It does not, because the time-varying rates affect all cells at the same time, so any bistability is at the plant level. What it *does* represent are any inputs that change with time, be it periodic or even spurious (assuming that stationarity

is reached fast during each spurious signal, and that these spurious signals act, on average, a fraction τ of the time).

Again, we set $b = 1$ here. In this case the value of b cannot strictly be considered to be irrelevant: because the system is dynamic, its specific timescales are important and do affect, for instance, how long it takes for the system to reach the steady state every time a changes. However, once we assume this relaxation to be instantaneous, b becomes a free parameter.

phenotype	AD	PD	ND
Col-0	0.04	0.1	0.86
bravo	0.23	0.47	0.30
bes1-D	0.5	0.19	0.31

Table 6.1 Fraction of plants in AD, PD and ND states, from data in Figure 6.1.

We then fitted these two models to three experimental cases of most interest: The wild type Col-0, the bravo mutant and the bes1-D gain-of-function (Table 6.1 and Figure 6.1), with experimental data provided by our collaborators in the group of Dr. Ana I. Caño-Delgado. To this end we defined an euclidean norm for the distance between $p_{ND,PD,AD}$ in our model and the frequency of AD, PD, ND in measurements (Ashyraliyev et al., 2009), similarly to chapter 4,

$$V_{MLE} = \frac{\sum_{X\in\{AD,PD,ND\}} \left(Frequency_X - p_X\right)^2}{\sigma_X^2}, \tag{6.12}$$

where we approximated the error in the measurements σ_X^2 according to the Bernouilli variance, $\sigma_X^2 \propto Frequency_X(1 - Frequency_X)$. We minimized this distance through a Nelder Mead method using Mathematica software (Wolfram Research, 2010), limiting the search range for τ from 0 to 0.5 (because a $0.5 < \tau < 1$ is equivalent to a $0 < \tau' < 0.5$ with switched definitions of a and α). Both models fit the data extremely well (Tables 6.2 and 6.3), which is to be expected, given that we only have 3 datapoints, and two (in the case of $a(n)$) or three parameters (in the case of $a(t)$) with which to fit them.

In the case of $a(n)$, we computed the fraction $\frac{\alpha}{a}$ to obtain a measure of how well synchronized is each phenotype. The results show the bravo mutant to have a

slightly impaired synchrony with respect to the wild type. Oppositely, bes1-D has more synchrony than the WT(Table 6.2).

phenotype	V_{MLE}	a	α	$\frac{\alpha}{a}$
Col-0	2×10^{-16}	5.65×10^{-3}	1.108	196
bravo	7.9×10^{-4}	6.19×10^{-2}	1.22	19.7
bes1-D	9×10^{-32}	3.55×10^{-3}	4.228	1191

Table 6.2 Fitting of the model with division transition probability per unit time $a(n) = a + \alpha n$.

The model with time-varying rates has one more parameter, so the good fit is even more expected. In any case, we can see how all three phenotypes are compatible with two global states, one with more divisions and the other one with less divisions, that alternate over time (Table 6.3). There are some interesting details, such as the fact that both *bravo* and *bes1-D* have more divisions than the wild type in each state, and that *bes1-D* is the only phenotype that spends more than half the period on its highly dividing state (Table 6.3).

However, it is hard to link these results to anything mechanistic about the behaviour of the module. For this reason, we made further measurements of existing experimental images taken by our collaborators, both in the wild type and the bravo mutant, to obtain another dataset with a higher level of detail. In this case, we distinguished between Partially Divided QCs with less or equal half of the cells divided, or with more than half (Table 6.4). Notice that these data do not fit perfectly with previous data. This is because observation of divisions uses morphological criteria that are not completely clear-cut. However, both data sets follow similar tendencies and, within each one, the same person did the measurements for every phenotype (with the later data set being measured by ourselves and the former by our collaborators), making the phenotypes fit for comparison. This is also the reason we perform two separate analyses: the previous dataset included the mutant *bes1-D* whereas this one does not.

Although the $a(t)$ model performed slightly worse in this case, the differences in the performance of both models are still not large enough to allow us to choose between them (Tables 6.6 and 6.5). The time-dependent model shows, like with the previous dataset, that *bravo* has an increased division rate in both states. In fact, its a is so large that we can consider it to be almost infinite, i.e. for a fraction of the time cells are almost continuously dividing. But even its α, the

phenotype	V_{MLE}	a	α	τ
Col-0	4×10^{-16}	2.7	1.1×10^{-7}	0.1
bravo	8×10^{-4}	5.6	0.17	0.44
bes1-D	4.4×10^{-15}	0.11	68	0.47

Table 6.3 Fitting of the model with time-varying division transition probability per unit time.

phenotype	AD	$PD_{>50\%}$	$PD_{\leq 50\%}$	ND
Col-0	0.055	0.127	0.2	0.618
bravo	0.394	0.243	0.333	0.03

Table 6.4 Fraction of plants in AD, $PD_{>50\%}$, $PD_{\leq 50\%}$ and ND states. Data from $N > 25$ plants in each case.

low division rate, is larger than the a of wild type (Table 6.5). We could think that, if the mechanism behind the synchrony is indeed a time-varying signal, the *bravo* mutant either is hypersensitive to it or at least does not process it in the same way, leading to these strange results of high divisions all the time. Notice also that, where the *bravo* mutant had a much larger τ than the wild type with the previous dataset, now has it smaller. This inconsistency, together with such a large value for α, point in the direction of this model not explaining well the results.

As for the model with the n-dependent division rate $a(n)$, it confirms the result from the previous dataset that *bravo* has an impaired synchrony (Table 6.6), since its ratio $\frac{\alpha}{a}$ is almost 10 times smaller than that of the wild type. Furthermore, this corroboration also increases the credibility of the other result of this model in the previous dataset: that *bes1-D* has enhanced synchrony.

phenotype	V_{MLE}	a	α	τ
Col-0	0.29	1.73	1.9×10^{-2}	0.34
bravo	0.81	6×10^4	2.67	0.26

Table 6.5 Fitting of the model with time-varying division transition probability per unit time to data with PD separated in two substates.

phenotype	V_{MLE}	a	α	$\frac{\alpha}{a}$
Col-0	0.017	0.038	0.73	19.2
bravo	0.48	0.5	1.1	2.2

Table 6.6 Fitting of the model with n-dependent transition probability per unit time to data with PD separated in two substates.

6.3 Discussion

We established, through simple probabilistic analysis of division data, that there is a synchrony in the division of Quiescent Centre cells. Rather than a synchrony in the decision to exit the quiescent state or to divide, it is a synchrony in the probability to observe cells within the same plant dividing, although those are highly likely sources for this synchrony.

Furthermore, both simple models of time-dependent rate of division or of a rate that depends on the state of other cells phenomenologically fit with the data. However, slightly worse fits and inconsistencies in its results seem to indicate that the synchrony being mediated by spurious or periodic signals that act on all cells at the same time is less likely than the possibility that division is synchronized through some sort of cell-to-cell communication. It is true, however, that the time-dependent model has more arbitrarily imposed conditions such as the shape of the time-varying function and, importantly, the fact that we neglect transient behaviours.

Still, if we consider that the driving force behind synchrony is, as it seems, cell-to-cell communication, we saw that the gain-of-function *bes1-D* has enhanced synchrony, whereas the *bravo* mutant has impaired communication, seeming to indicate different origins for the division phenotypes. However, to fully understand these phenotypes more information on the significance of the quiescent state would be needed.

A fair criticism to our modelling is that we impose a one step process, which means that cells decide sequentially and does not contemplate delays. Our model already has a relatively large number of parameters for the few data points available, even though making mechanistic assumptions allows us to greatly constrain the number of parameters. Other, more general models, would need arbitrary assumptions in the parameters, and the trials we have made led

to less clear results. Specifically, we tried a model in which there is a probability that all cells transition to the divided state or out of it at the same time, i.e. from 0d to 4d and back, with constant division and dedivision rates in the intermediate states. Preliminary results showed it to be a much poorer fit to experimental data.

In general, more data are needed, both to be able to build more complex models (considering separately the states with any number of divided cells) and to confirm the results from the *bes1-D* mutant. Furthermore, it would be interesting to incorporate to the model data from the *wox5* mutant, the third participant in our regulation module from chapter 5

Part IV

Final remarks and outlook

Chapter 7

Conclusions

7.1 Summary of results

All the work presented in this thesis revolves around different aspects of biological systems that can be understood as bistable. In the first two chapters, we theoretically analyzed different network motifs that enable bisability, and their dynamics under noise. The last three chapters, on the other hand, concentrate on a real system of stem cells: the Quiescent Centre of the root of *Arabidopsis thaliana*. In dialogue with experimental collaborators of the plant developmental biology group lead by Dr. Ana I Caño-Delgado (CRAG), we first tried to unravel how different genes that control the quiescence (cell cycle arrest) of these cells integrate in a module that yields different functions. Finally, we did a simple probabilistic model to study whether the release of this quiescence is synchronized, and in what way.

In the second chapter we showed in a simple Positive Feedback Loop, constituted by an autoactivation, that proper consideration of noise as multiplicative, derived from the dynamics of the system, instead of just as a perturbation of the deterministic behaviour, was sufficient to qualitatively account for an experimentally observed result (Frigola et al., 2012). The state-dependent noise due to the finite molecule number (in the nomenclature of Chapter 3, volume noise) generated an asymmetry in switching rates with respect to their deterministically predicted stability, a phenomenon that was observed in stochastic

cell state switching of yeast (Acar et al., 2005). Furthermore, noise was experimentally observed to be larger in one state than in the other, similarly to our theoretical results. The results in this chapter highlight the necessity to consider noise as an integral part of the system when studying its dynamics, rather than assuming deterministic dynamics and adding a perturbation to them.

We then moved forward to a fully stochastic analysis, in which we built a model of gene transcription that involved several reactions, each of which could generate noise with different impacts. In Chapter 3, we utilized this to model five different circuit architectures that generate bistability, and studied how noise coming from each of the different reactions affected each circuit. These five circuits were the classical Positive Autoregulation, Mutual Activation, and Mutual Inhibition, and the more novel Mixed Feedback Loop and Autoactivation with Complex, that include molecular titration in their mechanism of bistability generation. A global result of our study was that, surprisingly, the Autoactivation with Complex responds to noise quite similarly to the Positive Autoregulation and the Mutual Activation, whereas the Mixed Feedback Loop has a response very similar to Mutual Inhibition. This suggests some sort of general rule of how bistable switches are built and their response to noise, possibly related to the number of positive or negative trasncriptional regulations they have.

We also showed that each circuit is sensitive to specific noise sources, both in Global Stability of the circuit and in Relative Stability of each state with respect to the other. In particular, which noise source affects more the system is strongly dependent on the circuit that generates bistability. This suggests that each circuit may appear in biologically different contexts, depending on what noise sources dominate and which state needs to be more stable, both if they need to be robust against noise or when noise is constructively used as a tuning mechanism for their dynamics. In particular, the Relative Stability of Autoactivation with Complex is very sensitive to changes in volume, which suggests that it could appear in circuits that change their function during cell growth, and makes it unsuitable for other kinds of functions (unless it is coupled to other motifs that soften this sensitivity).

We then moved on to a specific biological system, in which we modelled the interactions of BRAVO, a gene shown by our collaborators to regulate stem cell quiescence in the root of *Arabidopsis thaliana*, and BES1, a transcription

factor that regulates gene expression according to the signalling of the Brassinosteroid hormone family. In Chapter 4 we used theoretical modelling to show that the autoactivation of BRAVO and its repression by BES1, together with their formation of a dimer, enables their expression to be strongly opposite for extremely wide ranges of parameter values (Vilarrasa-Blasi et al., 2014). Furthermore, it can drive bistability and an ultrasensitive switch between states upon a Brassinosteroid signalling threshold. Although we were unable to reproduce the bistable bifurcation diagram, we were able to experimentally observe a sharp transition upon a threshold external Brassinosteroid signalling.

Chapter 5 extended this model to include WOX5, a gene that is only expressed in the Quiescent Centre (Sarkar et al., 2007), and has been shown to directly regulate quiescence (Forzani et al., 2014). Including the interactions that were previously known and those unveiled by our collaborators, namely that WOX5 upregulates BRAVO and is also upregulated by it and by BES1, we were able to show that this module is, in principle, capable of excitability and even oscillations, although these behaviours do not seem to be happening in wild type, unstressed plants. According to our models, which contemplate the possibility of independent regulation of WOX5 by BES1 and BRAVO, and alternatively that the BES1-BRAVO complex could be doing the regulation, it is unlikely that WOX5 responds strongly to Brassinosteroid signalling. Therefore, we predict that it does its regulatory function upon quiescence together with BRAVO (which does respond sharply and strongly to hormone signalling), for instance by forming a complex that regulates it. This prediction remains to be tested.

Finally, in Chapter 6 we concentrate on the measurements of Quiescent Centre cell divisions done by our collaborators. We first noted that these divisions cannot be cell autonomous, with each cell independently deciding, since plants with all or none their cells divided are much too frequent. We then built minimal probabilistic models on how these divisions may be synchronized: by an external signal acting on all cells at the same time, or with rates that depend on the behaviour of the other cells. We showed that, despite both models being extremely simplistic, the model with cell-to-cell communication fits better the data and has more coherent results, suggesting that this synchronization mechanism is, at least, an important player in the biological system. We were also able to compare different phenotypes, seeing that the *bravo* mutant has a strongly diminished cell-to-cell communication, whereas the gain-of-function

bes1-D has increased synchronization. Since both mutants exhibit many more divisions than the wild type, but opposed behaviours regarding synchrony, this suggests that they have different roles in the regulation of quiescence and its synchronization.

7.2 Future perspectives

Most of the work in this thesis opens future perspectives and ways in which it can be either improved or built upon. After our comparison of additive and intrinsic multiplicative noise in chapter 2, the obvious questions are related to the effect of different noise sources or of extrinsic noise. However, both of these possibilities have already been considered by others since this work was first done (de Franciscis et al., 2014; Jaruszewicz et al., 2013). Even by ourselves, in the work presented in chapter 3.

The effect of extrinsic noise coupled to specific architectures has not received a lot of attention (Assaf et al., 2013; de Franciscis et al., 2014), despite its potential importance, since it can represent noise in the rest of the network in which the module is embedded. Therefore, one way to complete the results of chapter 3 would be to include this type of noise.

Other, more important ways to go forward with the work presented in chapter 3 is to confirm its results by studying other parameter sets (as discussed in the chapter), and try to link the different motifs to specific biological functions, as was done by Kittisopikul and Süel (2010). Another interesting question opened by the chapter is whether response to noise can be predicted by some characteristic of the network, such as the number of positive or negative interactions. This could be studied by generalizing the work to bistable Positive Feedback Loops with more than two genes, and try to find general rules that apply to all of them. Such a generalization would also be useful to the study of two-cell network motifs or circuits (Rouault and Hakim, 2012).

Moving on to our studies of the Quiescent Centre of *Arabidopsis* in Chapters 4 to 6, it remains to be seen if our results presented in Chapter 3 for the Autoactivation with Complex and Mixed Feedback Loop, the combination of which conforms the module presented in Chapter 4, apply to the BRAVO module.

Despite experimental limitations in the measurement of noisy dynamics, a theoretical study could be done. Furthermore, our study on the addition of WOX5 to the module in chapter 5 concentrates on steady states and on overall dynamical behaviours of the system, but the stochastic and deterministic switching between states can be studied. Depending on the predictions that arise, experiments could be proposed. An experimental question that would be *a priori* interesting is trying to ascertain the exact relationship of BRAVO expression, as measured through fluorescence, and division, which according to our measurements is unclear. Again, this study would require dynamical measurements which are technically challenging.

Dynamical measurements would also be needed to be able to study synchrony of divisions in more detail than we do in chapter 6: the static picture lumps together several phenomena as an observed division. With additional data, more complex models could be done, perhaps including single cell dynamics and cell to cell communication.

Experiments that can be more easily done are those related to the prediction, presented in chapter 5, that WOX5 and BRAVO act physically together to regulate quiescence. The first step would be to confirm if BRAVO and WOX5 actually dimerize, and if they do the role of this dimer would need to be tested. This is actually research in progress by our collaborators.

Overall, the work in this thesis opens up interesting perspectives in the field of gene regulatory circuits and their relationship with noise, in a more theoretical aspect, and also in more experimental questions that can be tackled with modelling.

7.3 List of publications

I David Frigola, Laura Casanellas, Jose M Sancho, and Marta Ibañes. Asymmetric stochastic switching driven by intrinsic molecular noise. *PLoS ONE*, 7(2):e31407, 2012.

II Josep Vilarrasa-Blasi, Mary-Paz Gonzalez-Garcia, David Frigola, Norma F'abregas, Konstantinos G Alexiou, Nuria López-Bigas, Susana Rivas, Alain

Jauneau, Jan U Lohmann, Philip N Benfey, Marta Ibañes and Ana I. Caño-Delgado. Regulation of plant stem cell quiescence by a brassinosteroid signaling module. *Developmental cell*, 30(1):36–47, 2014.

III David Frigola, Jose M Sancho, and Marta Ibañes. On the principles of multicellular organism development. *Contributions to science*, monographic number *Non-equilibrium physics*. Edited by Felix Ritort, Ignacio Pagonabarraga and Emma Sallent. (preprint)

The results presented in Chapters 3, 5 and 6 are in preparation for submission, and expected to be submitted shortly.

Part V

Appendix

Appendix A

Number of dividing cells given a number of observed divisions

When divisions are independent, it does not matter whether we model *detected* divisions or *observed* divisions. But if we propose a division probability that depends on how many cells are dividing the question could be raised: can we know, given an observed number of divisions, how many divisions are actually happening? Can we establish a relationship to better define the dependence of division probability of a given cell with the number of already divided cells? This can be done through Bayes' theorem

$$p(N_{div}|n_{divobs}) = \frac{p(n_{divobs}|N_{div})p(N_{div})}{p(n_{divobs})}, \tag{A.1}$$

where $p(N_{div}|n_{divobs})$ is the probability that N_{div} divisions are happening given an observed n_{divobs} number of divisions. $p(N_{div})$ is the *prior probability* that N_{div} divisions are happening. In the same vein, $p(n_{divobs})$ is the probability to observe a certain number of divisions. We do not know $p(N_{div})$ since N_{div} is not something we have observed, and in this section we assume no knowledge of $p(n_{divobs})$. However $p(n_{divobs}|N_{div})$, the probability to observe n_{divobs} divisions when the QC has N_{div} divisions, is known.

This is given by the hypergeometric distribution. Given N_{tot} cells among which N_{div} divide, and an observation of n_{obs} cells, the probability to see n_{divobs} cells dividing is

$$P(n_{divobs}) = \frac{\binom{N_{div}}{n_{divobs}}\binom{N_{tot}-N_{div}}{n_{obs}-n_{divobs}}}{\binom{N_{tot}}{n_{obs}}}. \tag{A.2}$$

If we assume a total of 10 cells and 4 observed cells, and take the simplified notation $N = N_{div}, n = n_{divobs}$,

$$P(n|N) = \frac{\binom{N}{n}\binom{10-N}{4-n}}{\binom{10}{4}} = \frac{\frac{N!}{(N-n)!n!}\,\frac{10-N!}{(6-N-n)!(4-n)!}}{210}. \tag{A.3}$$

Unfortunately, this function cannot be easily expressed in a simple way, such that we can extract a relationship between n and N to improve our functions of n-dependent division. We can, however, compute all possible values and tabulate them (Table A.1)

		Observed divisions n				
		0	1	2	3	4
Number of divisions N	0	1	0	0	0	0
	1	0.6	0.4	0	0	0
	2	0.333	0.533	0.133	0	0
	3	0.166	0.5	0.3	0.333	0
	4	0.071	0.381	0.429	0.114	0.005
	5	0.024	0.0238	0.476	0.238	0.024
	6	0.005	0.114	0.429	0.381	0.071
	7	0	0.033	0.3	0.5	0.166
	8	0	0	0.133	0.533	0.333
	9	0	0	0	0.4	0.6
	10	0	0	0	0	1

Table A.1 Probability to observe n divisions given N total divisions when there is a total of 10 cells of which 4 are observed.

If we normalize the columns, we obtain an estimation of $p(N_{div}|n_{divobs}) = p(N|n)$, assuming a uniform prior distribution $p(N_{div})$.

From this, we can compute the expected value of N given an observation n,

$$\langle N \rangle_n = \sum_{N=0}^{N=10} N \times p(N|n), \tag{A.4}$$

and we obtain that

$$\langle N \rangle_0 = 1, \quad \langle N \rangle_1 = 3, \quad \langle N \rangle_2 = 5, \quad \langle N \rangle_3 = 7, \quad \langle N \rangle_4 = 9, \tag{A.5}$$

which corresponds to the relation

$$\langle N \rangle_n = 2n + 1, \tag{A.6}$$

which is a linear function of n. Therefore, as long as our functions that regulate division are linear on n, they represent equally well the 'actual' functions in N, since the constants 2 and 1 will be absorbed into the parameters of the function.

This relationship is not universal, and it only works for 4 observed cells out of 10 total cells. For $n = 3$ out of $N = 10$ cells, for instance, it is $\langle N \rangle_n = 2.4n + 1.4 = n + 1.4(n + 1)$. However, it is still linear.

Appendix B

Resum en català

El desenvolupament d'animals i plantes és un procés complexe en el que, a partir d'una sola cèl·lula, sorgeixen les intrincades estructures de l'organisme multicel·lular. La formació d'aquestes estructures suposa una regulació molt acurada en l'espai i el temps del comportament de les cèl·lules, i en particular de la seva diferenciació en tipus cel·lulars distints, per part de la xarxa formada pels gens i les seves interaccions. Aquests processos són de gran interès biològic, però també físic, ja que aquesta regulació comparteix propietats amb sistemes que han estat, i són, estudiats des del punt de vista de la física.

Aquest estudi dels processos del desenvolupament amb les eines de la física es va iniciar ja fa més de cinquanta anys, però no és fins les últimes dècades que ha començat a ser realment fructífer. El gran avenç en les tècniques experimentals durant els últims quinze anys, amb una resolució en l'espai i el temps mai vista abans, ha suposat la recolecció de moltes i molt precises dades. Aquesta detallada informació experimental ha permès que els models físics i matemàtics estiguin ben fonamentats en la realitat biològica, així com també comprovar les prediccions detallades d'aquests models.

De tots els elements que aporta la física a l'estudi de sistemes biològics, en aquesta tesi ens centrem en dos. D'una banda en el comportament estocàstic de diversos processos cel·lulars, que apareix degut a les escales d'espai i temps de la cèl·lula, i als baixos nombres de molècules que participen en alguns d'aquests

processos. Aquest tipus de processos han estat estudiats en aquest i altres contexts per la física estadística de no equilibri. D'altra banda, també ens interessen les dinàmiques no trivials que sorgeixen quan petits grups de gens formen un circuit d'interaccions no lineals. Els sistemes dinàmics i la física no lineal ens permeten en aquests casos entendre els comportaments que emergeixen, com poden ser oscil·lacions o multiestabilitat.

La primera part de la tesi està dedicada a estudiar, a nivell teòric, com l'arquitectura de petites xarxes genètiques biestables interactuen amb les fluctuacions. En primer lloc estudiem com afecta l'estocasticitat al cas més simple de retroalimentació positiva, la autoactivació, en que una proteïna activa la seva pròpia expressió. Mostrem que considerar les fluctuacions com una simple pertorbació del sistema determinista no descriu el sistema de manera acurada, sino que cal derivar-ne el comportament a partir de la dinàmica del sistema, en el nostre cas obtenint el que es coneix com a soroll multiplicatiu. A més, observem com tenir en compte aquest soroll multiplicatiu és suficient per a reproduir qualitativament un resultat experimental: el fet observat en el llevat *S. Cerevisiae* que els ritmes d'escapament des d'un estat d'alta concentració de proteïna a un de baixa concentració són més ràpids, en proporció a la barrera energètica que ha de superar el sistema, que els ritmes per a canviar de l'estat de baixa concentració al que en té més (Acar et al., 2005; Frigola et al., 2012).

A continuació ampliem l'estudi, afegint a l'autoactivació quatre circuits biestables que involucren dos gens, i comparem com fluctuacions estocàstiques de cinc orígens diferents afecten a les transicions espontànies entre els dos estats de cada circuit. El nostre estudi mostra com cada circuit és sensible a fonts de soroll específiques, que poden canviar completament quin dels dos estats és més estable, així com canviar el ritme global de les transicions en varis ordres de magnitud. Quines són aquestes fonts de soroll canvia de circuit a circuit, i per tant aquests resultats suggereixen que els diferents circuits podrien aparèixer en contexts biològics diferents depenent de quina font de soroll domini i de quin estat cal que sigui més estable.

A la segona part de resultats de la tesi, ens centrem en un circuit genètic d'un sistema biològic específic. Estudiar aquests tipus de circuits permet, d'una banda, entendre millor les dinàmiques teòriques a través de veure com es fan efectives en casos concrets i, a més, respondre preguntes d'interés biològic. En el nostre cas estudiem, gràcies a la col·laboració amb el grup experimental de

biologia del desenvolupament en plantes dirigit per Ana I. Caño-Delgado al Centre de Recerca Agrigenòmica (CRAG)(CSIC-IRTA-UAB-UB), les cèl·lules del Centre Quiescent de l'arrel de la planta *A. thaliana*. Aquestes són un grup de cèl·lules mare a la punta de l'arrel que es divideixen amb molt baixa freqüència, i tenen la doble funció d'organitzar espaialment les cèl·lules mare del seu voltant (precursores dels diferents tipus cel·lulars), d'una banda, i de dividir-se en cas de dany per a restablir aquesta estructura i funcions, per l'altra.

Els nostres col·laboradors van descobrir la proteïna BRAVO, que regula la quiescència (la propietat de dividir-se a molt baixa freqüència) d'aquestes cèl·lules (Vilarrasa-Blasi et al., 2014), i van estudiar la seva interacció amb BES1, una altra proteïna que regula la transcripció de diversos gens en funció de la senyalització de les hormones Brassinoesteroides, i que fomenta la divisió de les cèl·lules quiescents. A partir dels seus resultats experimentals, construïm un model que mostra com el circuit format per aquestes dues proteïnes és capaç de generar biestabilitat i ultrasensibilitat, garantint transicions abruptes entre un estat amb una concentració elevada de BRAVO i molt baixa de BES1, i un estat oposat amb baix BRAVO i BES1 elevat. A més, el nostre model mostra com la interacció d'aquestes dues proteïnes, que formen un heterodímer, és essencial per a aquestes funcions (Vilarrasa-Blasi et al., 2014).

Després de mostrar això, ampliem el nostre model per a incloure una tercera proteïna, WOX5, que només s'expressa al Centre Quiescent i que recentment s'ha mostrat que regula la quiescència de manera directa. En incloure interaccions ja conegudes i d'altres trobades pels nostres col·laboradors, veiem que la inclusió de WOX5 fa que aquest mòdul sigui capaç de mostrar excitabilitat i oscil·lacions, tot i que aquests comportaments no semblen trobar-se en les plantes, com a mínim fora de situacions d'estrès. També veiem com, sota diverses hipòtesis, sembla poc probable que WOX5 sigui sensible als nivells de senyalització dels Brassinoesteroides, i per tant de BES1. Això ens porta a fer la predicció de que la regulació de la quiescència per part de WOX5 és conjunta amb BRAVO, que sí que és molt sensible (ultrasensible), possiblement formant un dímer BRAVO-WOX5.

Per últim, estudiem un altre aspecte de la quiescència però deixant d'estudiar els circuits genètics explícitament. L'observació de les divisions de les cèl·lules del Centre Quiescent en diferents fenotips mostra que les divisions no són autònomes, ja que els estats a on totes les cèl·lules estan dividides o cap ho

està es troben sobrerrepresentats. Construïm doncs models probabilístics senzills que intenten trobar quin és l'origen d'aquesta sincronia. En particular considerem la possibilitat de que hi hagi un senyal temporal senzill que fa que la probabilitat de les cèl·lules de dividir-se depengui del temps, o la de que aquesta probabilitat depengui de quantes cèl·lules ja s'han dividit (enlloc del temps). Trobem que malgrat els dos models són compatibles amb les dades, el model de comunicació cel·lular proporciona uns resultats més coherents que el del senyal temporal. Això ens du a dir que probablement aquesta comunicació sigui un agent important a la regulació de les divisions del centre quiescent. També observem com aquesta sincronia és de naturalesa diferent en els diferents mutants de la planta. En particular, el mutant *bravo* mostra una degradació de la sincronia, mentre que el guany de funció *bes1-D* l'augmenta. Això suggereix que els diferents gens participen de maneres diferenciades en la regulació de la quiescència i la seva sincronia.

En resum, podem dir que aquesta tesi gira al voltant de l'estudi de circuits genètics. D'una banda amb dos estudis teòrics sobre la relació de la seva arquitectura amb el soroll, i de l'altra amb dos models, directament basats en experiments, d'un circuit regulatori de cèl·lules mare en plantes. Aquest circuit ens du a fer també un breu estudi probabilístic de la sincronia en el comportament de les cèl·lules mare.

Bibliography

M. Acar, A. Becskei, and A. van Oudenaarden. Enhancement of cellular memory by reducing stochastic transitions. *Nature*, 435(7039):228–32, 2005.

M. Acar, J. T. Mettetal, and A. van Oudenaarden. Stochastic switching as a survival strategy in fluctuating environments. *Nat. Genet.*, 40(4):471–5, 2008.

M. Acar, B. F. Pando, F. H. Arnold, M. B. Elowitz, and A. van Oudenaarden. A general mechanism for network-dosage compensation in gene circuits. *Science*, 329(5999):1656–60, 2010.

E. Aichinger, N. Kornet, T. Friedrich, and T. Laux. Plant Stem Cell Niches. *Annu. Rev. Plant Biol.*, 63(1):615–636, 2012.

B. Alberts, A. Johnson, J. Lewis, M. Raff, K. Roberts, and P. Walter. *Molecular Biology of the Cell*. Other, 5 edition, 2007.

R. J. Allen, C. Valeriani, and P. Rein Ten Wolde. Forward flux sampling for rare event simulations. *J. Phys. Condens. Matter*, 21:463102, 2009.

U. Alon. Biological networks: The tinkerer as an engineer. *Science*, 301(5641): 1866–1867, 2003.

U. Alon. *An introduction to systems biology: design principles of biological circuits*. CRC press, 2006.

U. Alon. Network motifs: theory and experimental approaches. *Nat. Rev. Genet.*, 8(6):450–61, 2007.

M. Ashyraliyev, Y. Fomekong-Nanfack, J. a. Kaandorp, and J. G. Blom. Systems biology: parameter estimation for biochemical models. *FEBS J.*, 276 (4):886–902, 2009.

M. Assaf, E. Roberts, Z. Luthey-Schulten, and N. Goldenfeld. Extrinsic noise driven phenotype switching in a self-regulating gene. *Phys. Rev. Lett.*, 111 (2):1–5, 2013.

N. Q. Balaban, J. Merrin, R. Chait, L. Kowalik, and S. Leibler. Bacterial persistence as a phenotypic switch. *Science*, 305(5690):1622–1625, 2004.

A.-L. Barabasi and Z. N. Oltvai. Network biology: understanding the cell's functional organization. *Nature reviews genetics*, 5(2):101–113, 2004.

A. Becskei, B. Séraphin, and L. Serrano. Positive feedback in eukaryotic gene networks: cell differentiation by graded to binary response conversion. *EMBO J.*, 20(10):2528, 2001.

W. Bialek. Stability and noise in biochemical switches. 2000.

W. Bialek. *Biophysics : Searching for Principles*. Princeton University Press, Princeton, New Jersey, 2011.

N. E. Buchler and M. Louis. Molecular Titration and Ultrasensitivity in Regulatory Networks. *J. Mol. Biol.*, 384(5):1106–1119, 2008.

A. Caño-Delgado, J.-Y. Lee, and T. Demura. Regulatory mechanisms for specification and patterning of plant vascular tissues. *Annual review of cell and developmental biology*, 26:605–637, 2010.

G. Caravagna, G. Mauri, and A. D'Onofrio. The Interplay of Intrinsic and Extrinsic Bounded Noises in Biomolecular Networks. *PLoS One*, 8(2):e51174, 2013.

O. Carrillo, M. Ibañes, J. García-Ojalvo, J. Casademunt, and J. Sancho. Intrinsic noise-induced phase transitions: Beyond the noise interpretation. *Phys. Rev. E*, 67(4):1–9, 2003.

V. Castets, E. Dulos, J. Boissonade, and P. De Kepper. Experimental evidence of a sustained standing turing-type nonequilibrium chemical pattern. *Physical Review Letters*, 64(24):2953, 1990.

Z. Cheng, F. Liu, X.-P. Zhang, and W. Wang. Robustness analysis of cellular memory in an autoactivating positive feedback system. *FEBS Lett.*, 582(27): 3776–82, 2008.

J. L. Cherry and F. R. Adler. How to make a biological switch. *J. Theor. Biol.*, 203(2):117–33, 2000.

T. H. Cheung and T. A. Rando. Molecular regulation of stem cell quiescence. *Nature reviews Molecular cell biology*, 14(6):329–340, 2013.

F. Crick. Diffusion in embryogenesis. 1970a.

F. Crick. Central dogma of molecular biology. *Nature*, 227(5258):561–563, 1970b.

A. Cruz-Ramírez, S. Díaz-Triviño, I. Blilou, V. a. Grieneisen, R. Sozzani, C. Zamioudis, P. Miskolczi, J. Nieuwland, R. Benjamins, P. Dhonukshe, J. Caballero-Pérez, B. Horvath, Y. Long, A. P. Mähönen, H. Zhang, J. Xu, J. a. H. Murray, P. N. Benfey, L. Bako, A. F. M. Marée, and B. Scheres. A bistable circuit involving SCARECROW-RETINOBLASTOMA integrates cues to inform asymmetric stem cell division. *Cell*, 150(5):1002–15, 2012.

A. Cruz-Ramírez, S. Díaz-Triviño, G. Wachsman, Y. Du, M. Arteága-Vázquez, H. Zhang, R. Benjamins, I. Blilou, A. B. Neef, V. Chandler, et al. A scarecrow-retinoblastoma protein network controls protective quiescence in the arabidopsis root stem cell organizer. 2013.

R. D. Dar, B. S. Razooky, a. Singh, T. V. Trimeloni, J. M. McCollum, C. D. Cox, M. L. Simpson, and L. S. Weinberger. Transcriptional burst frequency and burst size are equally modulated across the human genome. *Proc. Natl. Acad. Sci.*, 109:17454–17459, 2012.

D. Darling. The Kolmogorov-Smirnov, Cramer-von Mises Tests. *Ann. Math. Stat.*, 28(4):823–838, 1957.

S. de Franciscis, G. Caravagna, and A. d'Onofrio. Gene switching rate determines response to extrinsic perturbations in a transcriptional network motif. *arXiv preprint arXiv:1410.6993*, 2014.

L. Dolan, K. Janmaat, V. Willemsen, P. Linstead, S. Poethig, K. Roberts, and B. Scheres. Cellular organisation of the Arabidopsis thaliana root. *Development*, 119(1):71–84, 1993.

R. M. Donovan, A. J. Sedgewick, J. R. Faeder, and D. M. Zuckerman. Efficient stochastic simulation of chemical kinetics networks using a weighted ensemble of trajectories. *J. Chem. Phys.*, 139(11):115105, 2013.

D. Dubnau and R. Losick. Bistability in bacteria. *Mol. Microbiol.*, 61(3):564–572, 2006.

A. Eldar and M. B. Elowitz. Functional roles for noise in genetic circuits. *Nature*, 467(7312):167–173, 2010.

M. B. Elowitz, A. J. Levine, E. D. Siggia, and P. S. Swain. Stochastic gene expression in a single cell. *Sci. Signal.*, 297(5584):1183, 2002.

J. Estrada and R. Guantes. Dynamic and structural constraints in signal propagation by regulatory networks. *Mol. Biosyst.*, 9(2):268–84, 2013.

J. E. Ferrell. Self-perpetuating states in signal transduction: positive feedback, double-negative feedback and bistability. *Curr. Opin. Cell Biol.*, 14(2):140–148, 2002.

J. E. Ferrell. Bistability, bifurcations, and Waddington's epigenetic landscape. *Curr. Biol.*, 22(11), 2012.

J. E. Ferrell Jr. The Biochemical Basis of an All-or-None Cell Fate Switch in Xenopus Oocytes. *Science (80-.).*, 280(5365):895–898, 1998.

C. Forzani, E. Aichinger, E. Sornay, V. Willemsen, T. Laux, W. Dewitte, and J. H. Murray. WOX5 Suppresses CYCLIN D Activity to Establish Quiescence at the Center of the Root Stem Cell Niche. *Curr. Biol.*, 24(16):1939–1944, 2014.

P. François and V. Hakim. Design of genetic networks with specified functions by evolution in silico. *Proc. Natl. Acad. Sci. U. S. A.*, 101(2):580–5, 2004.

P. François and V. Hakim. Core genetic module: The mixed feedback loop. *Phys. Rev. E - Stat. Nonlinear, Soft Matter Phys.*, 72(May):1–14, 2005.

N. Friedman, L. Cai, and X. Xie. Linking Stochastic Dynamics to Population Distribution: An Analytical Framework of Gene Expression. *Phys. Rev. Lett.*, 97(16):168302, 2006.

D. Frigola, L. Casanellas, J. M. Sancho, and M. Ibañes. Asymmetric stochastic switching driven by intrinsic molecular noise. *PloS one*, 7(2):e31407, 2012.

D. Frigola, J. M. Sancho, and M. Ibañes. On the principles of multicellular organism development. *Contributions to Science: "Non Equilibrium Physics"*, Submitted.

S. Froidure, J. Canonne, X. Daniel, A. Jauneau, C. Brière, D. Roby, and S. Rivas. Atspla2-α nuclear relocalization by the arabidopsis transcription factor atmyb30 leads to repression of the plant defense response. *Proceedings of the National Academy of Sciences*, 107(34):15281–15286, 2010.

J. Garcia-Ojalvo and A. Martinez Arias. Towards a statistical mechanics of cell fate decisions. *Curr. Opin. Genet. Dev.*, 22(6):619–626, 2012.

J. García-Ojalvo and J. Sancho. *Noise in spatially extended systems*. Springer Science & Business Media, 2012.

C. W. Gardiner. *Handbook of stochastic methods for Physics, Chemistry and the Natural Sciences*. Springer-Verlag, Berlin, 2008.

A. Gierer and H. Meinhardt. A theory of biological pattern formation. *Kybernetik*, 12(1):30–39, 1972.

D. T. Gillespie. Exact stochastic simulation of coupled chemical reactions. *J of Phys Chem*, 81(25):2340–2361, 1977.

D. T. Gillespie. The chemical langevin equation. *The Journal of Chemical Physics*, 113(1):297–306, 2000.

I. Golding, J. Paulsson, S. M. Zawilski, and E. C. Cox. Real-time kinetics of gene activity in individual bacteria. *Cell*, 123(6):1025–1036, 2005.

M.-P. González-García, J. Vilarrasa-Blasi, M. Zhiponova, F. Divol, S. Mora-García, E. Russinova, and A. I. Caño-Delgado. Brassinosteroids control meristem size by promoting cell cycle progression in arabidopsis roots. *Development*, 138(5):849–859, 2011.

T. G. W. Graham, S. M. A. Tabei, A. R. Dinner, and I. Rebay. Modeling bistable cell-fate choices in the Drosophila eye: qualitative and quantitative perspectives. *Development*, 137(14):2265–78, 2010.

R. Guantes and J. F. Poyatos. Multistable decision switches for flexible control of epigenetic differentiation. *PLoS Comput. Biol.*, 4(11):e1000235, 2008.

A. Haecker, R. Groß-Hardt, B. Geiges, A. Sarkar, H. Breuninger, M. Herrmann, and T. Laux. Expression dynamics of wox genes mark cell fate decisions during early embryonic patterning in arabidopsis thaliana. *Development*, 131 (3):657–668, 2004.

L. H. Hartwell, J. J. Hopfield, S. Leibler, and A. W. Murray. From molecular to modular cell biology. *Nature*, 402:C47–C52, 1999.

J. Hasty, D. McMillen, and J. J. Collins. Engineered gene circuits. *Nature*, 420 (6912):224–230, 2002.

J. Heyman, T. Cools, F. Vandenbussche, K. S. Heyndrickx, J. Van Leene, I. Vercauteren, S. Vanderauwera, K. Vandepoele, G. De Jaeger, D. Van Der Straeten, et al. Erf115 controls root quiescent center cell division and stem cell replenishment. *Science*, 342(6160):860–863, 2013.

W. Horsthemke and R. Lefever. Noise-induced transitions in physics, chemistry, and biology. *Noise-Induced Transitions: Theory and Applications in Physics, Chemistry, and Biology*, 1984.

S. Huang. The molecular and mathematical basis of waddington's epigenetic landscape: A framework for post-darwinian biology? *Bioessays*, 34(2):149–157, 2012.

J. Jaruszewicz and T. Lipniacki. Toggle switch: noise determines the winning gene. *Phys. Biol.*, 10(3):035007, 2013.

J. Jaruszewicz, P. J. Zuk, and T. Lipniacki. Type of noise defines global attractors in bistable molecular regulatory systems. *J. Theor. Biol.*, 317:140–51, 2013.

H. Jönsson, M. Heisler, G. V. Reddy, V. Agrawal, V. Gor, B. E. Shapiro, E. Mjolsness, and E. M. Meyerowitz. Modeling the organization of the WUSCHEL expression domain in the shoot apical meristem. *Bioinformatics*, 21 Suppl 1:i232–40, 2005.

T. Kalmar, C. Lim, P. Hayward, S. Muñoz Descalzo, J. Nichols, J. Garcia-Ojalvo, and A. Martinez Arias. Regulated fluctuations in nanog expression mediate cell fate decisions in embryonic stem cells. *PLoS Biol.*, 7(7):e1000149, 2009.

a. D. Keller. Model genetic circuits encoding autoregulatory transcription factors. *J. Theor. Biol.*, 172(2):169–185, 1995.

T. B. Kepler and T. C. Elston. Stochasticity in transcriptional regulation: origins, consequences, and mathematical representations. *Biophys. J.*, 81(6): 3116–36, Dec. 2001.

A. S. Khalil and J. J. Collins. Synthetic biology: applications come of age. *Nat. Rev. Genet.*, 11(5):367–379, 2010.

M. Kittisopikul and G. M. Süel. Biological role of noise encoded in a genetic network motif. *Proc. Natl. Acad. Sci. U. S. A.*, 107(30):13300–5, 2010.

S. Kondo, M. Iwashita, and M. Yamaguchi. How animals get their skin patterns: fish pigment pattern as a live Turing wave. *Int. J. Dev. Biol.*, 53(5-6):851–6, 2009.

M. Koornneef and D. Meinke. The development of Arabidopsis as a model plant. *Plant J.*, 61(6):909–21, 2010.

J. a. Kromer, L. Schimansky-Geier, and R. Toral. Weighted-ensemble Brownian dynamics simulation: Sampling of rare events in nonequilibrium systems. *Phys. Rev. E - Stat. Nonlinear, Soft Matter Phys.*, 87:1–11, 2013.

E. Kussell, R. Kishony, N. Q. Balaban, and S. Leibler. Bacterial persistence: a model of survival in changing environments. *Genetics*, 169(4):1807–14, Apr. 2005.

G. Lambert and E. Kussell. Memory and Fitness Optimization of Bacteria under Fluctuating Environments. *PLoS Genet.*, 10(9):e1004556, 2014.

P. Lawrence. Theoretical embryology: a route to extinction? *Current Biology*, 14(1):R7–R8, 2004.

J. H. Levine, Y. Lin, and M. B. Elowitz. Functional Roles of Pulsing in Genetic Circuits. *Science (80-.).*, 342(6163):1193–1200, 2013.

D. Li and C. Li. Noise-induced dynamics in the mixed-feedback-loop network motif. *Phys. Rev. E - Stat. Nonlinear, Soft Matter Phys.*, 77, 2008.

L. Li, X. Yu, A. Thompson, M. Guo, S. Yoshida, T. Asami, J. Chory, and Y. Yin. Arabidopsis myb30 is a direct target of bes1 and cooperates with bes1 to regulate brassinosteroid-induced gene expression. *The Plant Journal*, 58(2):275–286, 2009.

W. A. Lim, C. M. Lee, and C. Tang. Design principles of regulatory networks: searching for the molecular algorithms of the cell. *Mol. Cell*, 49(2):202–12, 2013.

A. Lipshtat, A. Loinger, N. Balaban, and O. Biham. Genetic Toggle Switch without Cooperative Binding. *Phys. Rev. Lett.*, 96(18), 2006.

R. Losick and C. Desplan. Stochasticity and cell fate. *Science*, 320(5872):65–8, 2008.

H. M. Meyer and A. H. K. Roeder. Stochasticity in plant cellular growth and patterning. *Front. Plant Sci.*, 5(September):420, 2014.

R. Milo, S. Shen-Orr, S. Itzkovitz, N. Kashtan, D. Chklovskii, and U. Alon. Network motifs: Simple building blocks of complex networks. *Science*, 298 (5594):824–827, 2002.

R. Milo, P. Jorgensen, U. Moran, G. Weber, and M. Springer. Bionumbers—the database of key numbers in molecular and cell biology. *Nucleic Acids Research*, 38(suppl 1):D750–D753, 2010.

M. J. Morelli, S. Tanase-Nicola, R. J. Allen, and P. R. ten Wolde. Reaction coordinates for the flipping of genetic switches. *Biophys. J.*, 94(9):3413–23, 2008.

B. Munsky, B. Trinh, and M. Khammash. Listening to the noise: random fluctuations reveal gene network parameters. *Mol. Syst. Biol.*, 5(318):318, 2009.

B. Munsky, G. Neuert, and A. van Oudenaarden. Using gene expression noise to understand gene regulation. *Science*, 336(6078):183–7, 2012.

J. D. Murray. *Mathematical Biology. II Spatial Models and Biomedical Applications {Interdisciplinary Applied Mathematics V. 18}*. Springer-Verlag New York Incorporated, 2001.

E. M. Ozbudak, M. Thattai, I. Kurtser, A. D. Grossman, and A. van Oudenaarden. Regulation of noise in the expression of a single gene. *Nat. Genet.*, 31(1):69–73, 2002.

E. M. Ozbudak, M. Thattai, H. N. Lim, B. I. Shraiman, and A. Van Oudenaarden. Multistability in the lactose utilization network of Escherichia coli. *Nature*, 427(6976):737–40, 2004.

J. Paulsson. Summing up the noise in gene networks. *Nature*, 427(6973):415–418, 2004.

T. J. Perkins and P. S. Swain. Strategies for cellular decision-making. *Mol. Syst. Biol.*, 5(326):326, 2009.

N. Perrimon and N. Barkai. The era of systems developmental biology. *Current opinion in genetics & development*, 21(6):681–683, 2011.

A. Pokhilko, P. Mas, and A. J. Millar. Modelling the widespread effects of TOC1 signalling on the plant circadian clock and its outputs. *BMC Syst. Biol.*, 7(1):23, 2013.

W. H. Press, S. A. Teukolsky, W. T. Vetterling, and B. P. Flannery. *Numerical Recipes in FORTRAN; The Art of Scientific Computing*. Cambridge University Press, New York, NY, USA, 2nd edition, 1993.

A. Raj and A. van Oudenaarden. Nature, nurture, or chance: stochastic gene expression and its consequences. *Cell*, 135(2):216–26, 2008.

A. H. K. Roeder, V. Chickarmane, A. Cunha, B. Obara, B. S. Manjunath, and E. M. Meyerowitz. Variability in the Control of Cell Division Underlies Sepal Epidermal Patterning in Arabidopsis thaliana. *PLoS Biol.*, 8(5):e1000367, 2010.

K. W. Rogers and A. F. Schier. Morphogen gradients: from generation to interpretation. *Annu. Rev. Cell Dev. Biol.*, 27:377–407, jan 2011.

H. Rouault and V. Hakim. Different cell fates from cell-cell interactions: core architectures of two-cell bistable networks. *Biophys. J.*, 102(3):417–26, 2012.

P. Rué and J. Garcia-Ojalvo. Gene circuit designs for noisy excitable dynamics. *Mathematical biosciences*, 231(1):90–97, 2011.

P. Rué and J. Garcia-Ojalvo. Modeling gene expression in time and space. *Annual review of biophysics*, 42:605–627, 2013.

F. Sagués, J. M. Sancho, and J. García-Ojalvo. Spatiotemporal order out of noise. *Rev. Mod. Phys.*, 79(3):829–882, 2007.

M. San Miguel and R. Toral. Stochastic effects in physical systems. In *Instabilities and nonequilibrium structures VI*, pages 35–127. Springer, 2000.

A. K. Sarkar, M. Luijten, S. Miyashima, M. Lenhard, T. Hashimoto, K. Nakajima, B. Scheres, R. Heidstra, and T. Laux. Conserved factors regulate signalling in Arabidopsis thaliana shoot and root stem cell organizers. *Nature*, 446(7137):811–4, 2007.

B. Scheres. Stem-cell niches: nursery rhymes across kingdoms. *Nat. Rev. Mol. Cell Biol.*, 8(5):345–354, 2007.

C.-C. Shu, A. Chatterjee, G. Dunny, W.-S. Hu, and D. Ramkrishna. Bistability versus Bimodal Distributions in Gene Regulatory Processes from Population Balance. *PLoS Comput. Biol.*, 7(8):e1002140, 2011.

D. Siegal-Gaskins, E. Grotewold, and G. D. Smith. The capacity for multistability in small gene regulatory networks. *BMC Syst. Biol.*, 3:96, 2009.

Z. S. Singer, J. Yong, J. Tischler, J. A. Hackett, A. Altinok, M. A. Surani, L. Cai, and M. B. Elowitz. Dynamic Heterogeneity and DNA Methylation in Embryonic Stem Cells. *Mol. Cell*, 55(2):319–331, 2014.

A. Singh, B. S. Razooky, R. D. Dar, and L. S. Weinberger. Dynamics of protein noise can distinguish between alternate sources of gene-expression variability. *Mol. Syst. Biol.*, 8(607):1–9, 2012.

Q. Smith, E. Stukalin, S. Kusuma, S. Gerecht, and S. X. Sun. Stochasticity and Spatial Interaction Govern Stem Cell Differentiation Dynamics. *Sci. Rep.*, 5: 12617, 2015.

P. Smolen, D. a. Baxter, and J. H. Byrne. Frequency selectivity, multistability, and oscillations emerge from models of genetic regulatory systems. *Am. J. Physiol.*, 274(2 Pt 1):C531–C542, 1998.

M. Strasser, F. J. Theis, and C. Marr. Stability and multiattractor dynamics of a toggle switch based on a two-stage model of stochastic gene expression. *Biophys. J.*, 102(1):19–29, 2012.

S. H. Strogatz. *Nonlinear dynamics and chaos: with applications to physics, biology, chemistry, and engineering*. Westview press, 2014.

G. M. Süel, J. Garcia-Ojalvo, L. M. Liberman, and M. B. Elowitz. An excitable gene regulatory circuit induces transient cellular differentiation. *Nature*, 440 (7083):545–550, 2006.

Y. Tao, X. Zheng, and Y. Sun. Effect of feedback regulation on stochastic gene expression. *J. Theor. Biol.*, 247(4):827–36, 2007.

T. Tian and K. Burrage. Stochastic models for regulatory networks of the genetic toggle switch. *Proc. Natl. Acad. Sci.*, 103(22):8372–8377, 2006.

T.-L. To and N. Maheshri. Noise can induce bimodality in positive transcriptional feedback loops without bistability. *Science*, 327(5969):1142–5, 2010.

R. Toral and A. Chakrabarti. Generation of Gaussian distributed random numbers by using a numerical inversion method. *Comput. Phys. Commun.*, 74 (3):327–334, 1993.

M. Turcotte, J. Garcia-Ojalvo, and G. M. Süel. A genetic timer through noise-induced stabilization of an unstable state. *Proceedings of the National Academy of Sciences*, 105(41):15732–15737, 2008.

A. M. Turing. The chemical basis of morphogenesis. *Philosophical Transactions of the Royal Society of London B: Biological Sciences*, 237(641):37–72, 1952.

J. J. Tyson, K. C. Chen, and B. Novak. Sniffers, buzzers, toggles and blinkers: Dynamics of regulatory and signaling pathways in the cell. *Curr. Opin. Cell Biol.*, 15(2):221–231, 2003.

C. Van den Berg, V. Willemsen, G. Hendriks, P. Weisbeek, and B. Scheres. Short-range control of cell differentiation in the arabidopsis root meristem. *Nature*, 390(6657):287–289, 1997.

N. Van Kampen. *Stochastic processes in Physics and Chemistry*. Elsevier B. V., Amsterdam, 2007.

J.-W. Veening, W. K. Smits, and O. P. Kuipers. Bistability, epigenetics, and bet-hedging in bacteria. *Annu. Rev. Microbiol.*, 62:193–210, 2008.

G. Vert, J. L. Nemhauser, N. Geldner, F. Hong, and J. Chory. Molecular mechanisms of steroid hormone signaling in plants. *Annu. Rev. Cell Dev. Biol.*, 21:177–201, 2005.

R. D. Vigil, Q. Ouyang, and H. L. Swinney. Turing patterns in a simple gel reactor. *Physica A: Statistical Mechanics and its Applications*, 188(1):17–25, 1992.

J. Vilarrasa-Blasi. *Spatial analysis of brassinosteroid signaling in the stem cell niche of Arabidopsis primary root*. PhD thesis, 2014.

J. Vilarrasa-Blasi, M.-P. González-García, D. Frigola, N. Fàbregas, K. G. Alexiou, N. López-Bigas, S. Rivas, A. Jauneau, J. U. Lohmann, P. N. Benfey, M. Ibanñes, and A. I. Caño Delgado. Regulation of plant stem cell quiescence by a brassinosteroid signaling module. *Developmental cell*, 30(1):36–47, 2014.

C. H. Waddington. The epigenotype. *Endeavour*, (1):18–20, 1942.

G. R. Walther, A. F. M. Marée, L. Edelstein-Keshet, and V. a. Grieneisen. Deterministic versus stochastic cell polarisation through wave-pinning. *Bull. Math. Biol.*, 74(11):2570–99, 2012.

M. Weber and J. Buceta. Noise regulation by quorum sensing in low mRNA copy number systems. *BMC Syst. Biol.*, 5(1):11, 2011.

M. Weber and J. Buceta. Stochastic stabilization of phenotypic States: the genetic bistable switch as a case study. *PLoS One*, 8(9):e73487, 2013.

Wolfram Research. Mathematica 8.0, 2010.

L. Wolpert. Positional Information and the Spatial Pattern of Cellular Differentiationt. 1968:1–47, 1969.

E. Yeger-Lotem and H. Margalit. Detection of regulatory circuits by integrating the cellular networks of protein-protein interactions and transcription regulation. *Nucleic Acids Res.*, 31(20):6053–6061, 2003.

J.-Y. Zhu, J. Sae-Seaw, and Z.-Y. Wang. Brassinosteroid signalling. *Development*, 140(8):1615–20, 2013.